Reactivity and burnout of wood fuels

Dall'Ora, Michelangelo; Jensen, Anker Degn; Jensen, Peter Arendt

Publication date:
2011

Document Version
Publisher's PDF, also known as Version of record

REACTIVITY AND BURNOUT OF WOOD FUELS

Ph.D. thesis

by

Michelangelo Dall'Ora

2011

DEPARTMENT OF CHEMICAL AND BIOCHEMICAL ENGINEERING

TECHNICAL UNIVERSITY OF DENMARK
DK-2800 Kgs. Lyngby, Denmark

PREFACE AND ACKNOWLEDGEMENTS

This Ph.D. thesis is submitted as part of the requirements for the Ph.D. degree at the Technical University of Denmark (DTU). The project was carried out at the Combustion and Harmful Emission Control (CHEC) Research Centre, Department of Chemical and Biochemical Engineering, Technical University of Denmark, in cooperation with Dong Energy Power and Vattenfall A/S. This study was supported by Energinet.dk, Dong Energy Power and Vattenfall A/S through PSO-F&U contract no. 6526.

The Ph.D. project was supervised by Professor Anker Degn Jensen (main supervisor) and Associate Professor Peter Arendt Jensen.

I would like to express my deepest gratitude to Anker Degn Jensen for his rigorous and generous guidance; his passion for science, commitment to tutoring and positive approach have been of great inspiration, especially during the toughest times of the project. I would like to thank Peter Arendt Jensen for his thorough review of the work and his stimulating criticism.

During my time at CHEC I have had the pleasure to work with excellent scientific and technical staff members; I am particularly grateful to Weigang Lin and Jørn Hansen for always being ready to share their invaluable knowledge and expertise.

Without the constant and loving support of my family and my friends I would not have been able to complete this project. I would especially like to thank Nathalie Lecordier and Matias Monsalvo for their support.

Michelangelo Dall'Ora

Copenhagen, April 2011

SUMMARY

This thesis deals with the combustion of wood in pulverised fuel power plants. In this type of boiler, the slowest step in the wood conversion process is char combustion, which is one of the factors that not only determine the degree of fuel burnout, but also affect the heat release profile in the boiler and thereby the overall operation and efficiency of the plant.

Chapter 1 consists of an introduction to thermal conversion of biomass fuels as well as a description of a Danish power plant where a measuring campaign was carried out as part of this project.

Chapter 2 is a brief literature review of different aspects relevant to wood combustion, including wood structure and composition, wood pyrolysis, wood char properties and wood char oxidation.

The full scale campaign, which is the subject of Chapter 3, included sampling of wood fuel before and after milling and sampling of gas and particles at the top of the combustion chamber. The collected samples and data are used to obtain an evaluation of the mills in operation at the power plant, the particle size distribution of the wood fuel, as well as the char conversion attained in the furnace.

In Chapter 4 an experimental investigation on the relation between pyrolysis of wood in boiler-like conditions and wood char properties is presented. Chars from pine and beech wood were produced by fast pyrolysis in an entrained flow reactor and by slow pyrolysis in a thermogravimetric analyser. The influence of pyrolysis temperature, heating rate and particle size on char yield and morphology was investigated. The applied pyrolysis temperature varied in the range 673 – 1673 K for slow pyrolysis and 1073 - 1573 K for fast pyrolysis. The chars were oxidised in a thermogravimetric analyser and the mass loss data were used to determine char oxidation reactivity. Char yield from fast pyrolysis (10^4 – 10^5 K/s) was as low as 1 to 6 % on a dry ash free basis, whereas it was about 15-17 % for slow pyrolysis (10 - 20 K/min); char yield decreased as pyrolysis temperature increased. During fast pyrolysis wood particles underwent melting, yet to different extents for the two investigated fuels: pine wood produced chars of porous spherical particles, whereas beech sawdust chars showed a somewhat less drastic change of morphology with respect to the parent fuel. Char produced by low heating rate pyrolysis fully retained the original fibrous structure of wood. Fast pyrolysis chars were significantly more reactive than slow pyrolysis chars (for the same activation energy, the pre-exponential factor was up to 2 orders of magnitude greater for chars

generated by fast pyrolysis); moreover, char oxidation reactivity decreased as pyrolysis temperature increased. The amount and composition of the ash forming matter of the wood fuels is believed to play an important role in determining the differences in char yield, morphology and reactivity.

The modelling of wood char combustion is the subject of Chapter 5. The lowest and the highest reactivities obtained for the chars produced in the EFR are used in a simple single particle combustion model in combination with a description of Avedøreværket's boiler. In the model the char particle is assumed to burn in a gas with constant temperature and constant oxygen fraction. The particle temperature is on the other hand determined taking reaction heat, convection through boundary gas layer and radiation into account. The model accounts for external diffusion of oxygen to the particle outer surface, internal diffusion in the pores and heterogeneous chemical reaction (CO is considered the only product). The model calculates an overall efficiency factor for combustion, yet assumes that all the reacting carbon is consumed at the outer surface of the char.

The model predicts that at an average furnace temperature of 1200 K the conversion of char particles with radius 20-350 μm is very much affected by the reactivity of the char. The influence of the particle's reactivity is lower at higher temperatures: at furnace temperatures of 1500 K and 1700 K the combustion of the char is mainly controlled by transport processes. The effect of the oxygen concentration in the bulk gas is investigated and it is found that an increase of oxygen in bulk gas leads to higher particle temperatures and shifts the controlling step of the combustion towards diffusion. As far as density is concerned, the model results indicate that the time of char conversion increases with increasing density. It is found that for larger char particles the residence time in the furnace can be considerably longer than for the gas (up to 6.4 s for 250 μm radius particle, compared with 4.6 s for the gas). According to the model high reactive chars with radius up to 285 μm attain a conversion of at least 99.80% in the furnace when burning in gas at 1200 K and 2% oxygen; in order to obtain 99.80% conversion for gas temperatures of 1500 K and 1700 K low reactive particles should have radiuses no greater than 260 μm and 300 μm and highly reactive chars no greater than 315 μm and 335 μm, respectively. Finally, the model results are compared to the full scale data from Avedøreværket power plant; the model provides a generally good prediction of the conversion attained by wood char in the furnace.

RESUMÉ

Denne afhandling omhandler forbrænding af træstøv i kraftværker. I denne type af kedler er trækulsforbrænding det langsomste trin, hvilket er den bestemmende factor ikke bare for brandselsomdannelse men også for varmeafgivelsesprofilen i kedlen. Dette har indflydelse på den overordnede drift og effektivitet af anlægget.

Kapitel 1 består af en introduktion til termiske omdannelse af biobrændsler samt en beskrivelse af et dansk kraftværk, hvor en målekampagne blev udført som en del af dette projekt.

Kapitel 2 er en kort litteraturoversigt af forskellige relevante aspekter af træforbrænding, hvilket inkluderer træstruktur og træsammensætning, træpyrolyse, samt egenskaber og forbrænding af koks fra træ.

Fuldskalakampagnen, som bliver beskrevet i Kapitel 3, bestod af indsamling af træbrændsel før og efter maling og indsamling af gas og partikler i toppen af brændselskammeret. De opsamlede prøver og data er blevet brugt til at evaluere møllerne i brug på kraftværket, partikelsstørrelsesfordelingen af træbrændsel og den opnåede omdannelse af koks i fyrrummet.

I Kapitel 4 bliver en eksperimentel undersøgelse af sammenhængen mellem pyrolyse af træ under kedellignende betingelser og trækuls egenskaber beskrevet. Kul fra gran og bøg blev produceret ved hurtig pyrolyse i en "entrained flow reactor" og ved langsom pyrolyse i en termogravimetrisk analysator. Det blev undersøgt, hvilken indflydelse pyrolysens temperatur, opvarmingshastigheden og partikel størrelsen har på koks udbyttet og morfologien. Pyrolyse temperaturen varierede mellem 673 – 1673 K for langsom pyrolyse og 1073 – 1573 K for hurtig pyrolyse. Koksen blev oxideret i en termogravimetrisk analysator, og vægttabet blev brugt til at bestemme dens oxidations reaktivitet. Koks udbyttet fra hurtig pyrolyse (10^4 – 10^5 K/s) var så lav som 1 – 6 % på tør askefri basis, hvorimod det var omkring 15 – 17 % for langsom pyrolyse (10 – 20 K/min); koks udbyttet faldt når pyrolysetemperaturen steg. Ved hurtig pyrolyse smeltede træpartiklerne, dog i forskellig grad for de to undersøgte brændsler: træ fra gran blev til porøse sfæriske partikler der indikerer fuldstændig smeltning, hvorimod koks fra bøg udviste mindre drastiske ændringer i morfologien m.h.t. det oprindelige brændsel. Koks produceret ved lav opvarmningshastighed bibeholdt den oprindelige fibrøse træstruktur. Koks fra hurtig pyrolyse var betydelig mere reaktivt end koks fra langsom pyrolyse (ved samme aktiveringsenergi er koks fra hurtig pyrolyse ca 100 gange mere reaktiv end koks fra pyrolyse i termogravimetrisk analysator); derudover faldt koks oxidations

reaktiviteten med stigende pyrolyse temperatur. Resultaterne indikerer at mængden og sammensætningen af de uorganiske stoffer i brændslet har stor indflydelse på koks udbyttet, samt dets morfologi og reaktivitet.

Modellering af koks forbrændning bliver behandlet i Kapitel 5. The lowest and the highest reactivity De højeste og laveste beregnede reaktiviteter for koks produceret i EFR bliver brugt i en simpel enkelt partikel forbrændningsmodel i kombination med en beskrivelse af Avedøreværkets kedel. Modellen antager, at kokspartiklen brænder i en gas med konstant temperatur og iltmolbrøk. Partiklens temperatur beregnes ved at tage reaktionsvarmen, konvektion gennem gasfilmen og stråling i betragtning. Modellen tager højde for ekstern diffusion af ilt til partiklens ydre overflade, intern diffusion i porerne og heterogen kemisk reaktion (CO antages som det eneste produkt). Modellen beregner en samlet effektivitetsfaktor for forbrændning og antager, at den reagerede carbon bliver forbrugt på den ydre overflade af kokspartiklen.

Modellen forudsiger at ved en fyrrumstemperatur på 1200 K påvirkes omsætningsgraden af partikler med radius 20-350 μm betydeligt af koksreaktiviteten. Indflydelsen af koksreaktiviteten er mindre ved højere fyrrumstemperaturer på henholdsvis 1500 K og 1700 K hvor forbrændingen hovedsageligt er kontrolleret af ekstern gasfilmkontrol. Indflydelsen af bulk iltkoncentrationen er blevet undersøgt i intervallet 0.1-4.0 vol.%. Stigende iltkoncentration fører til højere partikeltemperaturer og flytter forbrændingen mod en stigende grad af gasfilmkontrol. Modellen viser yderligere at udbrændingstiden stiger med stigende koksdensitet. Opholdstiden for partiklerne i fyrrummet stiger med stigende partikelstørrelse på grund af den større faldhastighed. Eksempelvis er opholdstiden for en partikel med radius på 250 μm 6.4 s hvorimod gassens opholdstid er 4.6 s. Ifølge modellen vil koks med høj reaktivitet kunne nå udbrændingsgrader større end 99.8 % ved en fyrrumstemperatur på 1200 K og iltprocent på 2, såfremt deres radius er mindre end 285 μm. Ved fyrrumstemperaturer på 1500 K og 1700 K skal partikler med lav reaktivitet have en radius mindre end henholdsvis 260 μm og 300 μm mens partikler med høj reaktivitet blot skal være mindre end henholdsvis 315 μm og 355 μm. Modellen er kvalitativt i god overensstemmelse med de målte udbrændingsgrader på Avedøreværket.

TABLE OF CONTENTS

CHAPTER 1

INTRODUCTION

1.1 ENERGY FROM BIOMASS

Biomass includes a wide range of products and by-products from forestry and agriculture as well as municipal and industrial waste streams. It thus includes trees, arable crops, algae and other plants, agricultural and forest residues, effluents, sewage sludge, manure, industrial by-products and the organic fraction of municipal solid waste. After a conversion process, biomass can be used as a fuel to provide heat, electricity or as transport fuel, depending on the conversion technology and the type of primary biomass.

In 2006, about 4% of the EU's total energy consumption was met from biomass [1]; nowadays about 1% of the world production of electricity is based on biomass fuels [2]. Environmental concerns are leading to more stringent regulations on energy production aiming at increasing the share of renewable sources of energy. Biomass is therefore increasingly being used as fuel for energy production.

A variety of wood species is burned in power plants nowadays, depending on the location of the plant, the wood-related activities in the area (pulp and paper industry, sawmills, etc.) and other economic reasons; wood from conventional forestry, residues from manufacturing of wood based products such as bark, sawdust and off-cuts from sawmills, demolition wood are some of the sources of wood fuel. In Denmark, the majority of the biomass used for power and heat production consists mainly of residues from forestry and agriculture (wood and straw) [3]. In the last decade, the consumption of wood for heat production has doubled in Denmark [2].

Worldwide, the utilisation of energy crops is also increasing; these are plants that are grown as a low cost and low maintenance harvest and that can either be used to make biofuels or directly exploited for energy production; willow and poplar are examples of fast growing trees that are used in short rotation forestry for wood fuel supply.

Apart from being a renewable source of energy, biomass contributes to the global reduction of CO_2 emissions. Combustion of wood or other plants is virtually a CO_2 neutral process, provided that the combustion is efficient and that land is replanted after harvesting. As the plants grow, they absorb

the same amount of CO_2 which is then released upon combustion. In fact, some CO_2 is produced due to transport and handling of the biomass fuels; yet, the overall CO_2 balance is much in favour of biomass fuels compared to fossil fuels. Moreover, usually the ash from the combustion of some types of biomass, like straw ash, can be used as a fertiliser, so that soil depletion is not an issue.

The most common ways of burning wood in power plants are grate firing and pulverised wood combustion. Compared with grate boilers, modern pulverised fired power plants do obtain a high electrical efficiency and have the capability to make fast changes in load and fuel type.

1.2 PULVERISED FUEL COMBUSTION

Suspension firing of pulverised fuel has been used to burn coal for decades; environmental concern and legislation have contributed to the conversion of some of those plants to wood combustion and to the building of new pulverised wood power plants.

Pulverised fuel firing is a combustion technique in which fuel is pulverised before being ignited. In practice, pulverised wood is transported to the power plant as wood pellets, which are then milled on site. This is an advantage compared with wood chip fired boilers: the common density of wood chips is about 250 kg/m^3, whereas the density of wood pellets is usually about 650 kg/m^3 and thereby the cost of transportation to the power plant is significantly reduced. On the other hand, the moisture content of wood chips can be as high as 45% [4], while the moisture content of pellets is usually about 6-10%; thus, higher efficiencies can be attained in pulverised fuel fired plants.

In suspension firing wood particles are heated up fast to high temperatures as they enter the furnace and thereby pyrolyse and leave a solid residue called char. The subsequent oxidation of char is the slowest step in the conversion of wood and influences the degree of conversion of the fuel as well as the heat release profile in the boiler, thus affecting the operation and efficiency of the plant. Nowadays, knowledge of wood char characteristics such as morphology and reactivity is still limited; among other reasons this is due to the wide range of wood fuels used and to the prevalence of char formation studies that are based on much milder conditions than the ones of a real pulverised wood furnace. Better knowledge of wood char reactivity would enable setting up better tools (models) to predict char conversion in this type of furnaces.

Biomass contains mineral matter which is converted to ash during combustion. The ash produced during straw combustion is often used as fertiliser to avoid soil depletion. As for plant operation, the mineral matter of the biomass can be an important issue. For example, straw gives rise to KCl containing deposits that hinder heat exchange and at times cause serious corrosion problems. Wood contains a much lower fraction of ash forming matter (<1%, as opposed to about 7-10% in straw) and a much lower amount of Cl; wood fired boilers experience fewer corrosion problems.

In the following section, a modern Danish power plant in which pulverised wood is used as fuel is described; full scale measurements at this plant were carried out as a part of this Ph.D. project.

1.2.1 PLANT DESCRIPTION

The Avedøre Unit 2 power plant is owned by Dong Energy A/S; initial proposals for the plant were made in 1994 and it was commissioned in 2001. It is a highly efficient multi-fuel power plant with advanced steam data (HP: 305 bar, 582 °C [4]), and can be operated in a pure condensing mode (to maximise power production), in pure back pressure mode (to maximise heat production) and in any combination in between. The full load capacity is 590 MWe for power (pure condensing mode) or 560 MJ/s and 510 MWe for heat and power operation (pure back pressure mode) [5]. The plant is connected to the Copenhagen area district heating system. Operating in pure condensing mode, a net electrical efficiency of 49% can be obtained; in pure back pressure mode using all the thermal energy in the condensed steam for district heating, the total efficiency is 94 % [5].

The unit consists of three types of combustors: a straw fired grate boiler (~100 MJ/s), the main multi-fuel boiler (~800 MJ/s) and two gas turbines (~2×50 MWe), as illustrated in Figure 1.1.

The main boiler is an ultra supercritical (USC), once through tower boiler of the Benson type; a sketch of this type of boiler is given in Figure 1.2.

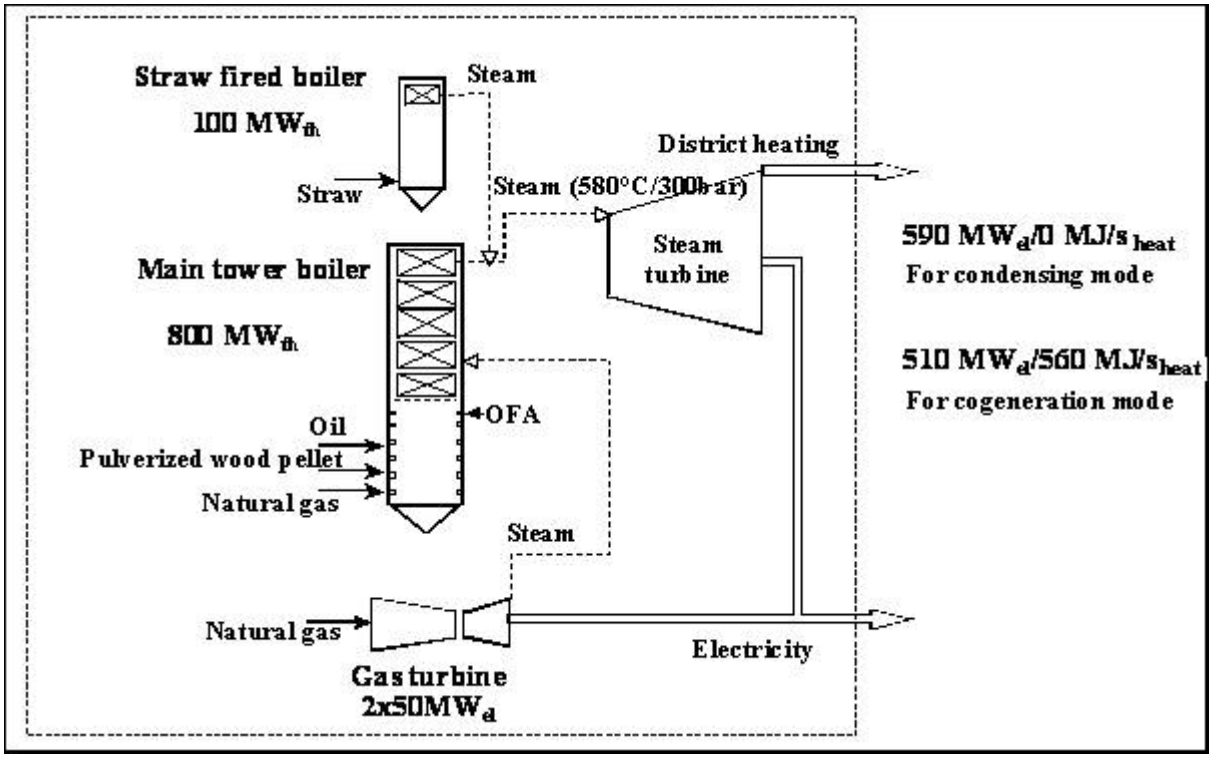

Figure 1.1 Schematic view of the Avedøre Unit 2 power plant. The high pressure steam from the main multi-fuel boiler and straw fired boiler are connected.

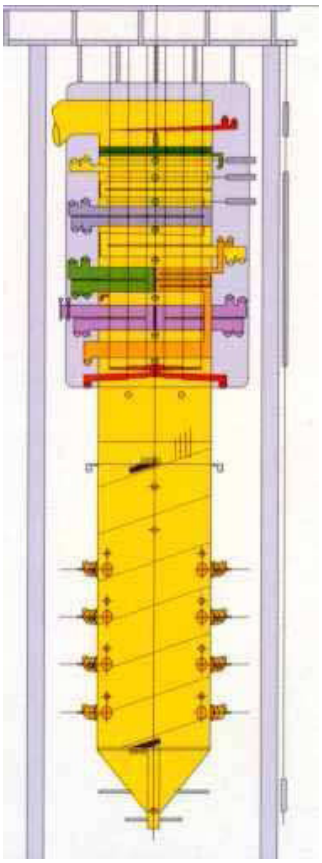

Figure 1.2 Sketch of a USC Benson type boiler, as the main multi-fuel boiler of Avedøre Unit 2 [4].

The full thermal capacity of the boiler is 800 MW. The boiler has a total height of 80 m. In the lower part is the combustion chamber with 16 burners on 4 levels, which are fired tangentially. Above the furnace chamber there is a screen evaporator that functions as a radiation shield. Superheaters and economisers are located above the screen. The USC boiler was commissioned in 2001 with oil and natural gas as fuels. In 2002 the combustion system was upgraded to allow firing of pulverised wood while keeping the gas and oil firing capacity unaltered. The maximum feed rate for the wood pellets is equivalent to the 70% of the full load of the boiler [6], i.e. 560 MJ/s or 120 tons of wood per hour. The yearly wood consumption is typically about 300,000 tons. Three out of the four burner levels, i.e. 12 out of 16 burners can be used for firing pulverised wood. Three roller mills are used to pulverise the wood pellets, each supplying wood to one burner level.

1.3 AIM OF THE PROJECT AND STRUCTURE OF THE THESIS

The work presented in this thesis is part of a larger project whose aim was to study co-firing of biomass and natural gas and NO_x emissions from pulverised biomass firing. Specific goals of this work were understanding and measuring wood char properties and reactivity in the conditions typical of a pulverised wood boiler. Furthermore, this work was intended to develop tools for the power industry to predict wood fuel burnout in pulverised wood boilers and optimise the operation of such power plants.

Chapter 2 is a brief literature review of different aspects relevant to wood combustion, including wood structure and composition, wood pyrolysis, wood char properties and wood char oxidation. Chapter 3 describes the full-scale campaign carried out at the Danish power plant Avedøreværket where the operation of the wood mills and the resulting wood particle size distribution as well as the CO concentration and char conversion after the combustion chamber were investigated. In Chapter 4 an experimental investigation into the relation between the pyrolysis of wood in boiler-like conditions and wood char properties is presented. This work has been published [7]. Chapter 5 includes an introduction to different approaches to single particle oxidation modelling, the description of the model used in this work and the results obtained. Wood char reactivity from pilot plant tests is used in combination with boiler conditions in the model and the predicted char burnout

is compared to the wood char burnout measured during the full-scale campaign. The general conclusions of the project are found in Chapter 6.

REFERENCES

1. How much bioenergy can Europe produce without harming the environment?, EEA Report No 7/2006
2. http://www.vattenfall.dk , Vattenfall A/S, 2010
3. Rising A., Vattenfall Opinion Paper on the Sustainability Aspects of Bioenergy, available at http://www.vattenfall.dk , 2010
4. Bendixen K., USC Technology in CCT Boilers Applying Biomass Cofiring, presented at Powergen Europe 2005
5. Ottosen P. and Gullev L., Avedøre Unit 2 – The World's Largest Biomass–Fuelled CHP Plant, News from Danish Board of District Heating, 2005
6. Gjernes E., Poulsen H.H., and Kristensen N., Large Scale Utilisation of Biomass in Fossil Fired Boilers, presented at Powergen Europe 2007
7. Dall'Ora M., Jensen P.A. and Jensen A.D., Suspension Combustion of Wood: Influence of Pyrolysis Conditions on Char Yield, Morphology, and Reactivity, Energy & Fuels, 2008, 22, 2955

CHAPTER 2

WOOD COMBUSTION REVIEW

2.1 INTRODUCTION

This Chapter is a brief literature review of different aspects relevant to wood combustion.

Section 2.2 gives an overview of wood structure and composition. In section 2.3 the first step in wood combustion is addressed, namely wood pyrolysis. The morphology and chemical composition of the solid residue of pyrolysis, char, is the subject of section 2.4; the dependence of these features on both original wood and pyrolysis conditions are outlined. The chapter ends with a section 2.5 dedicated to char oxidation.

2.2 WOOD STRUCTURE AND COMPOSITION

It is evident that the characterisation of the fuel is of major importance for the correct understanding and description of the combustion process. Utilisation of wood for the production of power is becoming more extensive, thus requiring an increasing amount of this fuel. A variety of wood species are burned nowadays in power plants, depending on the location of the plant, the wood-related activities in the area (pulp and paper industry, sawmills,…) and other economical reasons. In Denmark, local production of wood fuel mainly consists of pine and spruce, but wood fuel is also imported from other Countries. Wood from conventional forestry as well as residues from manufacturing of wood based products such as bark, sawdust, off-cuts from sawmills are some of the sources of the wood burned in power plants.

In this section a brief presentation of wood structure and chemical composition is carried out. Both structure and chemical composition vary slightly among the different species of wood, but the distinction between softwood and hardwood can be sufficient for the purposes of the present study.

2.2.1 WOOD STRUCTURE

Figure 2.1 shows the structure of a tree trunk with the major tissues including outer and inner bark, cambium, sapwood and heartwood.

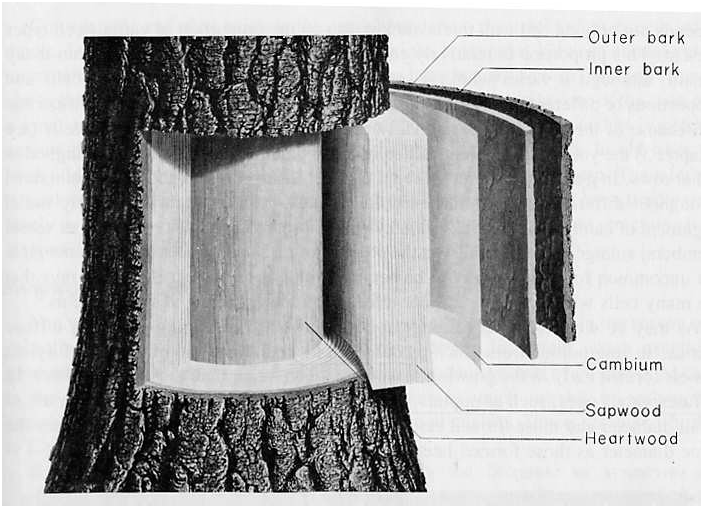

Figure 2.1 Generalised structure of a tree trunk showing orientation of major tissues including outer bark, inner bark, cambium, sapwood and heartwood [1].

The cambium consists of a thin layer of living cells between the sapwood (xylem) and the inner bark (phloem). The tree grows through the division of the cells that takes place at the cambial zone. More cells are produced towards the xylem on the inside than to the phloem on the outside; phloem cells divide less frequently than xylem cells. Phloem consists of vascular cells which carry sugar and nutrients throughout the plant. As much as about 90% of the cells forming the sapwood are dead cells [2]. The physiological function of the sapwood is to transport water and minerals from the roots to the growing part of the plant. Totally dead xylem tissue makes up the heartwood shown as the inner core in Figure 2.1.

Wood cells are elongated in shape and mostly oriented along the longitudinal direction of the stem. These cells not only provide for liquid transport and nutrients storage but also account for the mechanical strength of the tree. They mainly consist of cellulose, hemicellulose and lignin; cellulose makes up a skeleton surrounded by other substances functioning as matrix (hemicellulose) and encrusting (lignin) material. Wood cells are connected with each other through openings, referred to as pits [7].

There exist two sorts of wood, depending on the appearance of their seeds: if the seeds are covered with some kind of shell the wood is referred to as hardwood (*angiosperms*, e.g. birch, beech,

acacia), whereas in softwoods (*gymnosperms*, typical examples are spruce and pine) the seeds are uncovered. A general knowledge of the differences between softwoods and hardwoods might help interpret wood and wood char behaviour in the later stages of the study.

When describing wood structure it is common practice to refer to different cross sections of the tree trunk. The tangential, transverse and radial sections are shown in Figure 2.2, together with the surfaces and tissues described above in connection with Figure 2.1. In the transverse section wood rays, which radiate from the centre of the heartwood, are easily recognisable.

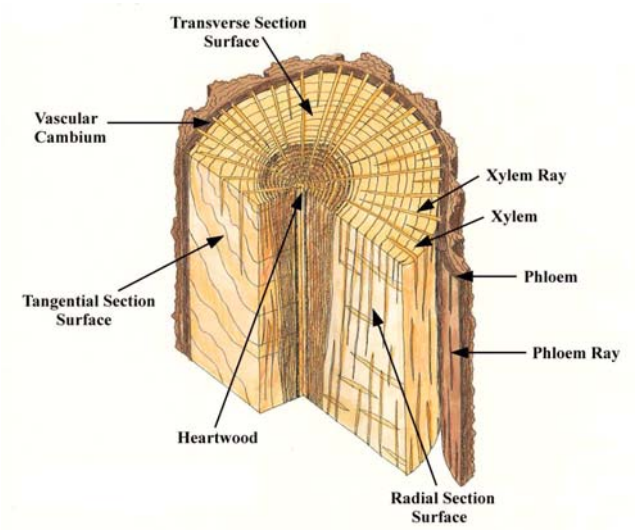

Figure 2.2 Methods of sectioning. Transverse cut, radial cut and tangential cut. Xylem and phloem rays can be recognised [3].

2.2.1.1 SOFTWOOD

Softwood is composed of two different cells: tracheas (90-95%) and ray cells (5-10%). Tracheas provide for both mechanical strength and water transport. The length and width of the tracheas ranges from 2.5 to 7 mm and 30 to 45 μm respectively [7]. Tracheas are normally referred to as fibres. The typical structure of softwood is shown in Figure 2.3 and Figure 2.4.

The liquid transport from one trachea to another takes place through the bordered pits; their amount in early wood tracheas is about 200 per trachea, most of them located in the radial walls. Latewood tracheas have only 10 to 50 rather small bordered pits. The bordered pits acts as a valve to keep the water flow under control and to prevent air and vapour bubbles to get into the liquid flow.

Another kind of cells in softwood is the parenchyma cell, accounting for storage of extraneous material such as starch, oils and fats. These cells are non-fibrous and much smaller than fibres; they

are arranged in radial strands called ray parenchyma. Some tracheas have the same direction of the parenchyma rays and are referred to as ray tracheas; they provide for transporting water horizontally and are connected to the tracheas by bordered pits. Both Figure 2.3 and Figure 2.4 show the presence in softwood of resin canals, which are intercellular spaces building up a uniform channel network in the tree. Average diameters of resin canals in pine are 80 µm for longitudinal canals and 30 µm for radial canals [7].

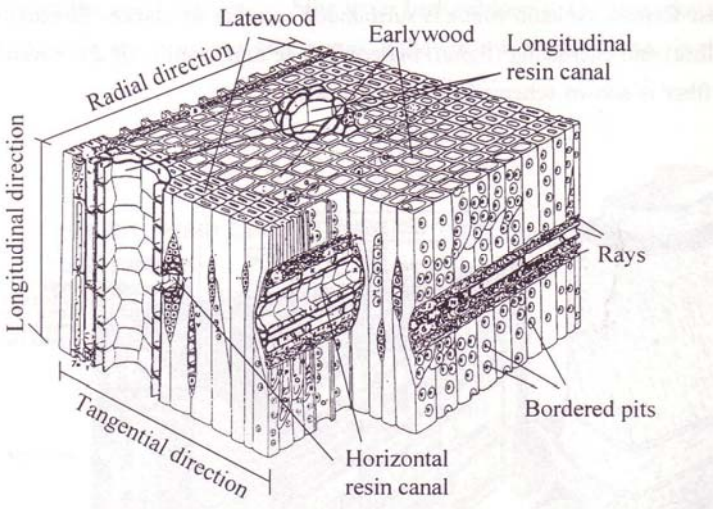

Figure 2.3 Gross structure of softwood [4].

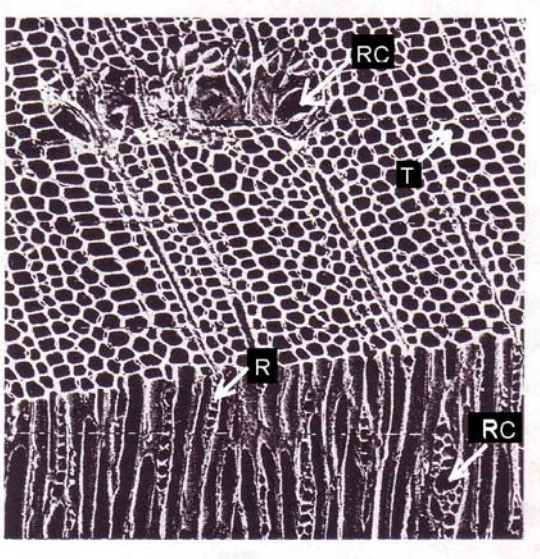

Figure 2.4 Transverse and longitudinal faces of softwood [5]. T: tracheas, R: Rays, RC: Resin canals.

Because of the large volume made up by tracheas (fibres) in softwoods, these woods tend to have a lower density than hardwoods. There are also seasonal changes in wood structure, since earlywood

produced early in the season is characterised by low density and fast growth, and latewood produced late in the season is characterised by slow growth and high density [2].

2.2.1.2 HARDWOOD

Hardwood structure is depicted in Figure 2.5 and Figure 2.6. The most apparent difference from softwood is the presence of large vessels along the longitudinal direction. Hardwood is a rapidly growing wood and vessels provide an effective conducting system for water. Vessels are non-fibrous tube-like elements with a large diameter compared to fibres and are joined together end-to-end; they appear as pores in the tangential view (see Figure 2.5). Vessel's length ranges commonly from 0.18 mm to 1.33 mm [7] while the thickness of their walls was found to range between 5 to 60 μm [6] .

In hardwoods, liquid transport in the radial direction is provided by tracheas while rays of parenchyma cells are present as in softwood. The fibre tracheas are thick walled with a small lumen, their length ranging approximately from 0.9 mm to 2.0 mm [7].

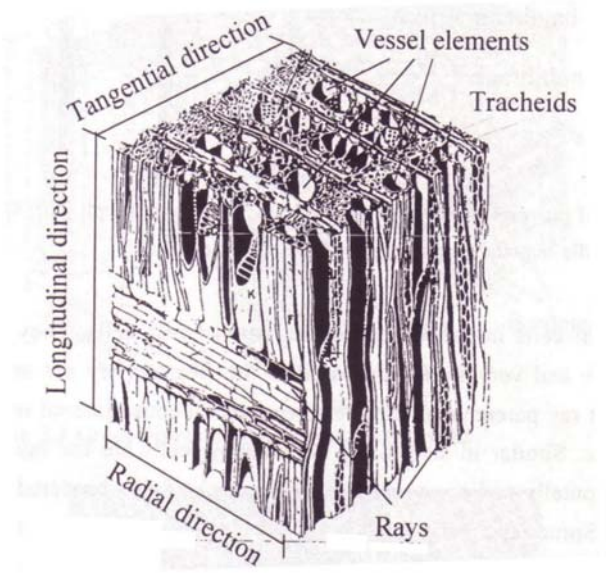

Figure 2.5 Gross structure of hardwood [4].

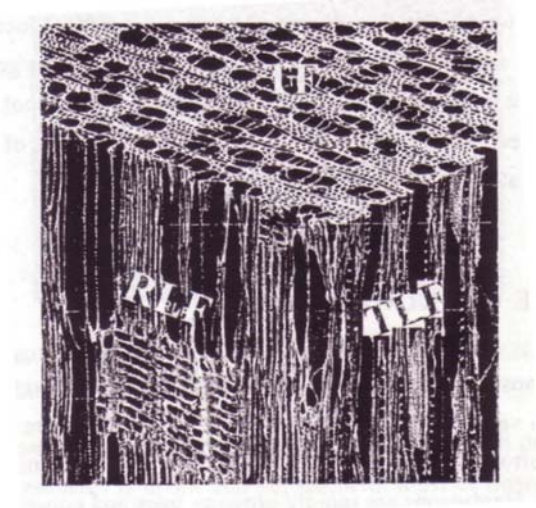

Figure 2.6 The three basic planes: transverse (TF), tangential longitudinal (TLF) and radial longitudinal (RLF) of a hardwood tree [5].

2.2.2 CHEMICAL COMPOSITION

The main components of wood are cellulose, hemicelluloses and lignin. These three substances account for 95% to 98% of the wood. Wood also contains other low molecular weight organic compounds that are referred to as extractives. Moreover wood contains a small amount of mineral matter, known as ash forming matter, which seldom exceeds 1% of the total mass [7]; in fact, the mineral matter is unevenly distributed among the different tissues, bark being the one with the highest ash fraction.

As a general rule, hardwoods contain a smaller fraction of lignin than softwoods. Some typical compositions of wood are presented in

Table 2.1.

Cellulose is the major constituent of the cell wall. It is a linear polysaccharide composed of ß-D glucopyranose units connected by (1→4) glucosidic bonds. The elementary formula of cellulose is $(C_6H_{10}O_5)_n$, where n is the degree of polymerisation, usually above 10000 in unaltered wood. Cellulose molecules are completely linear and have a strong tendency to form intra- and intermolecular hydrogen bonds. Aggregation of the linear chains of molecules within microfibriles provides a highly crystalline structure. As a consequence of its fibrous structure and strong hydrogen bonding, cellulose has a high tensile strength.

Hemicelluloses include all noncellulosic polysaccharides and related substances. Like cellulose most hemicelluloses function as supporting material in the cell walls. Hemicelluloses exhibit a

branched rather than a linear structure and the degree of polymerisation usually ranges from 50 to 200.

Lignin, the encrusting substance which binds the cell together and gives rigidity to the cell wall consists of complex three dimensional polymers of phenylpropane units.

Extractives include aliphatic, aromatic and alicyclic compounds, hydrocarbons, alcohols, ketones and various acids, esters, phenolic compounds, resins and other organic substances.

Table 2.1 Chemical composition of some wood species [8].

Species	*Cellulose*	*Hemicelluloses*	*Lignin*	*Extractives*
Softwoods				
Scandinavian Spruce	43	27	29	1.8
Scandinavian Pine	44	26	29	5.3
Douglas Fir	39	23	29	5.3
Scots Pine	40	25	28	3.5
Hardwoods				
Scandinavian Birch	40	39	21	3.1
Silver Birch	41	30	22	3.2
American Beech	48	28	22	2.0

Proximate and ultimate analyses of some wood fuels are reported in Table 2.2. The origin of the wood burned in power plant can be various. Usually bark is removed from stem wood (sapwood + heartwood), so in most cases when the fuel is referred to as wood it is to be considered stem wood; on the other hand, since the removal of the bark is not universally applied by all suppliers, it is necessary to take this part of the tree into account. Moreover, as has been said before, one of the attracting aspects of pulverised wood combustion is that waste wood from a wide spectrum of activities (sawmills, pulp and paper industry and others) can be utilised as fuel. A few examples of these “non conventional” wood fuels are included in Table 2.2.

Some important characteristics of wood as a fuel arise from Table 2.2. First of all, the volatile content of wood is much greater than that of coal, the most traditional solid fuel; the importance of

this characteristic will be outlined in section 2.3. A second, remarkable characteristic of wood is its high content of oxygen, which influences the evolution of the char morphology and possibly the fate of the ash forming minerals very much. As far as the ash content is concerned, a typical value for coal would be 10% on a dry basis [9], whereas for wood this value is much lower, as can be seen in Table 2.2. Obviously, it is not only the percentage of ash forming matter which determines how and how much the fuel can be troublesome (in relation to ash) when used in boilers; the specific fraction of each metal, its chemical form, distribution in the fuel and transformations and interactions during combustion are other determining aspects to be considered. Table 2.2 shows that the content of ash forming matter is higher in the bark than in other parts of the tree; on the other hand Müller-Hagedorn *et al.* [22] analysed separately sapwood and heartwood from pine and they found no significant differences in the amount and composition of metal salts. Thus when it comes to mineral content it seems appropriate to make a distinction between the metal-richer bark-derived fuel and the wood originating from any other part of the plant.

Typical ash compositions are shown in Table 2.3.

The inorganic, ash-forming elements absorbed from the pore water in the soil can be divided into macronutrients and micronutrients [2]. Essential nutrients, which are absorbed in larger amounts, are potassium, calcium, magnesium, phosphor and sulphur. Micronutrients are iron, manganese and chlorine, whereas silicon, aluminium and sodium are not considered to be essential for wood growth. Potassium, found as K^+, is highly coupled to the metabolic activity and is characterised by high mobility. Magnesium and calcium have a more structural function and their ions form stronger complexes than those formed by K^+; therefore their mobility is lower. Calcium is bound to cell walls, but can also be accumulated as oxalate [2].

The use of waste wood for heat and power production is certainly attractive, but some environmental aspects must be considered. In Table 2.3 only inorganic compounds are shown, but one must remember that waste wood has been, in most cases (for example when fibre board is considered), treated with organic additives which can result in the release of toxic compounds like furans and dioxins [10]. Moreover, waste wood may contain metals, some of which are listed in Table 2.3 (Zn, Cd, Ni,..), that can be released in the gas phase during combustion and thus possibly enhance the formation of dioxins and furans [10].

Table 2.2 Proximate and ultimate analysis of some wood fuels (wt % on dry basis).

	Birch [7]	*Spruce [7]*	*Pine [7]*	*Pine root [7]*	*Pine sawdust [37]*	*Softwood[a] sawdust [11]*	*Softwood[a] logging residue [11]*	*Softwood[a] bark[b,] [11]*	*Waste wood[c,] [2]*
Volatile matter	90.4	86.7	87.6	89.9	-	-	-	-	80.3
Fixed carbon	9.4	13.2	12.3	10.1	-	-	-	-	16.7
Ash	0.2	0.1	0.1	<0.1	0.3	0.5	2.7	3.6	3
LHV[d] (MJ/kg)	17.77	17.92	17.65	20.47		18.67	19.48	18.81	
C	47.1	47.4	46.9	53.6	47.0	51.9	51.6	52.5	48.5
H	6.2	6.3	6.3	6.5	6.3	6.0	6.0	5.7	6.1
N	0.11	0.07	0.07	0.10	0.0	0.12	0.48	0.40	1.4
S	-	-	-	-	-	0.0155	0.0525	0.0335	0.08
Cl	-	-	-	-	-	0.004	0.035	0.0265	0.07
O	46.6	46.2	46.7	38.5	46.4	41.8	39.0	39.3	40.91

[a] 60% Norway Spruce, 40% Scots Pine

[b] Bark contained about 20% stem wood

[c] includes painted wood, fibre board, untreated wood in unknown fractions

[d] Lower Heating Value

Table 2.3 Ash composition of wood fuels (wt% ash).

	Pine sawdust [37]	*Softwood*[a] *sawdust [11]*	*Softwood*[a] *logging residue [11]*	*Softwood*[a] *bark*[b] *(fresh)[11]*	*Waste wood*[c] *[2]*
CaO	72	31.55	32.39	40.00	29.79
K_2O	9	14.16	11.18	11.01	3.92
MgO	8	5.13	5.46	4.53	5.34
SO_3	5				
MnO_2	4[d]	4.87	5.50	3.30	-
SiO_2	2	27.20	29.90	27.75	20.61
Na_2O		1.70	2.18	1.58	2.78
Al_2O_3		4.85	3.05	4.39	3.89
P_2O_5		5.72	7.81	5.31	-
Fe_2O_3		4.81	1.52	2.12	6.17
TiO_2					-
ZnO					1.36
PbO_2					0.50
CdO					0.19
CuO					0.07

[a] 60% Norway Spruce, 40% Scots Pine

[b] Bark contained about 20% stem wood

[c] includes painted wood, fibre board, untreated wood in unknown fractions

[d] MnO

2.3 WOOD PYROLYSIS

Pyrolysis is the process of devolatilisation of a solid due to heating in an inert atmosphere. Wood releases volatile matter during this process. The amount of volatiles released varies with process conditions and can be much different from the volatile matter amount determined during proximate

analysis tests [15]; the volatiles consist of gases and tar. Tar is the fraction of hydrocarbons in the volatiles that appears as a liquid at 20ºC. Pyrolysis also yields a solid residue, char.

The yield of pyrolysis depends strongly on the conditions of the process; this stage significantly affects the overall process of wood combustion by determining yield and influencing morphology, composition and properties of the char.

2.3.1 TYPES OF PYROLYSIS

In full-scale plants different ranges of operation are encountered depending on the scope of pyrolysis. In the following pyrolysis will be referred to as slow/intermediate when the heating rate applied is up to 200-300 ºC/s and the final temperature is 700 ºC or lower; fast pyrolysis of wood, used particularly when a high tar yield is desired, applies heating rates of some hundreds to several thousands ºC/s. As it enters the furnace of a pulverised fuel fired boiler, the solid fuel is exposed to very high temperature which can be as high as 2000 K; the resulting heating rate of the particles is thus very high (10^4 - 10^5 ºCs^{-1}) [12]. Table 2.4 summarises the conditions and applications of different types of pyrolysis.

Table 2.4 Different conditions of pyrolysis for different applications.

Type of Pyrolysis	*Temperature range*	*Heating rate*	*Applications*
Conventional	400 – 700 ºC [15]	10^{-2} – 10^2 ºCs^{-1}	activated carbon, filter carbon
Fast	~500 ºC [13]	10^2 – 10^3 ºCs^{-1}	production of bio-oil
Pulverised Fuel Combustion	up to 1750 ºC [12]	10^4 – 10^5 ºCs^{-1}	combustion, gasification

As far as research on wood pyrolysis is concerned, many of the studies on this subject are based on thermogravimetry (TG) and differential scanning calorimetry (DSC). When investigating pyrolysis kinetics, one wants to work at kinetically controlled conditions; in a TG apparatus this requirement can be met by using samples of low mass at relatively low temperatures, in order to avoid mass and heat transfer limitations. Table 2.5 shows typical operating temperatures and heating rates for TG and DSC studies. Data and models of pyrolysis derived from experimental conditions reported in Table 2.5 apply primarily to slow/intermediate pyrolysis and their relevance to suspension combustion in full-scale plants is doubtful [14,15]. As a matter of fact, it has been pointed out

[15,40] that at the much severer conditions (temperature, heating rate) experienced by pulverised fuel the pyrolysis process presents major differences from the slow/intermediate type.

Table 2.5 Typical TGA and DSC conditions of studies found in literature (for wood and biomass).

Final temperature (ºC)	*Heating rate (ºC/min)*	*Reference*
1100	3 - 100	[12]
600 – 900	30 - 600	[15]
75 – 500	10	[16]
600	40	[17]
480	0.1 - 60	[18]

A paper by Grønli *et al.* [19] highlights that when operating a TGA an increase of the heating rate causes the scatter among different measurements to broaden, i.e. the uncertainty of the results increases; this result was based on very low values of heating rate (5ºC/min and 40ºC/min) and a relatively large amount of data (5 different types of TG apparatus were used to pyrolyze cellulose in 8 different laboratories) [19]. One should keep this observation in mind when considering TGA studies where the heating rate was increased in an attempt to operate in combustion relevant conditions ($10^2 – 10^3$ ºCs^{-1} in Svenson *et al.* [14]). Other authors have found evidence of significant influence of the experimental procedure used in TGA and DSC experiments on the resulting pyrolysis process [16,17,18]; in the work of Milosavljevic *et al.* [18] different results were obtained depending on whether the crucible with the sample (cellulose) had or did not have a lid (see also Rath *et al.*[16], who obtained similar results operating with beech and spruce wood; these papers are treated in greater detail in the following paragraph). Thus, it is not always straightforward to compare results from different researchers and, above all, it is clear that the extrapolation of data on pyrolysis to conditions (primarily temperature) other than those for which they were obtained has to be avoided.

Few authors investigated wood pyrolysis with reactors that could reproduce the conditions of a pulverised fuel furnace. The reactors used by these authors are wire mesh reactor [15,40], electrodynamic TG balance [15], screen heater reactor [20], drop tube [40], tubular reactor [40] and free-fall reactor [21]. Their findings will be presented in the following paragraphs and sections.

Changing the conditions of pyrolysis causes major morphological differences in the solid residue obtained; this issue is addressed in section 2.4. Another major difference among slow, fast and pulverised fuel pyrolysis is the yield of char. Table 2.6 shows the char yield obtained by several authors by pyrolyzing wood (pure cellulose in one instance) at different heating rates and temperatures. Data from each source should be compared independently.

Cellulose [18] and spruce [16] data in Table 2.6 show that an increase of the residence time of the released volatiles around the pyrolyzing wood (obtained by using a lid during TGA runs) determines a higher char yield. Results from Di Blasi and Branca [23] show the importance of the pyrolysis temperature on the char yield (decreases with increasing T), while data for birch and white quebracho [21] demonstrate that higher heating rates during pyrolysis lead to a lower char yield. Finally, minerals may also affect char yield, as illustrated by the results of Nik-Azar *et al.* [20]. These observations, relating char yield to pyrolysis conditions and wood characteristics, are treated in the following paragraphs.

Table 2.6 Char yields from pyrolysis of wood as reported in literature.

Reference	*Solid*	*Temperature (ºC)*	*Heating Rate (ºC/min)*	*Char yield (wt%)*
[18]	Cellulose (no lid)	NA	1.1	9
[18]	Cellulose (with lid)	NA	1.1	19
[16]	Spruce (no lid)	500	10	19.5
[16]	Spruce (with lid)	500	10	24.3
[23]	Beech	300	1000	37
[23]	Beech	435	1000	11
[21]	Birch	800	High	5.5
[21]	Birch	NA	Low	15
[21]	White quebracho	800	High	8.2
[21]	White quebracho	NA	Low	20
[20]	Beech	1000	6×10^4	10-15
[20]	Acid washed beech	1000	6×10^4	6

2.3.2 CHEMICAL REACTIONS AND PHYSICAL PHENOMENA DURING PYROLYSIS

The process of pyrolysis at the severe conditions of a pulverised fuel boiler is very complex. In order to understand and interpret the experimental data it may be useful to follow the development of the process as it occurs in a TGA with relatively low final temperatures and heating rates. Rath *et al.* [16] studied the pyrolysis of spruce and beech wood by means of DSC and TG in order to determine the heat of pyrolysis. The applied heating rate was 10ºC/min and the investigated temperature range was 75 to 500ºC. They observed, in accordance with the findings of many authors, the typical wood weight loss behaviour, i.e. two weight loss steps. Figure 2.7 shows a typical TG curve obtained by Rath *et al.* [16]. The main weight loss occurred between 200 and 390ºC, which is usually referred to as primary pyrolysis. At higher temperatures, 390 to 500ºC the weight loss shows a much lower rate; this "tail" is known as secondary pyrolysis. It has been suggested that this low-rate loss is due to reactions of aromatisation and dehydrogenation of the primary char [16].

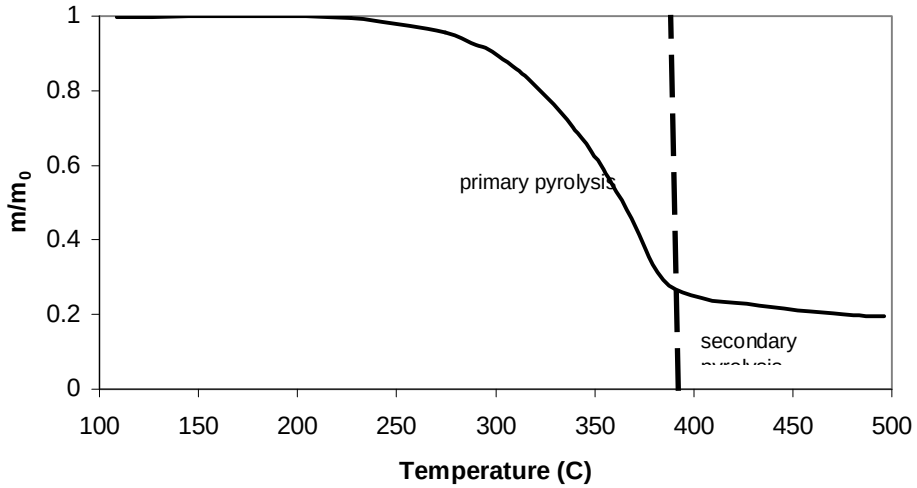

Figure 2.7 Results from TG pyrolysis experiments of spruce wood. Data from Rath *et al.*[16].

The DTG curve shown in Figure 2.8 reveals that the rapid mass loss (primary pyrolysis) consists of two peaks: Müller-Hagedorn *et al.* [22] associated the lower temperature (280 to 360ºC) and lower intensity peak (which appears as a "shoulder" in Figure 2.8) to the degradation of hemicellulose and the peak at higher temperatures (360-400ºC) to cellulose pyrolysis (lignin was believed to decompose throughout the whole range); this is in agreement with Milosavljevic *et al.*[18] who studied the pyrolysis of cellulose and found the weight loss to occur between 380 and 430ºC.

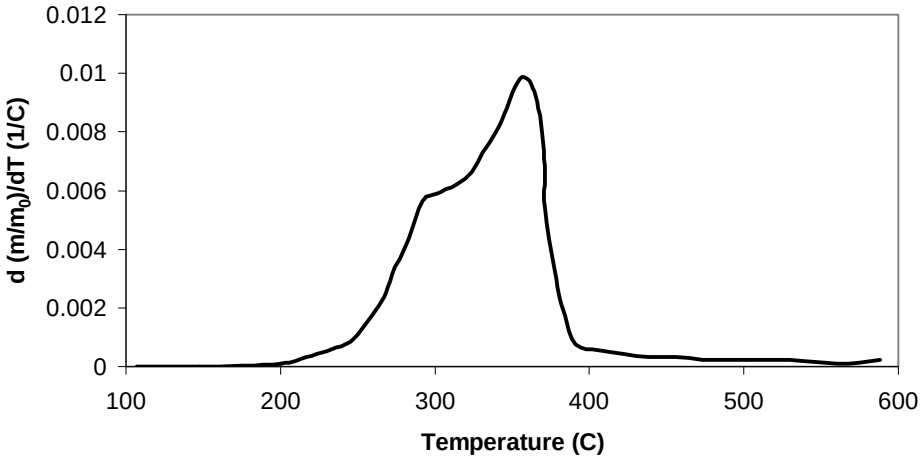

Figure 2.8 DTG curve of hornbeam wood, heating rate 10 ºC/min. Data from Müller-Hagedorn *et al.* [22].

At temperatures above 450ºC the tar produced can undergo secondary reactions as cracking [23]. These reactions lead to the formation of what is referred to as secondary char. In fact, several authors showed evidence that the volatiles released during pyrolysis further react with char to yield secondary char and gases; the extent of these secondary reactions varies significantly with the conditions of pyrolysis [16-18]. Figure 2.9 summarises the concept of secondary reactions, primary and secondary char.

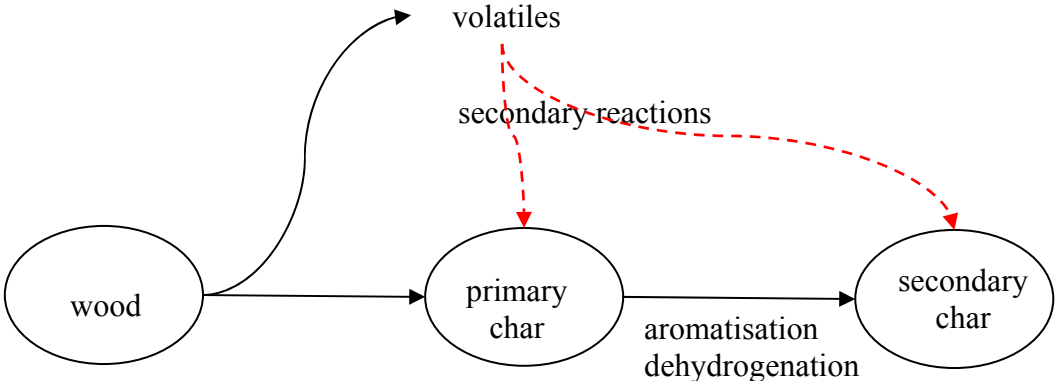

Figure 2.9 Secondary reactions during wood pyrolysis.

Rath *et al.*[16] obtained a higher yield of char when pyrolysing beech and spruce wood in a crucible with a lid than in a crucible without lid (24.3 and 19.5 wt% respectively, pyrolysis temperature was 500 ºC) [16]. Also, Rath *et al.* [16] found that a sample of higher mass yielded a higher fraction of char; similar results were obtained by Stenseng *et al.* who studied cellulose pyrolysis [17]. Both the effects of the presence of a lid in TG (see also Milosavljevic *et al.* [18]) and the influence of the sample mass on the yield of char are interpreted as a result of the above mentioned secondary reactions [16]; in fact, it appears that an increase of the residence time of the volatiles within (sample mass) or in the proximity (lid) of the sample leads to higher char yields, i.e. secondary reactions are enhanced. Thermodynamic investigation of the pyrolysis process by DSC confirms this consideration. As a matter of fact, both Rath *et al.* [16] and Milosavljevic *et al.* [18] found that heat of pyrolysis (of cellulose for Milosavljevic *et al.* and wood for Rath *et al.*) linearly decreased with increasing char yield; Figure 2.10 shows some of their results.

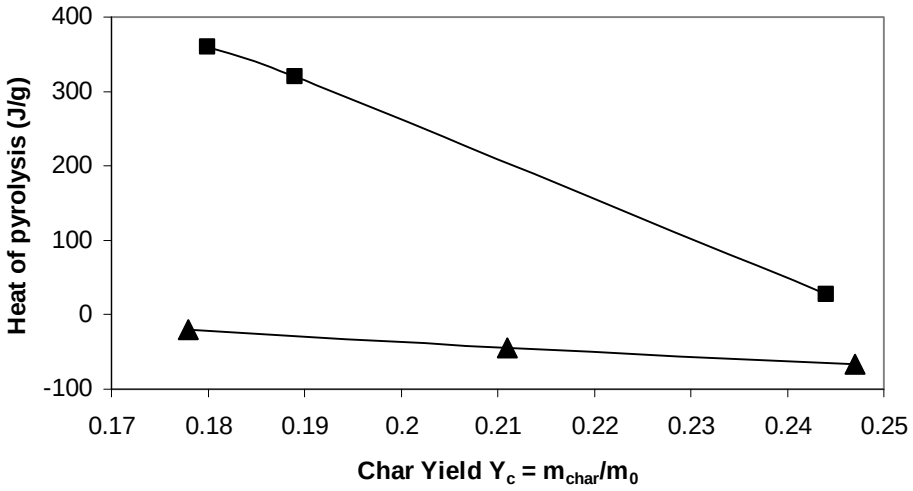

Figure 2.10 Dependence of the heat of pyrolysis of spruce wood on the yield of char. ■, primary pyrolysis; ▲, secondary pyrolysis. Data From Rath *et al.*[16]

The curves in Figure 2.10 can explain the observed linear dependence of heat of pyrolysis on char yield: the primary devolatilisation process is endothermic, while the secondary char-forming processes are exothermic [16,18] (with reference to Figure 2.10 note that during primary pyrolysis both devolatilisation and secondary reactions occur, while during secondary pyrolysis mainly secondary reactions occur). A higher yield of char would thus correspond to a higher exothermicity (or lower endothermicity) of the global process. In the study of Rath *et al.* [16] during the runs with

a lid the char yield was higher and the primary pyrolysis was almost exothermic (primary volatiles are retained near the solid so that secondary reactions can start at lower temperatures); this confirms that the resistances to the flow of the volatiles from the particle influence the extent of the secondary reactions occurring and thus play a role in determining the final yield of char.

Nevertheless, one should also observe that given the turbulent conditions characterizing suspension firing, the existence of a "lid-like" resistance to the flow of volatiles would be unexpected in these boilers; on the other hand, the size of the wood particles may still have a significant influence on the char yield.

2.3.2.1 *INFLUENCE OF TEMPERATURE ON CHAR YIELD*

Figure 2.11 shows the influence of pyrolysis temperature on the final yield of char. Pyrolysis was carried out in a screen heater reactor; samples of beech wood were heated at a rate of approximately 1000 ºCs^{-1} to the final temperature and subsequently cooled by air convection (≈200 ºCs^{-1}); holding time at the final temperature is zero [20].

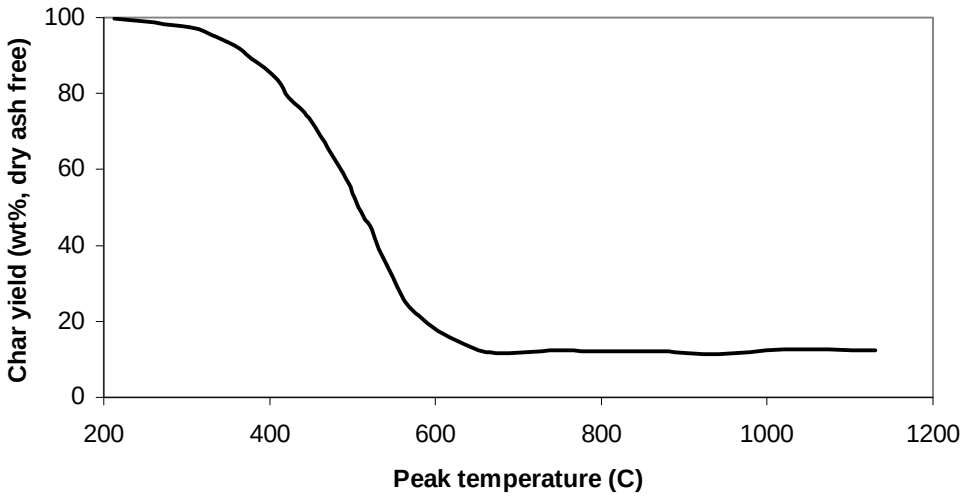

Figure 2.11 Influence of final pyrolysis temperature on char yield. Beech wood, heating rate ≈1000 ºCs^{-1}. After Nik-Azar [20].

It clearly appears from Figure 2.11 that the temperature at which pyrolysis is carried out has a strong influence on the final yield of char. The peak temperature and the holding time are known to determine to a large extent the yield of char in pyrolysis processes. The final value of about 10%

yield (on a dry ash free basis) for temperatures above 700 ºC (from Figure 2.11) seems to agree well with other literature data on rapid wood pyrolysis (see Table 2.6).

2.3.2.2 *INFLUENCE OF HEATING RATE*

Biagini *et al.* [15], Cetin *et al.* [40] and Di Blasi and Branca [23] pointed out that at higher temperatures and heating rates the above described stages in wood pyrolysis occur simultaneously and their interactions bring about substantial changes to the process. This has major effects on pyrolysis yield, as it appears from Table 2.6, as well as on char particle morphology and composition. At high heating rates (up to 10^5 ºCs^{-1}) Biagini *et al.* [15] observed swelling of the particle (they used various kinds of biomass, including hazelnut shells and pine sawdust). They explain this by arguing that the simultaneous release of volatiles and the melting of solid (which was also observed during their work [15]) can make the particle swell, generating large internal cavities. Similar results were obtained by Cetin *et al.* [40] (see Figure 2.16 and Figure 2.18 for a description of the morphological changes observed). Nevertheless Biagini *et al.* [15] suggested that more knowledge of the process is needed to enable prediction of the extent of the volatiles release and of the swelling on the basis of proximate analysis or wood species. When it comes to the influence of the process conditions on these phenomena they observed, as a general rule, that the amount of volatiles released increased with the applied heating rate, which is in agreement with the above mentioned inverse relation between heating rate and char yield.

2.3.2.3 *THE ROLE OF MINERAL MATTER IN THE PYROLYSIS OF WOOD*

Inorganic salts have a well known major influence on the pyrolysis of wood, especially with respect to the composition of the products (char, tar, gases) [22]. Müller-Hagedorn *et al.* [22] suggest that only water–washed wood TG analysis should be compared and investigated when the kinetics of pyrolysis is addressed: the question would then have to be answered whether the risk of depicting a quite unrealistic scenario of mineral-free wood is to be preferred to comparing and reviewing data from different woods keeping in mind the role of their mineral content.

A paper by Nik-Azar *et al.* [20] highlights the effects of mineral matter in wood (beech) during rapid pyrolysis. Beech wood was pyrolised with a heating rate of 1000 ºCs^{-1} to a final temperature of 1000 ºC [20]. Prior to pyrolysis the wood was washed with acids in order to remove the cations (K^+, Na^+, Ca^{2+}); in these runs the char yield was lower (6 wt%) than in those where untreated wood

was pyrolised (10-15 wt%). Also, the yield of gases from the pyrolysis of cation-impregnated wood (58 wt%) was higher compared to the gas yield of acid-washed wood (34wt%). These two observations were ascribed to the catalytic effect of the above mentioned cations [20]. In fact potassium, sodium and, to a lower extent, calcium cations are believed to catalyze the cracking of tar and repolymerisation, thus enhancing the extent of secondary pyrolysis [20]. As a confirmation, Nik-Azar *et al.* noticed that the molecular weight of tar (i.e. the degree of polymerisation) decreased in their experiments as the concentration of the cations in the wood increased. It appears evident that the mineral matter content in wood is a major factor to be considered when investigating wood pyrolysis.

2.3.3 MODELLING WOOD PYROLYSIS

All of the available models of wood pyrolysis make necessary simplifications; the complexity of the process has prevented an exact model to be attained. The number of reactions involved in wood degradation and devolatilisation both in the solid and gas phase is very large, so that detailed kinetics is not available. Besides, heat and mass transport in and around the porous wood particles are complex and strongly influenced by the operating conditions.

The rate of devolatilisation can be controlled by decomposition kinetics, heat transfer (internal and external) or mass transfer (internal and external). When considering pulverised fuel boilers, the dimensions of the wood particles are (probably) small enough to allow the assumption of uniform temperature in the particle; account is thus not made for intra particle heat transfer.

2.3.3.1 SINGLE FIRST ORDER REACTION

One simple way of modelling wood pyrolysis is by means of a single first order reaction of the remaining volatile. If intra particle mass transfer is neglected along with internal heat transfer then the devolatilisation rate is uniform throughout the particle and can be expressed as follows:

$$\frac{dV}{dt} = k \cdot \left(V^* - V \right) \qquad (2.1)$$

where V^* is the initial volatile content of the particle (total amount of volatiles released when devolatilisation is complete), V is the cumulative amount of volatiles released up to time t and k is the rate constant of the Arrhenius type:

$$k = k_0 \cdot e^{-\frac{E}{RT}} \qquad (2.2)$$

where k_0 is the pre exponential factor, E is the activation energy, R is the gas constant and T is the absolute temperature.

Assuming that the pyrolysis occurs at a constant temperature T, *k* in equation (2.1) would be a constant and thus integration of (2.1) would yield:

$$V = V^* \cdot \left(1 - e^{-kt}\right) \qquad (2.3)$$

Since in practical applications and in common laboratory experiences pyrolysis does not occur at a constant temperature, a correction must be made to account for the time-temperature profile of the particle. Still, the single first order reaction model has major limitations. Since the pre-exponential factor k_0 and the activation energy E depend on the heating rate of the particle, the single first order kinetics is strongly dependent on the conditions for which it has been derived, i.e. it can not be successfully applied to pyrolysis processes at conditions other than those for which the parameters were determined. Stenseng [29] compared diverse single-first-order-reaction kinetics for the pyrolysis of wood from literature. The data in Figure 2.12 are taken from Appendix A in Stenseng [29] and the original references are reported in the legend [24,25,26,27,28].

Figure 2.12 shows that the range of pyrolysis reactivity for wood is very wide in the available literature. For the data shown in Figure 2.12 the activation energy E of the first order reaction varies between 68 kJ/mol and 140 kJ/mol, while the pre exponential factor k_0 ranges from $8.5 \cdot 10^2$ s^{-1} to $1.0 \cdot 10^8$ s^{-1}. The wide range of values for k_0 and E may be due not only to the differences between various species of wood, but also (and possibly to a larger extent) to the different conditions at which these parameters were determined. When working at high heating rates (for example those applied by Nik-Azar *et al.* [26]) accurate temperature measurements can be quite difficult and thus uncertain; this may result in large uncertainties of the kinetics. Moreover, different kinetics were obtained for samples of different mass; this warns us that when deriving kinetics data a careful account for possible heat and mass transport limitations must be made.

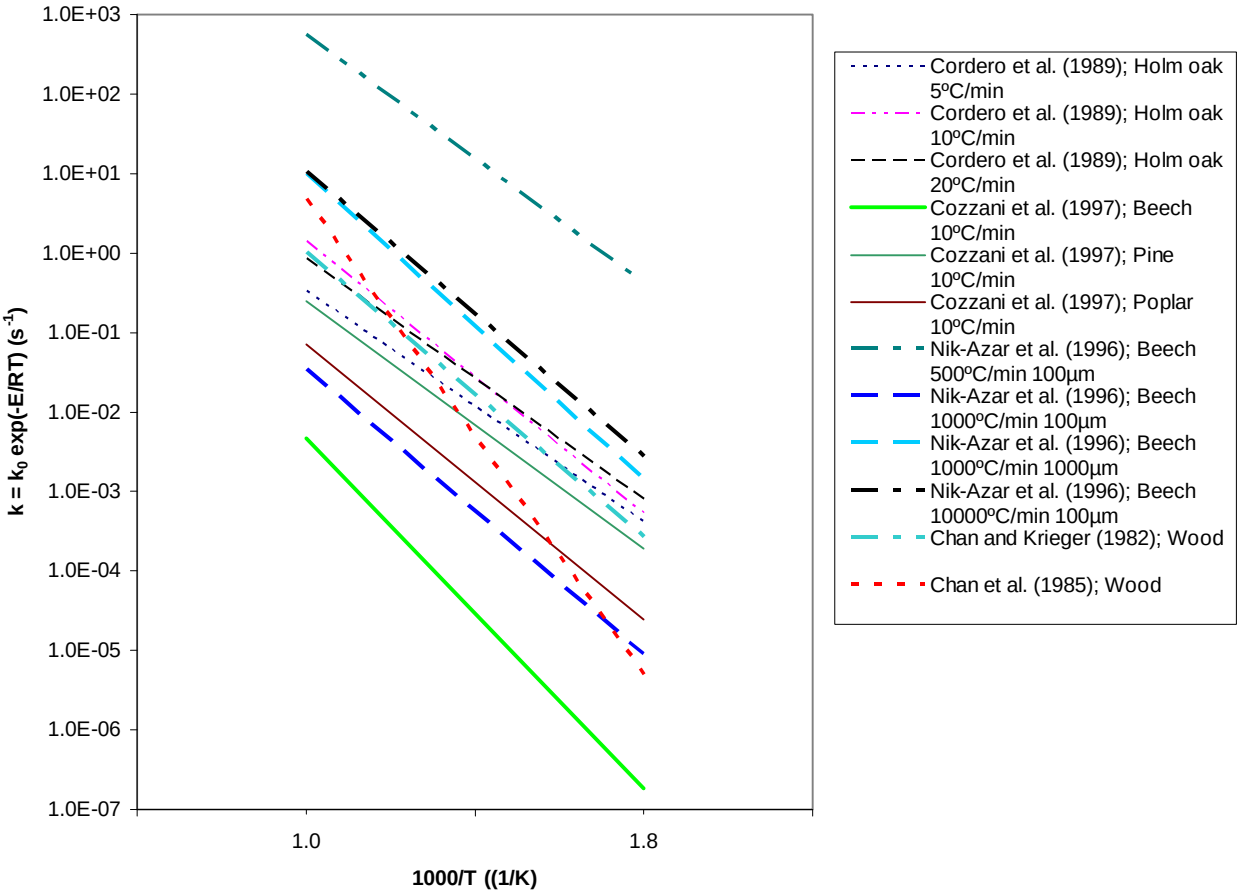

Figure 2.12 Single-first-order-reaction kinetics for pyrolysis of different sorts of wood at different conditions. After Stenseng [29].

2.3.3.2 DISTRIBUTED ACTIVATION ENERGY

One way to overcome the dependence of the kinetic parameters on the heating rate is the utilisation of a distributed activation energy model. This model ideally account for the variety of reactions occurring during wood degradation (all these models were developed for coal pyrolysis, but they can be adapted to wood pyrolysis). The reactions are all given the same pre-exponential factor, while the activation energy changes as a continuous distribution (e.g. Gaussian distribution). The activation energy distribution function f(E) will satisfy the following expression:

$$\int_0^\infty f(E)dE = 1 \qquad (2.4)$$

The expression for the amount of volatiles released up to time t will then become:

$$V = V^* \cdot \left[1 - \int_0^{\infty} \exp\left(\int_0^t k_0 e^{-\frac{E}{RT}} \right) \right] \cdot f(E) dE \qquad (2.5)$$

The distributed activation energy model was found by Stenseng [29] to be the most suitable to describe wheat straw pyrolysis; in this case the distribution function f(E) was logarithmic normal distribution.

2.3.3.3 COMPETING PARALLEL REACTIONS

Another common way to model wood pyrolysis is by means of a set of competing parallel reactions. Grønli and Melaanden [30] developed a model with three parallel competitive reactions to account for primary production of gas, tar and char, and a consecutive reaction for the secondary cracking of tar; the predictions of the model agreed well with experimental data from the pyrolysis of a cylinder of Norwegian spruce (diameter 20mm,length 30mm). Hastaoglu and Al-Khalid [31] used in their model two parallel reactions, one for the production of tar and one for the production of gas and char; further cracking of the primary tar is also considered, as well as drying of the wood.

2.3.3.4 SUPERPOSITION

Some models consider wood as consisting of several macro components that act independently during pyrolysis. Each component follows its own kinetic path and the global rate of devolatilisation is the sum of the individual rates. The pyrolysis of each component can thus be modelled by a first order reaction or a set of reactions in series. These models often associate each of the reactions to one of the wood macro components [22,32,33] (cellulose, hemicellulose, lignin), but the use of pseudo components is not rare either. These models can be referred to as superposition models.

It is worth mentioning that no model accounts for the presence of the mineral matter. Better, it is evident that the parameters determined for each of the models (if derived from e.g. TG analysis of an unaltered wood particle) implicitly account for the mineral content and its effect; this may cause the risk that a model derived for a certain wood does not prove satisfactory for a wood (or part of the same plant) with a significant difference in amount and/or distribution and/or chemical appearance of metals. Some researchers, as Müller-Hagedorn *et al.* [22], used washed

(demineralised) wood when running the experiments for the determination of the kinetic constants of their models. Thus, the model obtained is not dependent on the minerals; in this case though, it seems that the model should include a sort of species/mineral matter- dependent correction factor, if it is to describe pyrolysis realistically. Since the effect of the mineral matter is very complicated and not fully understood yet, it appears that the extrapolation of model parameters from unaltered wood would be preferable, although the above mentioned limitations to the range of application of the model apply.

2.4 WOOD CHAR: STRUCTURE, PROPERTIES AND THEIR CHANGES DURING COMBUSTION

Char conversion is the slowest step in pulverised fuel combustion [34] and the reactivity of the char is influenced by its structure as well as its chemical composition. An understanding of the char structure and properties is thus a basic step for modelling the combustion process and predict the burnout.

Wood char is a highly heterogeneous material, its structure, chemical composition and properties depending on the original wood material and the conditions of pyrolysis. As an example of the heterogeneity of char, Table 2.7 presents some wood char ultimate analyses found in published literature.

Table 2.7 shows that chars from one wood species can exhibit large variations in composition. The chemical composition of pine char, for example, is substantially different for the three studies [35 - 37] considered in Table 2.7: this strong variability is caused by differences in pyrolysis conditions and, probably to a higher extent, differences in virgin wood composition which in turn depends on the region where the tree grew, part of the tree and type of wood (roots, stem, sapwood, heartwood, bark), possible impurities and contamination (for example, wind can carry soil that can get stuck on the tree). Both pyrolysis and chemical composition of parent fuel have been investigated by several researchers with respect to char yield (see previous section), physical structure and reactivity; the following paragraphs will present some of the results obtained.

Table 2.7 Ultimate analysis (on a dry basis) of some wood char found in literature.

	Pyrolysis conditions	*C(%)*	*H(%)*	*N(%)*	*S(%)*	*O(%)*	*Ash(%)*
Pine [35]	873 K, >300 K/s	69.7	3.13	0.52	0.05	19.1	9.2
Beech [36]	800 K, fast pyrolysis	78.0	3.2	0.25	-	15.9	2.8
Douglas fir [36]	800 K, slow pyrolysis	76.8	3.5	0.10	-	18.6	1.0
Pine [36]	800 K, slow pyrolysis	75.3	3.8	0.10	-	19.7	1.2
Redwood [36]	800 K, slow pyrolysis	78.3	3.4	0.09	-	17.5	0.66
Chestnut [36]	800 K, slow pyrolysis	76.8	3.1	0.11	-	16.7	3.4
Pinewood sawdust [37]	900 K, vortex reactor	76	2.4	1.1	-	13.5	7

2.4.1 CHAR MORPHOLOGY

There is wide agreement in the literature on the conclusion that the conventional type (see Table 2.4) of pyrolysis does not alter the morphological structure of wood [7,39,46]. Even when the pyrolysis temperature reaches values as high as 1000ºC the structure of the char may appear very similar to that of the original wood, provided the heating rate is sufficiently low (and, most likely, the soaking time sufficiently short). Figure 2.13 shows scanning electron microscopy (SEM) images of wood char obtained by Kumar and Gupta [46] after pyrolysis of a 15 mm^3 acacia wood particle at 600ºC. In Figure 2.13a some constitutive elements of wood structure, namely vessels, fibres and pits are seen to retain their original morphology upon pyrolysis and are recognised by Kumar and Gupta as the origin of the discontinuous pore size distribution of the acacia char (in fact, they don't provide a quantitative description of the pore size distribution). The cell cross-sectional structure of the wood is easily recognisable in Figure 2.13b. Eucalyptus chars produced at similar conditions retained the wood structure to the same extent as acacia chars [46]. When observing Figure 2.13 note that Kumar and Gupta classify pores according to the following: micropores (width less than 2μm), mesopores (2-50μm), macropores (width exceeding 50μm). This classification differs from the commonly used IUPAC classification: micropore (<2 nm), mesopore (2-50 nm), macropore (>50 nm) [38]. According to the IUPAC classification, all of the pores considered in Kumar and

Gupta [46] are macropores. This is in agreement with the pore size distribution of a Moraballi wood char obtained by Wildman and Derbyshire [39] (see Figure 2.20 and related comment).

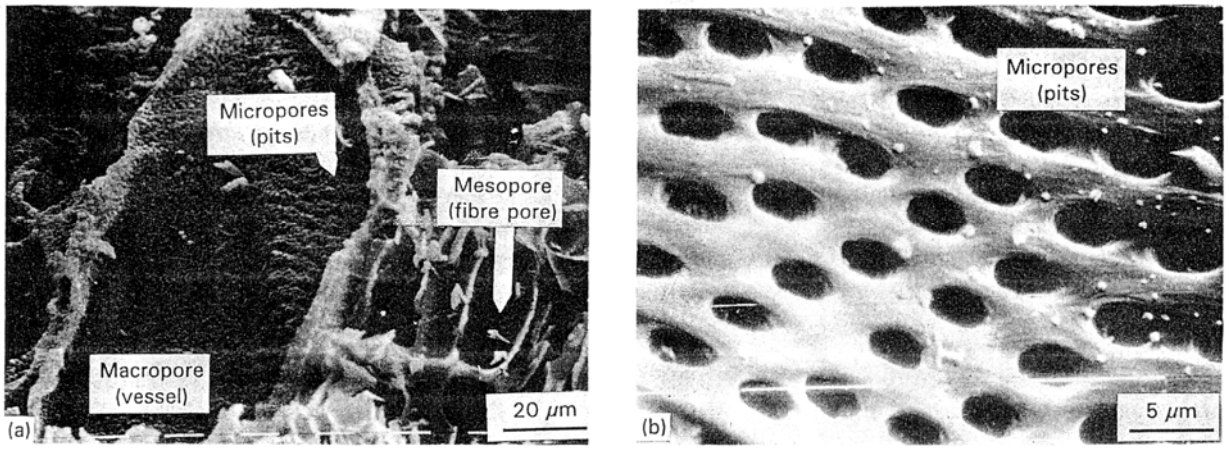

Figure 2.13 SEM images of acacia wood char prepared at 600ºC. Conventional pyrolysis. [46]

Typical techniques used to investigate and characterise the structure of a char are mercury porosimetry, optical microscopy and SEM. By means of these techniques Wildman and Derbyshire [39] studied the macroporosity of coal and hardwood (Moraballi) derived chars and activated carbons. The precursor (coal or wood) was pyrolised at 600 ºC and some of the produced chars were activated by reaction with steam. Chars retained the typical wood structure after pyrolysis, although severe shrinkage had occurred during the thermal treatment; in Figure 2.14 (after Wildman and Derbyshire [39]) the cellular fibrous structure is easily recognised.

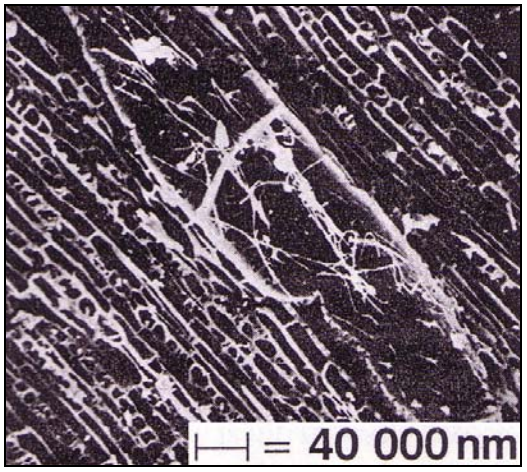

Figure 2.14 SEM image of a Moraballi wood char prepared at 600ºC. Conventional pyrolysis. [39]

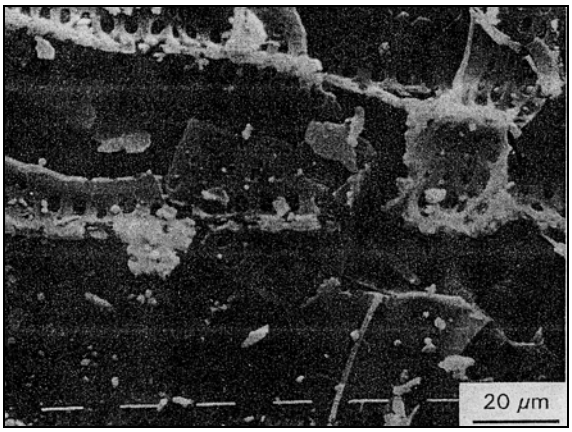

Figure 2.15 SEM images of acacia wood char prepared at 1050ºC [46].

Figure 2.15 reports an image of an acacia char produced at 1050ºC [46]; the heating rate of the pyrolysis is not clearly specified by Kumar and Gupta, but is believed to be of the order of some hundreds to several thousands ºC/min, which may be considered as moderate heating rate. The presence of some cracks and voids in the char, visible in Figure 2.15, reveals that pyrolysis at moderate heating rates did bring about some changes in the structure [46]. Nevertheless, in Figure 2.15 it is still possible to recognise the cross sectional cell structure, even though in fragments.

Recently, in an attempt to relate the pyrolysis conditions to char reactivity Cetin *et al.* [40] investigated the structural evolution and morphological changes of biomass (pine, eucalyptus, bagasse) char during pyrolysis. The chars were generated in different reactors including a wire mesh reactor, a tubular reactor and a drop tube reactor. In the drop tube reactor the wood particle could be heated to 1000ºC with a heating rate of 1×10^5 ºCs^{-1} [40]. The high heating rate and short residence times obtained with this reactor resemble the conditions in a pulverised fuel boiler. Cetin et al. [40] came to the conclusion that under high heating rates wood particles do not preserve the wood cell structure; they show evidence (see Figure 2.16) that the particle underwent plastic deformation as a result of melting [40].

Figure 2.16 reports SEM images after Cetin *et al.* [40] of pine sawdust chars produced under different conditions. It is evident that high heating rates produced severe changes in the morphology of the char (Figure 2.16d) whereas the char generated at lower heating rate preserved the typical structure of wood cells (Figure 2.16b). The char produced at 500 ºCs^{-1} shows an intermediate behaviour (Figure 2.16c): the surface of the char appears smooth, thus indicating the occurrence of some melting. Similar results were obtained using eucalyptus wood, although it should be noticed

that eucalyptus char (hardwood) showed somewhat less tendency to melt than pine char (softwood) [40].

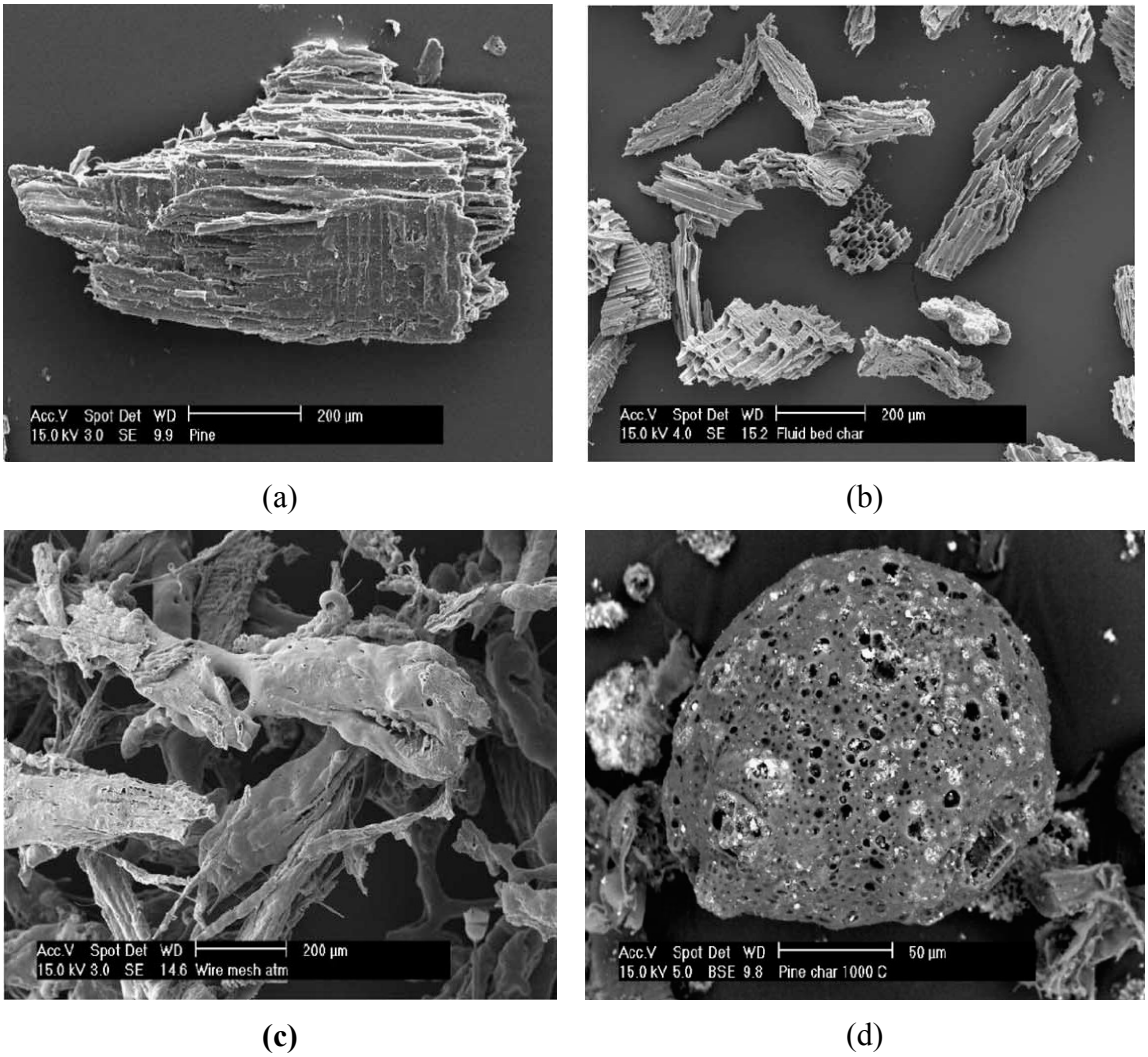

Figure 2.16 SEM images of pine sawdust: (a) parent material, (b) char generated at 950ºC by low heating rate (20ºCs^{-1}), (c) 950ºC with moderate heating rate (500ºCs^{-1}), (d) 1000ºC at very high heating rate (1×10^5 ºCs^{-1}) [40].

This divergence of the behavior of the eucalyptus from the pine particles may be a result of the higher lignin content of softwoods compared to hardwoods (usually 28-30 % in softwoods and 20-23% in hardwoods). In fact, when pyrolyzed alone lignin has a great tendency to become liquid during pyrolysis and swells leaving a macroporous crust [41]: the higher lignin content of the pine wood could thus contribute to the observed higher tendency to melt of this wood compared to eucalyptus wood.

Smoother char particle surfaces in conjunction with higher pyrolysis temperature were also observed by Zolin, who studied the pyrolysis of wheat straw [51]. SEM images of the char particles

obtained by Zolin are shown in Figure 2.17. These chars were produced in an entrained flow reactor at 1200 and 1340 ºC. Cast and loose samples pictures are shown. The similarity of the morphology of the char particles in Figure 2.17 with those of Figure 2.16 c) and d) is evident. Moreover, the char produced at 1200 ºC appears to preserve to a little extent the original morphology of the biomass, whereas the char produced at 1340 ºC is very similar to the one in Figure 2.16 d). The cast samples in Figure 2.17 reveal that the straw char particles are hollow, with a wall that becomes thinner as pyrolysis temperature increases; this confirms that melting and subsequent reorganisation of the structure (including pore structure) has occurred during pyrolysis.

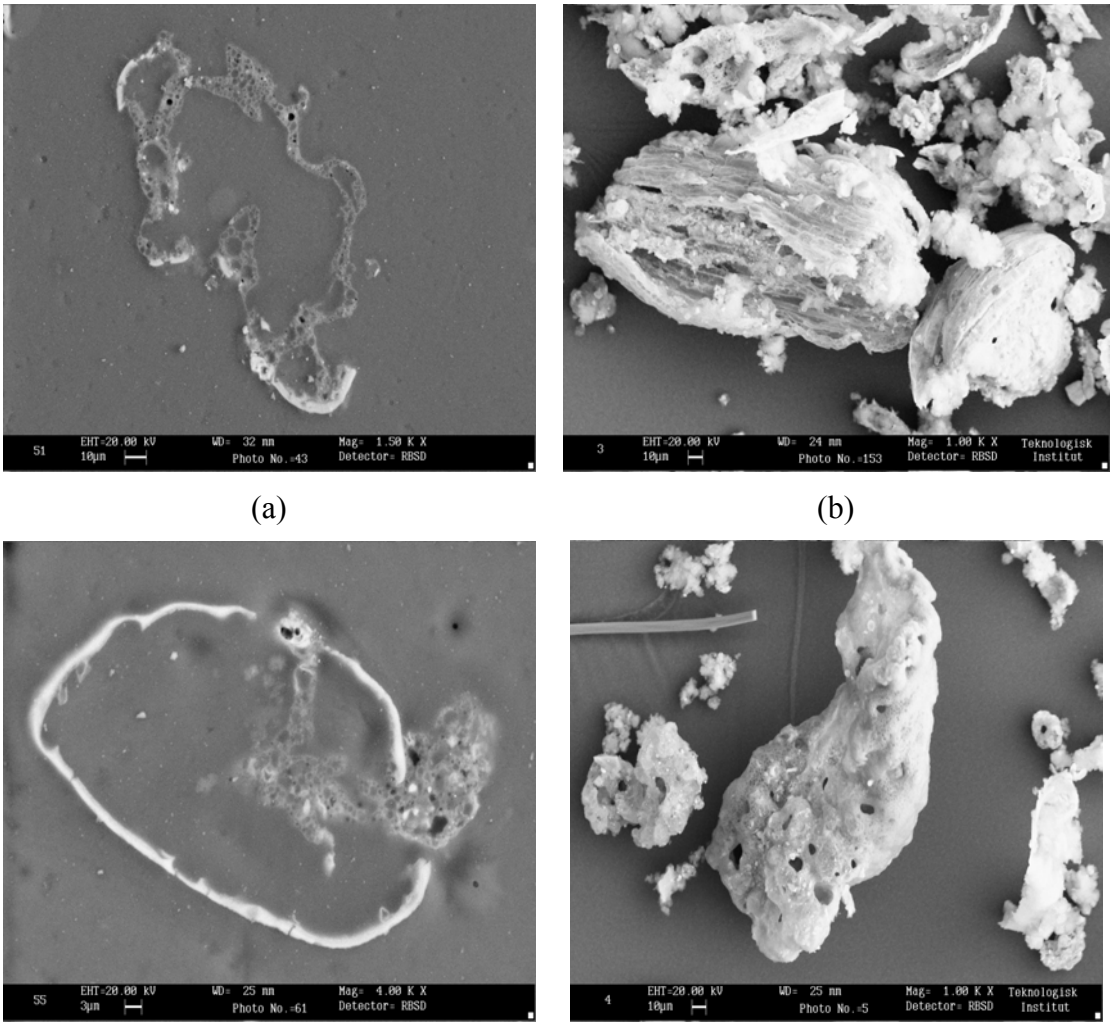

Figure 2.17 Scanning electron microscopy (SEM) pictures of wheat straw chars produced in an entrained flow reactor at two different temperatures. (a) 1200ºC, cast sample; (b) 1200ºC, loose sample; (c) 1340ºC, cast sample and (d) 1340ºC, loose sample. After Zolin [51].

Figure 2.18 shows a pyrolysis sequence for a pine particle of the same type as those of Figure 2.16. It can be seen that the particle first swells then completely melts and evolves into a droplet before rupturing and loosing its volatile matter [40]. Cetin *et al.* [40] also studied the influence of pyrolysis pressure on the structure of the resulting char and concluded that melting has a stronger effect on char morphology compared to swelling as pyrolysis pressure increases.

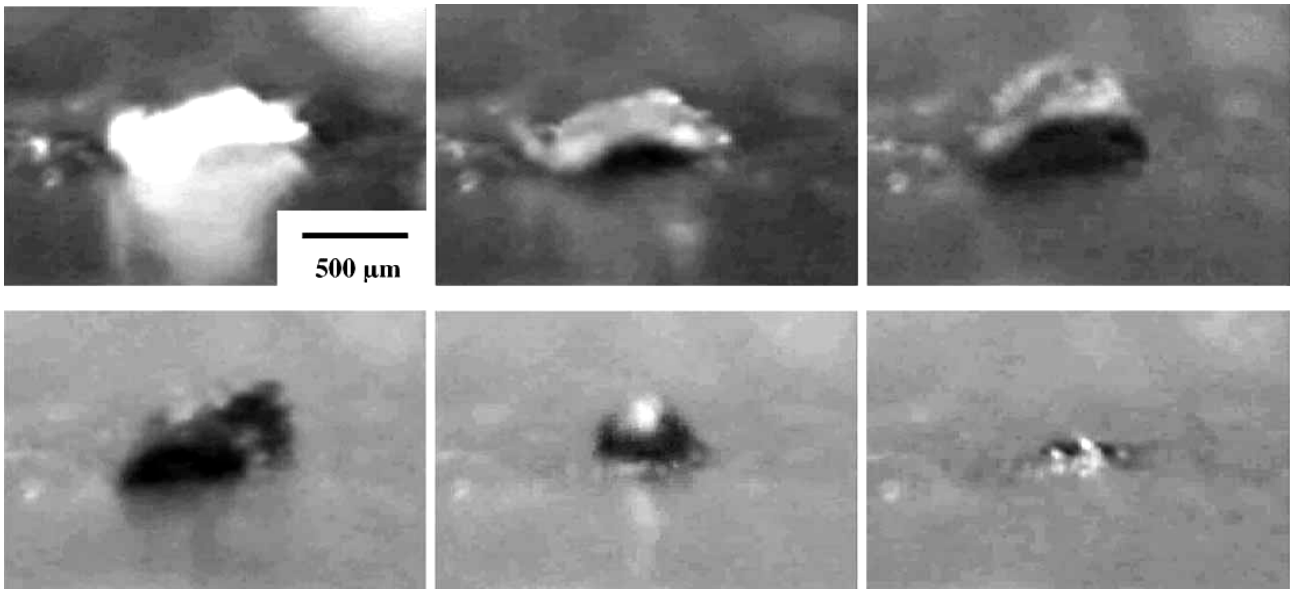

Figure 2.18 Pyrolysis of pine particles at high heating rates: swelling and transition through liquid phase [40].

The pictures of Figure 2.16 to Figure 2.18 show that swelling is most likely to happen in wood particles during pyrolysis at severe conditions.

Some authors, as Davidsson and Pettersson [42] exclude a priori the possibility for a wood particle to swell during pyrolysis. Davidsson and Pettersson studied the shrinkage of cubic birch particles with edge length of 5 mm during pyrolysis at temperatures ranging from 350 to 900 ºC; the particles entered a preheated furnace at the final temperature, thus being subject to relatively high heating rates [42]. They conclude that a maximum shrinkage of up to 40% in the radial and tangential directions is obtained at 500-700 and 400 ºC respectively; when the pyrolysis temperature was further increased the shrinkage in these directions decreased. Their results are shown in Figure 2.19.

Davidsson and Pettersson do not explain the behaviour of the curves in Figure 2.19; in fact, this tendency could be explained if some swelling of the particles was allowed to have occurred at temperatures higher than those for which maximum shrinkage was measured. However, it is difficult to compare results from the work of Davidsson and Pettersson [42] to those of Cetin *et al.*

[40], since Cetin *et al.* [40] used particles of significantly smaller size (50 to 2000 μm compared to 5 mm) and the heating rate attained in their work in the drop tube reactor (10^5 ºCs^{-1}) was far higher than that of the work of Davidsson and Pettersson [42]. Indeed, the size of the particles employed in the study by Cetin *et al.* is far closer to that of pulverised wood than that of the study by Davidsson and Pettersson; a similar consideration can be done for the heating rates, those in Cetin *et al.* being of the same order as those of a pulverised wood boiler. It is thus quite straightforward to assume that the results of Cetin *et al.* [40] represent the phenomena occurring in the pulverised wood boiler better.

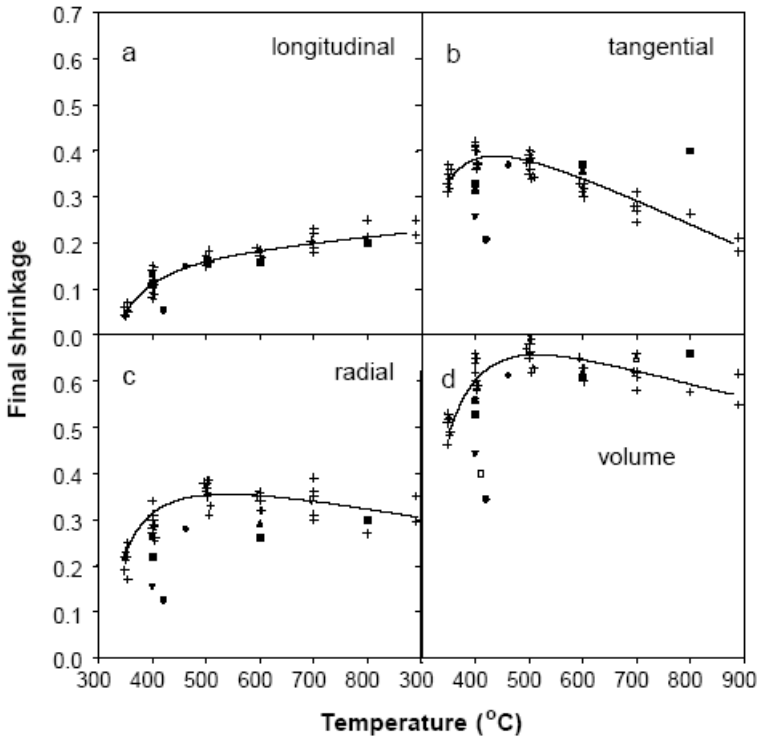

Figure 2.19 Shrinkage as a function of temperature for (a) longitudinal, (b) tangential and (c) radial directions, and for (d) volume. Experimental data obtained by Davidsson and Pettersson (+) and their trend-lines are given. Other symbols are literature data from references in Davidsson and Pettersson. After Davidsson and Pettersson [42].

It is worth noting that the apparent disagreement of the conclusions on the changes in particle morphology during pyrolysis between Cetin *et al.* [40] and other authors [39,46] is due to the range of pyrolysis conditions investigated in their works. In fact if one considers low to moderate heating rates the results of Cetin *et al.* [40] are a clear confirmation of what Kumar and Gupta [46] and Wildman and Derbyshire [39] have observed. Melting of wood particles during pyrolysis was only

observed when the heating rate was well above those of the investigations by Kumar and Gupta [46] and Wildman and Derbyshire [39]. These high heating rates happen to be those experienced by the pulverised wood in a suspension fired boiler. Therefore the work of Cetin *et al.* is believed to be the most relevant to our future investigation.

2.4.2 PORE STRUCTURE AND PORE SIZE DISTRIBUTION

As far as pores are concerned, many researchers agree that the pore size distribution in chars is bimodal [39,43,46,47].

For a char derived from Moraballi wood (hardwood) Wildman and Derbyshire [39] obtained by mercury porosimetry the pore distribution reported in Figure 2.20. The distribution in Figure 2.20 is bimodal and shows that a large fraction of the pore volume of the char was made up by macropores. The high proportion of macropores was a general feature of the wood derived chars considered in the work of Wildman and Derbyshire [39]. As the char retained the structure of the original wood, the origin of the pores was recognised in the fibres and vessel cells of the wood [39].

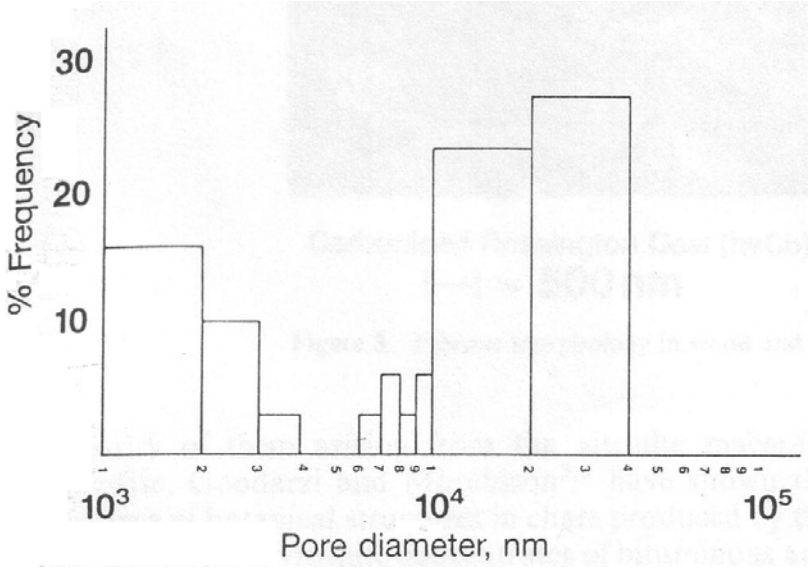

Figure 2.20 Pore size distribution of a Moraballi wood char [39].

Figure 2.21 shows the pore size distribution of larch wood and of a char from larch wood obtained by mercury porosimetry by Klose *et al.* [43]. For larch wood, maxima of the pore size distribution can be recognised at pore radii of 10nm, 100nm and 10μm [43]. During pyrolysis, which was carried out by heating 3K/min up to a final temperature of 800 ºC, the mesopores and macropores

volume increased, as can be inferred from Figure 2.21. This result is in accordance with the above presented results of Wildman and Derbyshire [39]. Unfortunately, Wildman and Derbyshire do not describe in detail in their paper the char production process that they used, only the final temperature of 600 ºC is reported [39]. This information may actually be sufficient to advise the reader that the pyrolysis conditions were not relevant to pulverised fuel combustion; the same can be said about the work by Klose and Schinkel [43], in that the applied heating rate of 3 K/min was very low.

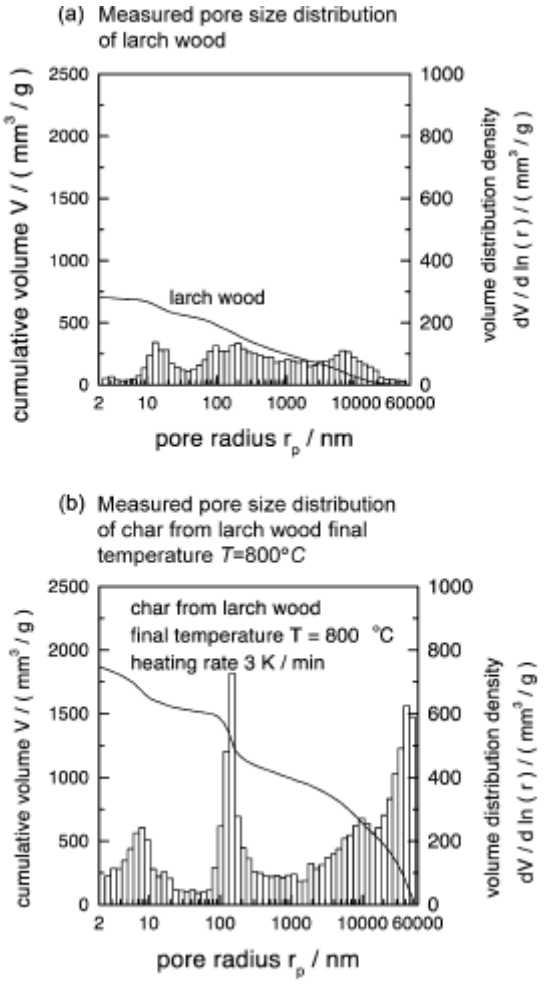

Figure 2.21 Measurements of pore size distribution [43].

Although the volume fraction made up by the different sized pores helps characterise the morphology of the char, a more important role is played by the fraction of total surface area associated with the different classes of pores. The available surface area for oxidation is indeed a

most relevant parameter for the determination of the rate of conversion of the char. In this respect, micropores usually make up the main source of surface area in a char particle; the accessibility of this surface is dependent on the structure of the pores (micro, meso and macro) network.

Cetin *et al.* [40] measured the surface area of char produced at moderate heating rate (up to 500 ºCs^{-1}) by means of N_2 and CO_2 adsorption. Although they provided a different description of the structural changes of wood particle during pyrolysis at this heating rate, they found that increases in the heating rate of pyrolysis led to an increase of the fraction of the macropores in the char [40]. This was considered a result of melting [40], i.e. the origin of the char pores was no longer recognised in the fibrous structure of the wood but in the plastic transformation of the particle subsequent to the appearance of a molten phase (see Figure 2.16c-d and Figure 2.18).

Pastor-Villegas *et al.* [44] prepared chars by heating rockrose under dynamic and isothermal conditions between 200 and 1000ºC; they found that the resulting char porosity was influenced by the shrinkage which accompanied pyrolysis. They concluded that the pore opening due to the loss of volatile matter is somewhat hindered by pore narrowing caused by the structural shrinkage which becomes more severe as the temperature increases from 400 to 1000ºC. A systematic study on the shrinkage of wood particles during pyrolysis was carried out by Byrne and Nagle [45]. They found that the shrinkage of a wood particle is strongly influenced by the heat treatment temperature and that the actual extent of the shrinkage varies, as expected, with the direction considered as a result of wood anisotropy. Byrne and Nagle [45] pyrolyzed 2.5 cm cubes of tulip poplar, with a nominal heating rate of 10°C/min; they observed a maximum tangential shrinkage of about 40% whereas the radial shrinkage was about 33%. These results compare quite well with Davidsson and Pettersson [42] who found a maximum shrinkage of 40% for both tangential and radial direction. However, it is important to notice that Pastor-Villegas *et al.* [44] and Byrne and Nagle [45] worked at pyrolysis conditions which are far from those encountered in a suspension fired boiler, and the dimensions of the particles used in their studies (1 to 3.15 mm in Pastor Villegas *et al.*; 2.5 cm in Byrne and Nagle) were larger than those of a pulverised fuel. These aspects have to be carefully borne in mind when applying the results of these works to the investigation of pulverised wood combustion. Pyrolysis temperature and heating rate are parameters to be taken into account when assessing the influence of pyrolysis conditions on pore structure development. Kumar and Gupta [46] pyrolyzed acacia and eucalyptus wood at different temperature and heating rate and then investigated the char morphology by SEM. Their particles were large with respect to pulverised wood (15 mm^3) and the maximum temperature that they employed was 1050 ºC. As far as pores are concerned, they found

that pore size decreased as pyrolysis temperature/heating rate increased. Figure 2.22 (a) and (b) show SEM images of acacia wood chars prepared at 600 and 1050 ºC respectively. An image analyser measured a decrease of 30% for the pit size when the pyrolysis temperature was increased from 600 to 1050 ºC [46]; the results from Byrne and Nagle [45] would predict a reduction in size of the pits of 10-15% between these two pyrolysis temperature. The more severe size reduction may be a consequence of the much higher heating rate applied by Kumar and Gupta [46].

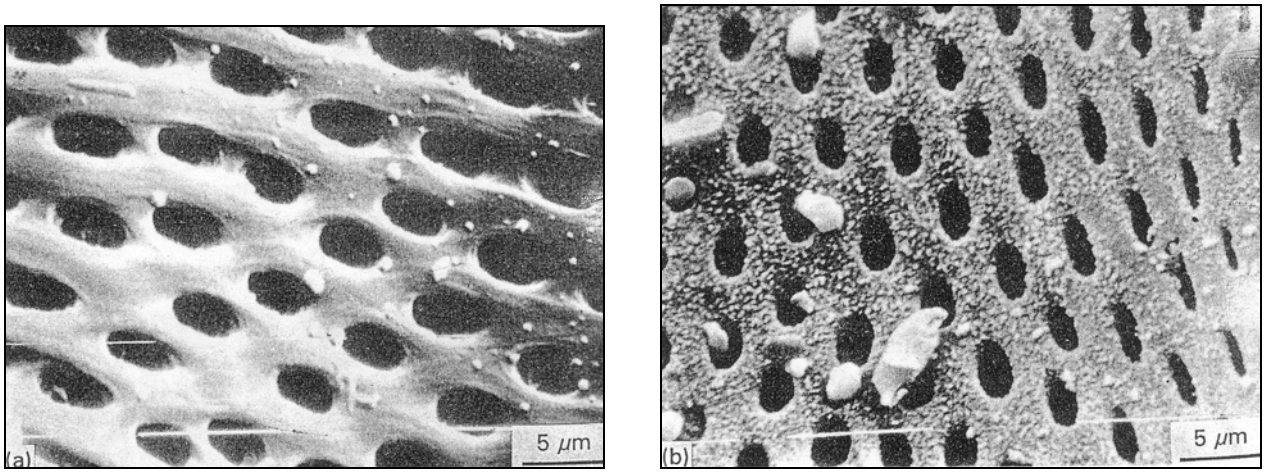

Figure 2.22 SEM images of acacia wood char prepared by fast pyrolysis at (a) 600ºC and (b) 1050ºC [46].

2.4.2.1 *WOOD MACRO COMPONENTS AND PORE DEVELOPMENT DURING PYROLYSIS*

Gergova *et al.* [47] investigated a number of activated carbons from agricultural residues. The residues were pyrolyzed at final temperature 600, 650 and 700 ºC and activated at the same temperatures by reaction with steam. They showed that the elemental composition and macromolecular structure and composition of the precursor had a strong influence on, for instance, the adsorption characteristics of the activated carbon. BET surface and pore volume were measured for the activated carbons as well as for a lignin and a cellulose char, produced from lignin and cellulose subjected to the same heat treatment as the biomass raw materials. Macropores in lignin char made up as much as 70% of the pore volume (as stated earlier, lignin easily melts and swells during pyrolysis), while the cellulose char contained almost equal volumes of micro- and macropores [47]. As Gergova *et al.* underline, with respect to pyrolysis/activation reactions the behaviour of cellulose and lignin combined in biomass is most probably different from that of the single substances. However, the agricultural residue derived chars seem to develop a greater fraction of macropores as the lignin content of the parent material increases. As an example, almond shell and grape seeds contain 42% and 30% cellulose (weight on a dry basis) and 34% and 49%

lignin respectively; the macroporosity of almond shell derived char was 0.02 cm^3g^{-1}, while that of grape seeds was 0.25 cm^3g^{-1} [47]. In a recent study [48] the relative amount of lignin and cellulose in the parent material has been related to the reactivity of the chars with respect to the activation reaction (reaction of the char with carbon dioxide; both pyrolysis and activation were carried out at final temperature 850 ºC). Char derived from biomass with a higher content of lignin (palm shell), i.e. a less fibrous structure, revealed a lower rate of the activation reaction than those derived from material with higher cellulose and holocellulose fibres (coconut shell). On the other hand, results from the work of Wan Daud and Wan Ali [48] do not seem to show a strong dependency of pore distribution on the lignin/cellulose fraction of the parent fuel. A paper by Pastor Villegas *et al.* [49] shows evidence of the influence of wood composition on char morphology and properties. In this work rockrose wood and rockrose wood extracted in petroleum ether exhibited a different temperature dependence of pore development during devolatilisation. In general, chars from extracted rockrose exhibited greater porosity than chars from raw rockrose. All other conditions being equal, the differences in these properties of the chars were attributed to the extraction process (this process is used to extract labdane which is employed in the perfume industry).

Although some relations between wood and char characteristics have been pointed out, there exist (to my knowledge) no such works on wood char morphology dependence on the parent wood as the one on coal derived char by Bailey *et al.* [50]. This work is a systematic study relating coal characteristics such as rank and petrographic composition to the fraction of different types of char that are obtained upon pyrolysis at different conditions. The char morphology system set by Bailey *et al.* is based on char physical and optical characteristics relevant to pulverised coal combustion. As said, the knowledge of wood char properties and their dependencies on parent fuel is not particularly extensive, especially when it comes to char prepared under suspension combustion relevant conditions.

2.4.3 CHAR REACTIVITY

Prior to the discussion on how different parameters (both during pyrolysis and during char conversion) influence wood char reactivity, some general considerations are given. Once again, the illustration of wood char characteristics is based on a comparison with char from coal. Figure 2.23 shows an Arrhenius plot of the oxidation reactivity of some coal chars, straw char and pine char. The data of Figure 2.23 were found in Zolin [51] (coals and straw) and in Janse *et al*. [37] (pine).

As can be seen in Figure 2.23, the char obtained from pine wood has the highest reactivity. It is seen that biomass chars (straw and wood) exhibit higher reactivity to oxygen than coal char. This is a general observation of very important practical implications.

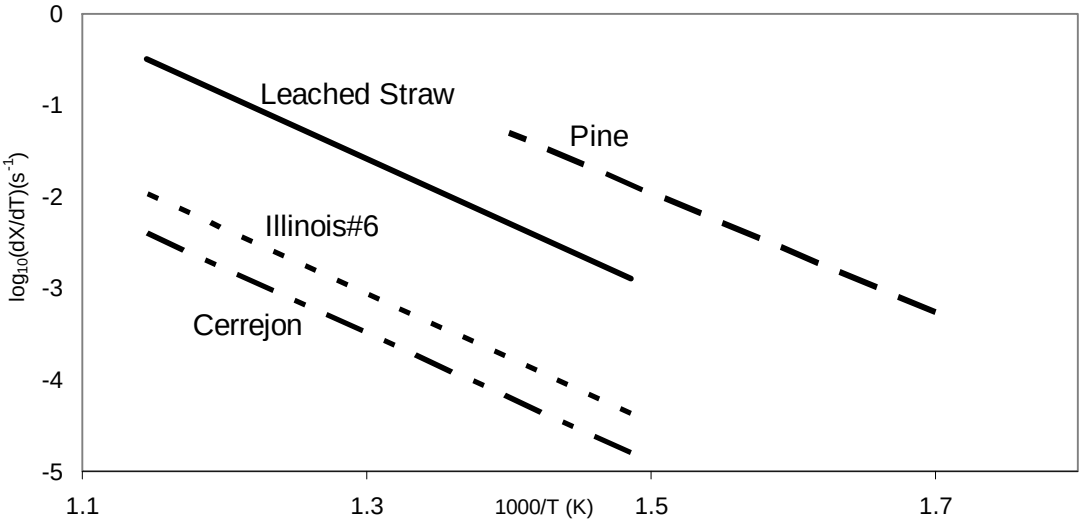

Figure 2.23 Arrhenius plot (reaction rate versus temperature) of the oxidation reaction of chars. Data for coals and straw are derived from Zolin [51] (char produced in a TGA, heating rate 45 K/min, peak temperatures: Cerrejon and Illinois#6 900°C, leached straw 700°C), whereas data for pine char are taken from Janse *et al.* [37] (char produced in a screen heater reactor, estimated heating rate 300 K/s, peak temperature 600°C) .

Understanding char morphology and structure is a major step when modelling char burnout in combustion processes in that physical and chemical properties of the char determine its oxidation reactivity. However, useful information can be gained by trying to relate char reactivity directly to the conditions of pyrolysis. The observations that one can make about char reactivity can be determining in validating conclusions drawn about the actual development of the fuel particle during pyrolysis.

The conditions of flash pyrolysis are closer to those of a suspension burner than those of conventional pyrolysis, thus results from flash pyrolysis studies might be more applicable to this investigation than the conclusions drawn for conventional pyrolysis. Janse *et al.* [37] investigated the effect of flash pyrolysis temperature, heating rate and pyrolysis time on the pine wood char produced. By means of a so called screen heater reactor (described in their paper [37]) and of a packed bed reactor they varied the parameters between the range of 500 to 600 ºC for the final pyrolysis temperature, 20 to 100 s for the pyrolysis time, while the heating rate was either 1 or 300 Ks^{-1} [37]. The heating rate turned out as the parameter which most influenced the char properties;

due to the narrow range of temperature investigated (500-600 ºC) this observation should not be considered as a general statement. In fact, the final pyrolysis temperature is known to have a very strong influence on char reactivity.

From the burn-off curves of the chars obtained by Janse *et al.* [37] (see Figure 2.24) it appears that the char produced at the highest heating rate was highly reactive compared to the one produced at low heating rate. Nevertheless, the fact that the two chars (low and high heating rate) were subject to different soaking times (see caption of Figure 2.24) may play an important role, since it most likely results in a different thermal deactivation ratio for the two chars (thermal deactivation is treated in detail in the next paragraph). Thus, the distinct behaviour of the two pair of curves of Figure 2.24 may not be the sole effect of the heating rate but should rather be considered a combined effect of heating rate and holding time (in other words, the effect of the thermal history of the particle on its reactivity).

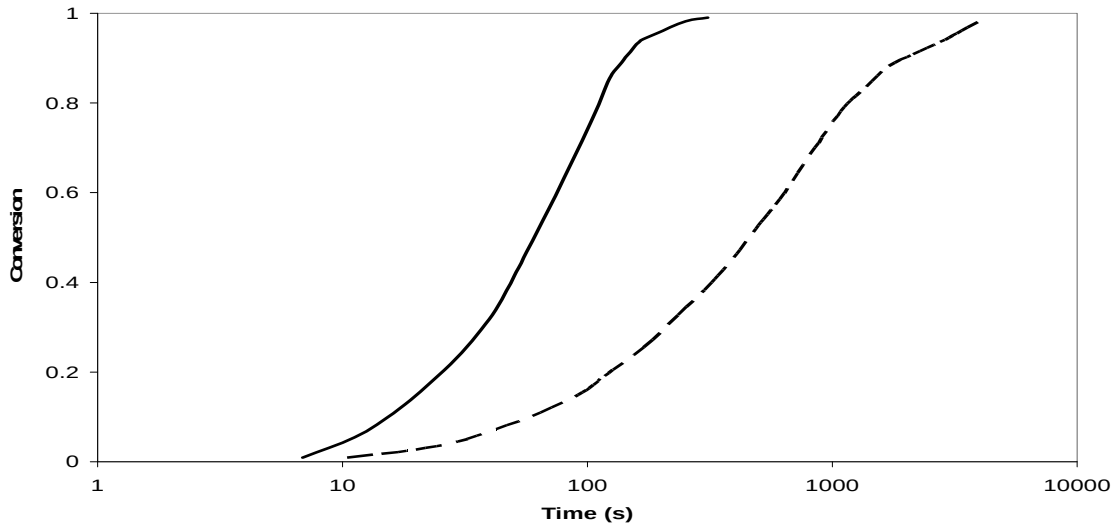

Figure 2.24 Influence of the heating rate on the burn-off curve of a pine char. Combustion at 425ºC in 18% O_2. Char preparation conditions: pyrolysis temperature, 600ºC; holding time at 300K/s, 60s (solid curve); holding time at 1K/s, 375s (dashed curve) [37].

Janse *et al.* [37] compared the reactivity of the char produced during their work with literature data and they found that their char had a significantly higher reactivity, as can be seen in Figure 2.25. It was shown that the higher concentration of catalytic metals due to the lower char yield of flash pyrolysis could have a significant influence on this result.

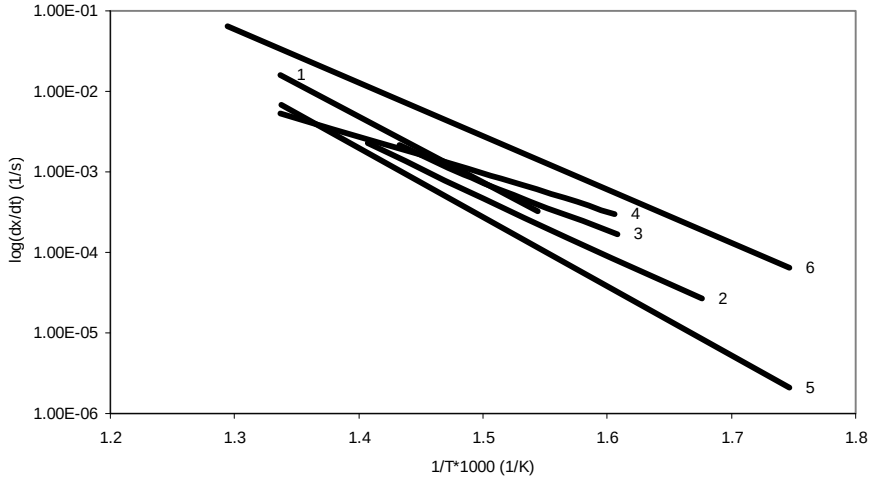

Figure 2.25 Arrhenius plot (reaction rate versus temperature) of the best fit rate equation of the work of Janse *et al.* (line 6, pine wood char) and other literature data: 1, Mc Carthy (E. Marginata wood char)[82]; 2, Burggraaf and Prins (wood char)[83]; 3, Magnaterra *et al.* (hardwood char) [84]; 4, Magnaterra *et al.* (hardwood char) [85]; 5, Kashiwagi and Nambu (cellulosic paper) [86]. After Janse *et al.* [37].

The literature values of char reactivity that Janse *et al.* considered were all derived for chars that had been produced at a much lower heating rate (1 to 20 ºC/min compared to at least 300 ºC/s in the work of Janse *et al.* [37]). It was suggested that the higher heating rate could result in a higher H/C ratio of the char [37] (the ratio H/C is known to influence char reactivity, see next paragraph). The higher reactivity of char from flash pyrolysis may also be related to morphological changes of the particle; in this view the findings of Janse *et al.* [37] could be related to the results of Kumar and Gupta [46] and Cetin *et al.* [40] who observed a rupture of the characteristic fibrous cell structure when pyrolysis of wood was carried out at similar heating rates and final temperatures (see Figure 2.15 and Figure 2.16b). In fact, it may be thought that the morphological changes undergone by the particle at high heating rate result in higher char reactivity. What is clear is that the heating rate is a major factor to be considered when studying suspension combustion of wood.

2.4.4 CHANGES OF WOOD CHAR STRUCTURE, COMPOSITION AND REACTIVITY DURING COMBUSTION

The process of char conversion consists of two steps, namely devolatilisation and oxidation [36]. The modifications of char from coal during combustion have been extensively studied

[51,52,53,54,55,56]. Much less has been done to investigate these changes for wood-derived chars. Two papers by Wornat *et al.* [57,35] address this issue and their results are reported here.

The chars were produced from pine particles in a vortex reactor at 625ºC and their combustion was carried out in a laminar flow reactor at 6 and 12 vol% O_2 and a mean gas temperature of approximately 1330ºC [57]. Nominal char particle size ranged from 75 to 106µm. Ultimate analysis of the char is reported in Table 2.8. Table 2.9 and Table 2.10 show the results obtained by Wornat *et al.* [57]: the chars were extracted from the reactor at different residence times and the conversion reported in the tables was calculated by using Si as a tracer [57].

During the earlier stages of char conversion (0-52.8% in Table 2.9) further volatiles are released (in addition to those released during pyrolysis). As can be seen from Table 2.9, this process is accompanied by a strong decrease in the oxygen and hydrogen content of the char; on the other hand, the fraction of nitrogen released during this first step is much lower. In fact, the main species released in this stage, deriving from the breakage of the weaker aliphatic bonds are CO, CO_2 and H_2O, together with hydrocarbons [57]. The higher retention of nitrogen in the char is attributed to the presence of this element in heterocyclic ring structures [57] that require more energy to be broken than aliphatic bonds. As conversion proceeds a steady decrease of all organic elements appears, as can be seen in Table 2.9. Despite the rapid decrease of the oxygen content of the char during the first stages of conversion, this element still represented a fraction as high as 15-25% of the organic portion of the char at high conversion [57]. This observation helps interpret the behaviour of the inorganic elements present in the char (Table 2.10). Wornat *et al.* [57] believe that Na, Ca and K are present in the char in the form of ion-exchanged metals onto oxygen functionalities. This would subject Na and K to vaporisation. It is seen in Table 2.10 that during the early stage of conversion the release of these elements is very low. Wornat *et al.* explain this by suggesting that the temperatures reached by the particles during devolatilisation may not have been high enough for vaporisation to occur. On the other hand, during combustion the particle temperature is higher and some loss of Na and K is observed (see Table 2.10); according to Wornat *et al.* the full vaporisation of these alkali metals could be prevented by the formation of silicates or aluminosilicates due to the interaction of their oxides with SiO_2 or Al_2O_3 [57]. Similar considerations can be done with respect to alkaline earth metals Mg and Ca. They may also exist as ion-exchanged metals onto oxygen functional groups [57] and therefore form silicates; other processes that are suggested as explanation of the high retention of Ca and Mg in the solid char are sintering and coalescence [57]. Actually, as burnout proceeded, Wornat *et al.* [57] found evidence

of migration of the inorganics to the surface; notably, the surface concentration of Si and Ca becomes much higher as indicated in Table 2.11.

Table 2.8 Ultimate analysis (dry basis) of pine char used in the work of Wornat *et al.* [35].

	C (%)	*H (%)*	*N (%)*	*S (%)*	*O (%)*	*Ash (%)*	*K (%)*	*Si (%)*
Pine char	69.7	3.13	0.52	0.05	19.1	9.2	1.03	1.93

Table 2.9 Organic element retention in the pine chars (normalised fractions) [57].

Char conversion (% dry ash-free)	*Mass*[a]	*C*	*H*	*O*	*N*
0	1	1	1	1	1
52.8[b]	0.472	0.562	0.082	0.157	0.694
73.0[b]	0.270	0.314	0.054	0.126	0.532
86.4[b]	0.136	0.154	0.020	0.088	0.394
94.6	0.054	0.053	0.010	0.049	0.172

[a] Normalised char mass on a dry ash-free basis.

[b] These samples produced at 6% O_2; other samples produced at 12% O_2.

Table 2.10 Inorganic element retention in the pine chars (normalised fractions) [57].

Char conversion (% dry ash-free)	*Na*	*Mg*	*Al*[a]	*K*	*Ca*
0	1	1	1	1	1
52.8[b]	1	0.980	0.762	0.982	0.997
73.0[b]	0.455	0.931	0.692	0.887	0.962
86.4[b]	0.449	0.917	0.729	0.599	0.973
94.6	0.313	0.827	0.878	0.468	0.789

[a] Al values uncertain due to low absolute Al levels.

[b] These samples produced at 6% O_2; other samples produced at 12% O_2.

Table 2.11 Overall elemental surface analysis of pine chars (net X-Ray counts from each element on the char surface) [57].

Char conversion (% dry ash-free)	*C*	*O/C*	*Mg/C*	*Al/C*	*Si/C*	*K/C*	*Ca/C*
0	20384	0.243	0.0212	0.0137	0.256	0.093	0.055
52.8[a]	30513	0.161	0.0473	0.0111	0.445	0.149	0.136
73.0[a]	21994	0.252	0.0727	0.0202	0.750	0.275	0.282
86.4[a]	11641	0.348	0.1045	0.0582	1.468	0.441	0.497
94.6	9271	0.737	0.1290	0.0681	2.847	0.597	0.466

[a] These samples produced at 6% O_2; other samples produced at 12% O_2.

SEM analysis of the char at different stages of combustion reveals that Si-rich spherical beads are formed on the surface of the burning wood char [57]. Also, the data in Table 2.11 show that the increase of the surface concentration of metals was accompanied by an increase of the oxygen surface concentration; this consideration, as well as the high stability of some metal oxides as MgO and CaO, are used by Wornat *et al.* [57] to support the assumption that the metals present in the char are bound to oxygen [57]. Surface enrichment of metal species has recently been confirmed by the work of Frandsen *et al.* [58]. They pyrolyzed (at low heating rates) and combusted different fuels (spruce, bark, waste wood, straw) and noted for all of the chars a surface enrichment of K, Ca, Mg P and Mn; in the SEM images of Figure 2.26 the formation of cotton-like ash on the surface of spruce samples can be seen, as well as Ca-rich cubic crystals on a bark sample [58]. The composition of the crystals and the area referred to in Figure 2.26 were obtained by Frandsen *et al.* [58].

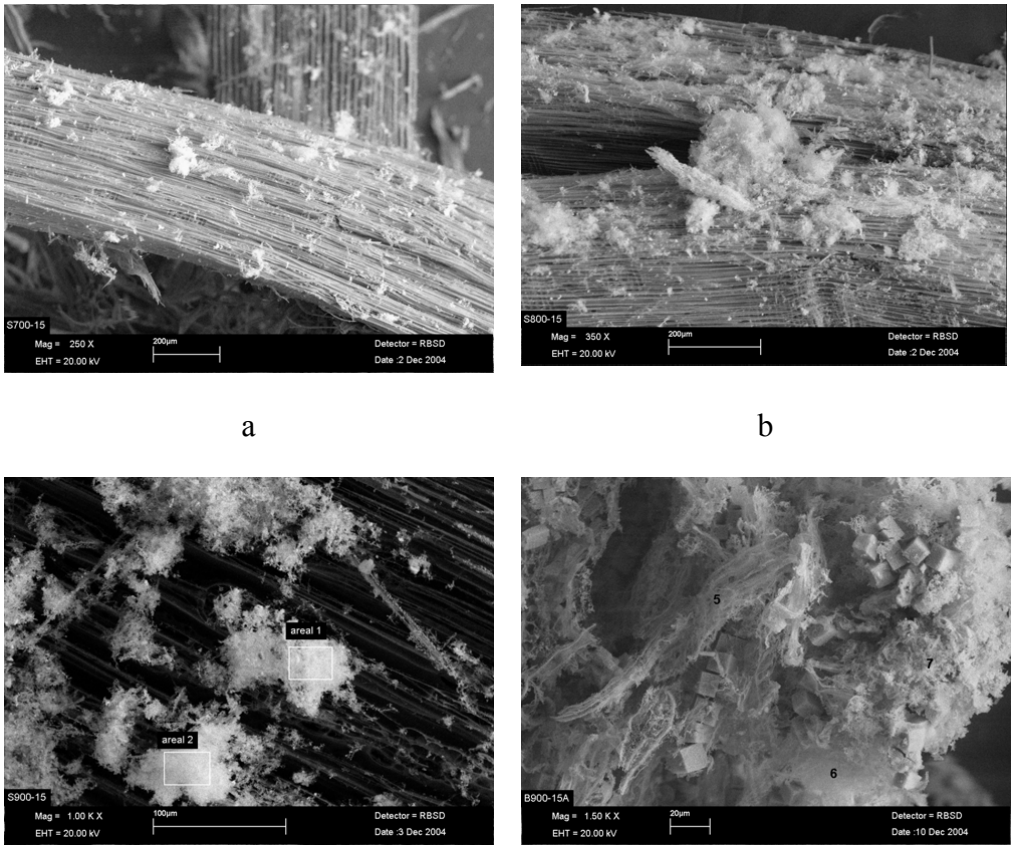

Figure 2.26 After Frandsen *et al.* [58] : Spruce samples pyrolysed and subsequently combusted in 2.5% O_2 at 700°C (image a), 800°C (image b) and 900°C image c). In image d Ca-rich cubic crystals are shown inside a residual ash particle from combustion of bark in 21% O_2 at 900. Composition, % (mol/mol), C- and O- free: Spot 5: 66% Ca, 21% Mg, 6% P, Spot 6: 77% Ca, 15% Mg, 4% P, Area1: 54% Ca, 14% Mg, 14% Mn, 7% K, 4% P.

Figure 2.27 summarises the results that Wornat *et al.* [57] obtained by X-Ray diffraction investigation of the partially converted chars. Part (a) of Figure 2.27 refers to pine wood char, part (b) shows the results for switchgrass. For pine, diffraction patterns of chars at different conversions are shown, from which some important considerations arise. Firstly, it seems likely that the hump centred at 25º in the spectrum of the pine char sample represents amorphous material [57]; its disappearance as conversion increases from 0 to 95% would signify a loss in amorphous material, i.e. an ordering (at least to some degree) of the organic portion of the char. Actually, high resolution transmission electron analysis seems to show that some ordering happens during the first stage of char conversion [57]. This consideration can be valid in that during devolatilisation the char releases oxygen-rich molecules and this could make some order of the amorphous carbon material attainable. In fact, oxygen is known to enhance cross linking of carbon, thus limiting the attainable degree of order of (the organic portion of) the char [57]. The high oxygen content of wood (and

biomass in general) chars seems to be one of the characteristics that make the behaviour of wood char different from that of low-oxygen coal char.

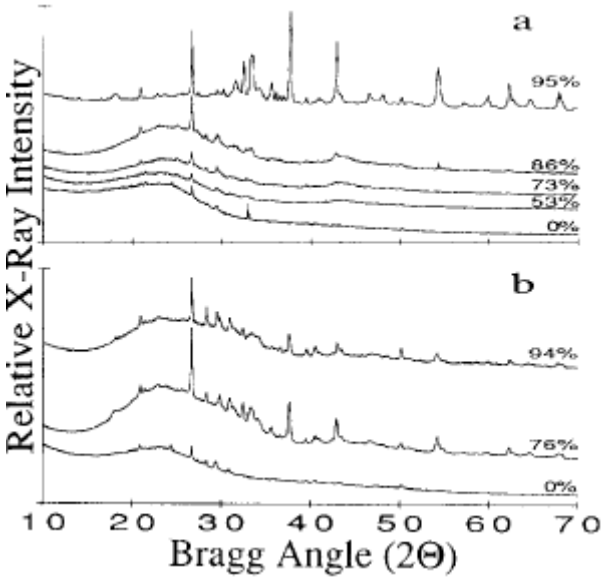

Figure 2.27 X-ray diffraction patterns for biomass chars at various extents of reaction. (a) Pine char, uncombusted and at conversions of 53%, 73%, 86% and 96% daf. (b) Switchgrass char, uncombusted and at conversions of 76% and 94% daf [57].

As far as inorganics in the char are concerned, Figure 2.27 (a) proves that the inorganic portion of the pine char develops a high degree of crystallinity during char conversion; in fact, the narrow distinct peaks of the char sample at 95% conversion are associated with inorganic crystalline material [57].

Wornat *et al.* [35] (see Figure 2.28) followed the temperature history of pine chars during combustion; the temperatures were derived from optical measurements (two colour pyrometer) and the particle size was measured by a coded-aperture device (this technique gives the particle dimension along its axis of flow as it passes an optical window). The experiments of Figure 2.28 are the same as those of the previously considered paper [57]; T_g indicates the mean gas temperature in the laminar flow reactor. It can be seen the particles have different temperatures, i.e. they burn with different rates (the presence in Figure 2.28 of some particles at a lower temperature than the average gas temperature T_g is due to radiation losses of the particles to the quartz walls of the reactor [35]).

A number of different factors can affect this heterogeneity. For example, the part of the wood from which the char was derived can influence char reactivity in more than one way: mineral matter is not evenly distributed in the tree (the catalytic activity of some minerals like Ca and K is widely

recognised), variations in the composition of the wood are encountered (e.g. bark and heartwood do not have the same composition in terms of macro components). Moreover, char particles have very different shapes and sizes, as seen in Figure 2.29 (Figure 2.29 shows that many of the pine char particles had a high aspect ratio; this may be one of the reasons why the particle diameter measured by the coded aperture technique gave the wide range of diameters of Figure 2.28 even though the original nominal size of the particles was 75-106 μm [35]).

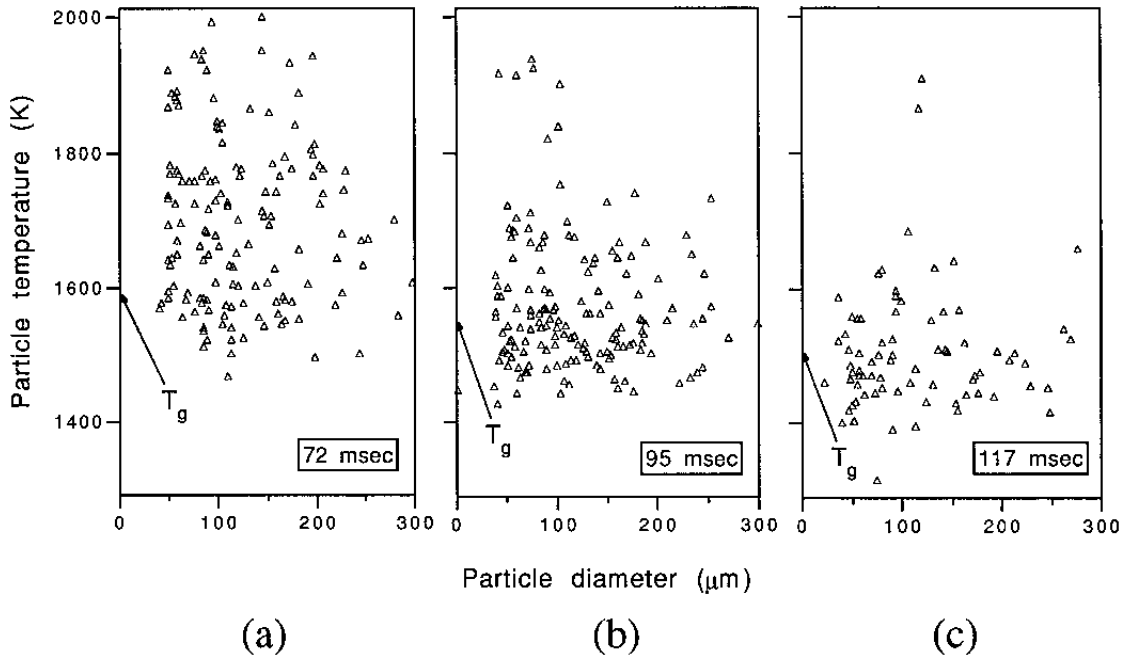

Figure 2.28 Optical measurements of temperatures and sizes of single particles of Southern pine char burning in 12 mole% O_2 in a laminar flow reactor. Initial particle size, 75-106 μm. Particle residence times: (a) 72ms, (b) 95ms, and (c) 117ms. Particle diameters determined by coded aperture technique. T_g denotes mean gas temperature [35].

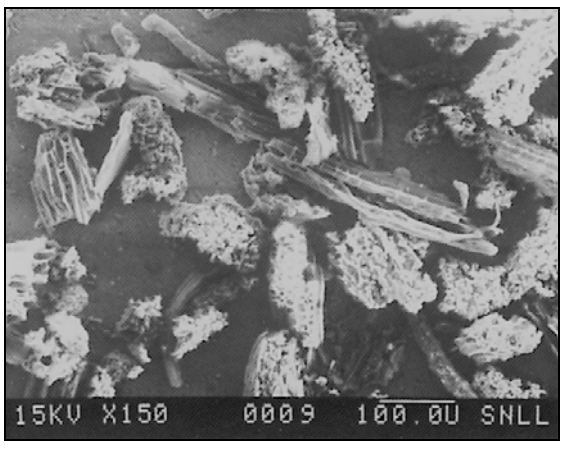

Figure 2.29 SEM image of pine char particles produced in a vortex reactor at 625ºC [35].

Considering the sequence of Figure 2.28 one can see that the range of particle temperatures becomes narrower at higher residence times (i.e. higher conversions) and that the mean temperature (burning rate) decreases as burnout increases.

One of the causes of the decreased reactivity of the char is the release of oxygen and hydrogen rich compounds during the early stages of conversion. It has already been said that the presence of oxygen in wood chars limits the possibility for the char to rearrange its organic matrix. Nevertheless, although to a much lower extent than in coal chars, it has been shown that the decrease in oxygen concentration and the exposure of the char to the high temperatures of combustion bring about some ordering. When rearranging its carbon matrix, the char loses edge carbons that are converted to basal plane carbons. The loss of edge carbon resulting from the ordering of the carbon matrix of the char is known to cause a decrease in reactivity in coal chars [52] and there is no reason to doubt that this would have the same effect in wood chars. Geometrically, edge carbon atoms can readily form bonds with chemisorbed oxygen due to the availability of unpaired sp^2 electrons. Basal plane carbon atoms presumably have their π-electrons forming chemical bonds with adjacent carbon atoms [59].

Another factor that may contribute to the loss of reactivity of the char as conversion proceeds is the evolution of the concentration and of the form of appearance of metals. The transition of the inorganic portion of the char through a molten phase (documented by the occurrence of the Si-rich beads [57]) and the possible incorporation of metals in silicates and/or aluminosilicates as well as the partial vaporisation of these metals can affect significantly their catalytic activity.

The two phenomena mentioned above, i.e. ordering of the carbon structure and changes in the inorganic matter, are accounted for as one factor in some char combustion models and referred to as thermal deactivation. As the name suggests, this effect (that can be seen as a measure of the degree of order and the extent of the changes in the inorganics) is strongly dependent on (and increases with) temperature. A more detailed discussion of thermal deactivation is given in paragraph 2.4.4.2.

Along with thermal deactivation, another factor must be considered when describing Figure 2.28, namely shrinkage of the char particles as the carbon is consumed by the reaction with oxygen. For larger particles at higher temperatures, it is likely that the rate of external mass transfer controls the burning rate. Smaller and less reactive (deactivated) particles are more likely to burn under chemical reaction control. This certainly contributes to the decrease of the average particle

temperature observed from Figure 2.28 (a) to Figure 2.28 (c) (this issue is treated in more detail in section 2.5).

At this point, it seems appropriate to underline once more that a very limited number of papers deal with wood char transformations during combustion; therefore the description of the phenomena reported here would need to be further investigated for a validation.

2.4.4.1 *FRAGMENTATION*

The morphology of char particles influences the combustion process and so does their size. A good description of the evolution of the size distribution and of the structure – shape, porosity - of the char particles during conversion is of utmost importance to predict char burnout. Fragmentation of char particles is known to happen during pulverised coal combustion [53,56] but its extent does not seem to be clearly predictable. Mitchell and Akanetuk [56] conducted combustion experiments in a laminar flow reactor (1230ºC, 12% O_2). They used synthetic char particles of known porosity (23 and 36%) and controlled pore structure [56]. The chars were produced from the polymerisation of furfuryl alcohol with p-toluenesulfonic acid; porosity and pore structure were controlled by addition of carbon black (micropores are formed around the carbon black intrusions) and lycopodium plant spores during polymerisation [56].

Following the evolution of both burnout and size number distribution during conversion (by extracting chars at different residence times), they noted that at any residence time both the burnout and the number of small particles in the distribution were higher for the higher porosity samples [56]. This seems to suggest that the extent of fragmentation (which Mitchell and Akanetuk believe to be percolative, i.e. forming a set of different sized particles from one particle) increases, for coal char, with increasing porosity. On the other hand Zhang *et al.* [53], who also investigated synthetic spherical char (Spherocarb), observed only a low degree of fragmentation, although the original particles were highly porous (60-80% [53]). Zhang *et al.* used a TGA at 500ºC and an electro dynamic balance reactor in their study. They observed that only those particles whose physical continuity was broken during oxidation experienced fragmentation [53]. Feng and Bhatia [60] investigated fragmentation of three microporous coal chars by measuring electrical resistivity during conversion and by direct observation. They concluded that when the reaction is controlled by diffusion of oxygen (as is most likely to be the case for pulverised wood particles at the high temperatures of a suspension boiler) perimeter fragmentation is to be expected, i.e. the outer shell of

the particles fragments (by percolation) when the local conversion of the shell (or the porosity of the shell) becomes greater than a critical value (in their study the critical porosity was 0.91 - 0.99) [60].

These observations highlight that the prediction of the effect of fragmentation on char burnout would need a good knowledge of the shape of the fragments generated. In fact, as underlined by Mitchell and Akanetuk [56], depending on the size and shape of the generated fragments the effect of fragmentation can be twofold, i.e. it can enhance or decrease the burnout. For example, fragmentation may lead to the transition from external mass transfer-controlled-combustion (kinetic regime III, see section 2.5) to combined diffusion and chemical reaction controlled conversion (regime II); depending on the burning temperature of the particles, which is affected by the surface-to-volume ratio, this change causes either an increase (for instance if all fragments were spherical) or a decrease of the combustion rate.

As said, the studies of Mitchell and Akanetuk [56] and Zhang *et al.* [53] were carried out with synthetic carbon particles; these particles contain virtually no mineral matter [53]. With consideration to the influence of metals on the oxidation reaction and possibly on the structural changes of the char particle during its conversion one would expect that the mineral content (and its physical distribution) of the wood char particles also plays a role in determining particle fragmentation behaviour. To my knowledge, no studies on wood combustion address this issue.

2.4.4.2 *THERMAL DEACTIVATION*

As for fragmentation, char thermal deactivation has been primarily studied in relation to coal combustion. The expression “thermal deactivation” refers to the reduced reactivity of the char as it is subjected to increasing temperatures both during pyrolysis and oxidation. Two processes contribute to this effect: thermal annealing and changes in the inorganic minerals of the char [55]. The relative importance of the two processes depends on the nature of the parent fuel and on combustion conditions [55]. Thermal annealing is the result of a series of transformations in the organic matrix of the char that include the loss of hydrogen and oxygen, elimination of edge carbon sites and defects elimination [51]. These transformations result in the ordering of the organic portion of the char that we mentioned earlier in this paragraph. It seems now interesting to present some results obtained for coal char, for which more systematic and extensive work has been carried out. As far as inorganic phase transformations are concerned, their description has also been reported earlier and their effect on the burning rate will be considered here.

Beeley *et al.* [54] pyrolyzed four monomaceral-rich coals in a high temperature wire mesh reactor. The heat treatment to which the coals were subjected was: heating rate of 10^4ºCs^{-1}, maximum temperature of either 1000 or 1800 ºC, holding time of 2s. The samples were then oxidised in a TGA (thermal path: 40 ºC/min up to 400 ºC , 15 ºC/min to 900 ºC, hold for 2 minutes at 900 ºC. 7% O_2) and the derivative mass loss curves (DTG) were compared. DTG curves obtained for Illinois #6 lithotype chars prepared at 1000 and 1800 ºC are shown in Figure 2.30 [54]. The vitrain char oxidation reaction peak is shifted to much higher temperatures by the increase of the heat treatment temperature. Beely *et al.* [54] extracted the mass loss rate value of the vitrain rich samples at 50% conversion and found a reduction of the reaction rate of the order of 30-50 when increasing the pyrolysis temperature from 1000 to 1800 ºC. Thus, despite the short treatment time (2s), the increase of the severity of the heat treatment brought about major changes in char reactivity.

The effect of the pyrolysis temperature is less significant for the fusain chars (see Figure 2.30). This is a clear indication that the deactivation tendency of a char strongly depends on the parent fuel. Furthermore, by means of high resolution transmission electron microscopy Beeley *et al.* also found that the deactivation tendency of the chars correlates with the extent of crystalline order developed during heat treatment and oxidation [54].

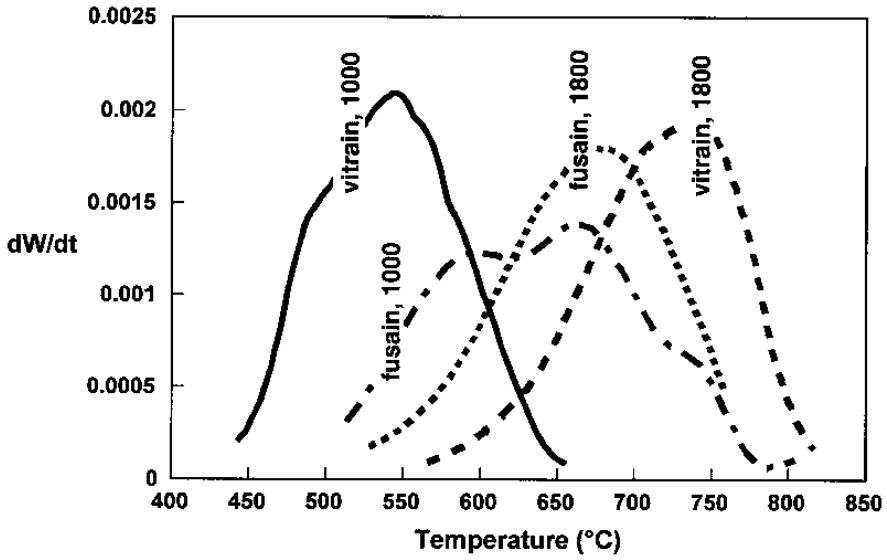

Figure 2.30 Derivative thermograph (DTG) profiles for Illinois #6 lithotype chars produced at 1000ºC and 1800ºC. W is the normalised sample weight, *d*W/*dt* is the instantaneous reaction rate (s^{-1}) [54].

Senneca *et al.* [55] studied the gasification reactivity (with CO_2) of a bituminous coal that was subjected to heat treatments in the range 900 to 1400 ºC with holding times from 1 to 300 min; after

heat treatment the char was gasified in a thermobalance with CO_2 partial pressure between 0.25 and 1bar [55]. The effect of heat treatment temperature on char reactivity is shown in Figure 2.31 [55] where the gasification reaction rate at 50% conversion is reported as a function of treatment temperature. The effect of thermal deactivation is evident in Figure 2.31: the reactivity of the char prepared at 900ºC is about five times as high as the reactivity of the char prepared at 1400ºC. The trend of the curve in Figure 2.31 may suggest that the deactivation could become severer at temperatures higher than 1400ºC. X-ray diffraction analyses showed that in the work of Senneca *et al.* [55] the bituminous coal experienced both an ordering of the carbon matrix (which increased with increasing heat temperature and holding time) and changes in the mineral matter. To account for both these effects, they proposed to model the char as consisting of two types of carbon, the more reactive type turning into the less reactive as heat treatment proceeds [55]. In fact, for some types of coal Zolin [51] found that increasing the heat treatment temperature the oxidation DTG curves did show two peaks, as if the char had split into two phases of different reactivity. He studied the oxidation reactivity of chars from straw (biomass) and coals at temperatures in the range 700 to 1400ºC in a TGA and, consistently with the other authors, he noted that the DTG curves shifted to higher temperatures when the heat treatment was conducted at higher temperatures [51].

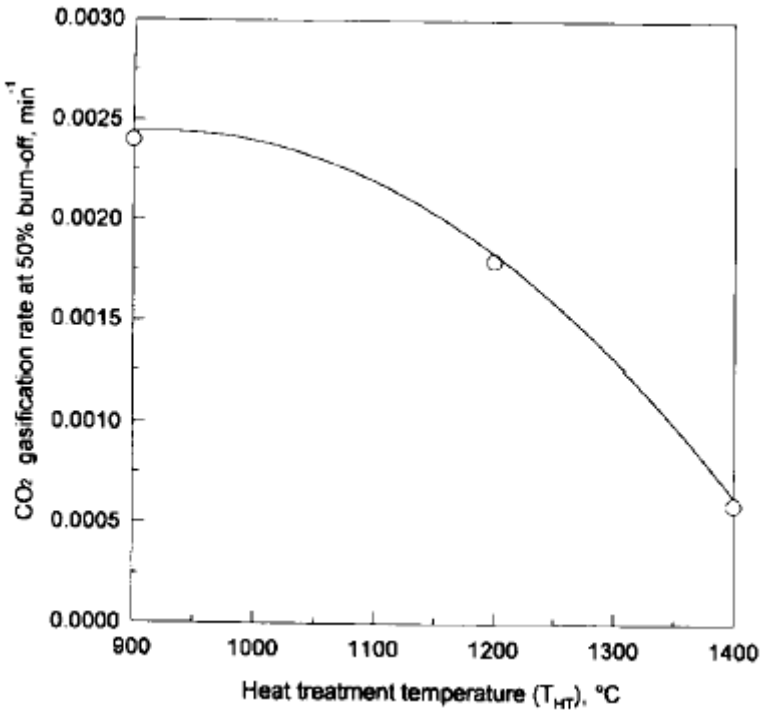

Figure 2.31 Thermal deactivation: gasification rate at 50% conversion at 900ºC and p_{CO2}=1bar of a bituminous coal. Samples heat treated for 30 min [55].

Another result of the study of Zolin [51] was a new confirmation of the important role played by catalytic minerals during char oxidation: for chars produced in an entrained flow reactor at temperatures in the range 1200-1400ºC the oxidation reactivity (measured by means of a simultaneous thermal analyser STA) of a char of leached straw was lower than the reactivity of untreated straw by a factor of 30 (the effect of leaching is extraction of the mineral matter from straw).

Indeed, the relative importance of thermal annealing and mineral transformations during heat treatment is not yet known for biomass and in particular wood fuel. Still, it is important to investigate the extent of their combined effect (thermal deactivation) for wood fuels, because this aspect can be of significant importance to predict char reactivity and burnout in pulverised fuel furnaces. Wood particles may either experience a severe heat treatment prior to oxidation (for example by going through a fuel-rich region in a low NO_x burner) [54] or be ignited at a very early stage in the combustor, as discussed by Zolin *et al.* [87]: in both cases the high temperatures reached by the particles require that the effect of thermal deactivation be carefully considered when assuming char reactivity values for burnout calculation.

2.5 CHAR OXIDATION

2.5.1 DEFINITIONS

Coupling transport phenomena and chemical reactions is vital for investigating and modelling the combustion of char.

The overall reaction rate between char and oxygen can be controlled by different phenomena depending on the conditions at which oxidation is carried out, char characteristics and degree of conversion. Three different situations may occur that are commonly referred to as regime I (or zone I), regime II and regime III [34, 61].

Figure 2.32 illustrates the relation between burning rate and temperature. In Figure 2.33, the concentration profile of reactant gas (oxygen) across the gas boundary layer and in the particle is shown for the three regimes.

Regime I: the overall burning rate is controlled by the chemical heterogeneous reaction between O_2 and the carbon on the surface of the char. In this regime neither external mass transfer of oxygen to

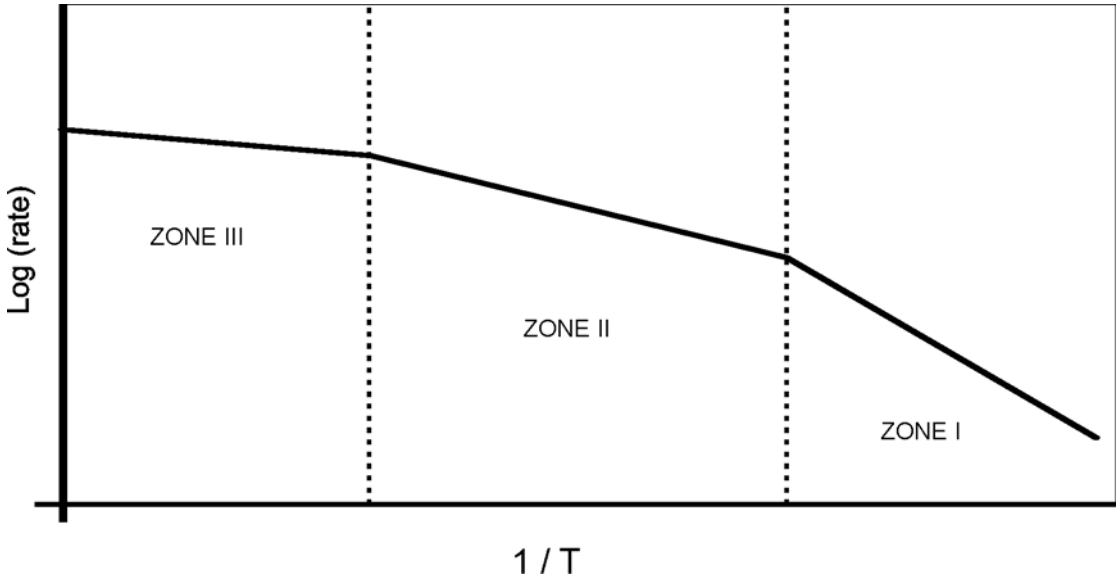

Figure 2.32 Change in rate of char oxidation with temperature; kinetic regimes [59].

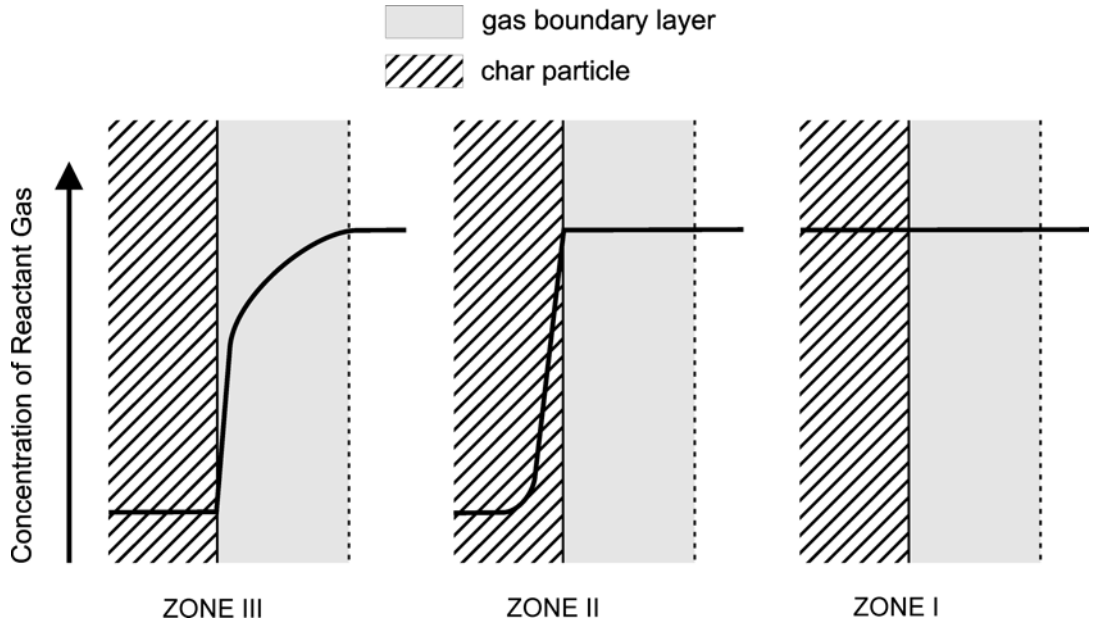

Figure 2.33 Oxygen concentration profile in the char particle and its proximity (gas boundary layer); changes with different oxidation regimes [59].

the char particle nor internal diffusion of O_2 through the pores influences the burning rate. The kinetics of the chemical reaction determines the overall rate and the whole internal and external (very low compared to the internal because of the porous nature of the char) surface areas of the particle are exposed to the same concentration (partial pressure) of O_2, equal to the bulk concentration. In regime I the effectiveness factor η, which can be seen as a measure of how far the

reactant gas diffuses into the porous particle before reacting, is 1, i.e. oxygen fully penetrates into the particle.

Regime II: the overall burning rate is controlled by chemical reaction (between carbon and oxygen) as well as by diffusion of reactant (O_2) through the pores. The rate of diffusion of O_2 through the pores of the char particle is of the same order as the intrinsic reaction rate, which leads to a concentration gradient of O_2 in the particle. In these conditions the effectiveness factor decreases, describing the fact that not all of the internal surface area of the char is reacting with oxygen at the same rate.

Regime III: the overall burning rate is controlled by the diffusion of reactant O_2 from the bulk phase to the external surface of the char particle. The reactivity of the char is thus high enough to consume all the oxygen at the external surface of the particle and no internal diffusion occurs.

At the high temperatures of a pulverised fuel furnace it is most likely that the char particles burn under regime II and III, especially at the beginning of the conversion. As conversion proceeds, both particle size and particle temperature (burning rate) decrease; thus, at higher levels of burnout burning under regime I, i.e. kinetic control, can be attained. Important parameters in determining in which regime the combustion of the char proceeds are char density and porosity and particle size [61], together with bulk temperature and intrinsic reactivity of the char (which in turn depends on catalytic impurities and active sites concentration).

2.5.2 REACTION MECHANISM

The kinetics of char oxidation has been studied by many authors [37,62,63,64,88,89,90]. Hurt and Calo [91] proposed a reaction mechanism that explains the observed trends in experimental data from many authors, yet being simple enough to be used in char combustion models. This is a three-step semi-global mechanism whose simple rate law describes the major trends in reaction order, activation energy, and CO/CO_2 ratio from 600 to 2000 K. They define semi-global kinetics as those comprising more than one explicit reaction step; the steps themselves are not necessarily elementary. Intrinsic kinetics are defined as those not influenced by transport processes.

The first step in char oxidation is the adsorption of oxygen to the carbon surface; subsequently, oxygen forms intermediate complexes and, finally, the gaseous products CO and CO_2 are formed and desorb. As discussed before, the carbon atoms that constitute the carbonaceous matrix of the char do not have the same stability and reactivity; depending on which active sites the oxygen

attaches to, various complexes can be formed that also have different stability and reactivity. These oxide complexes, like all surface species, can migrate, diffuse and interact with one another; they can also react with molecular gaseous oxygen [90,91].

The three-step model developed by Hurt and Calo [91] includes reaction between gaseous oxygen and surface complex, C(O). This reaction was shown by Hurt and Calo [91] to enable the description of the high reaction orders in the low temperature Zone I regime observed by various authors: a summary of the global kinetic parameters found in recent literature is given in Table 2.12, from Hurt and Calo [91].

Table 2.12 Global intrinsic kinetic parameters observed in atmospheric char combustion. After Hurt and Calo [91].

	Low temperatures (600–800 K)	*High temperatures (1200–1700 K)*
Global reaction order, n	0.6–1.0	0 (with some reports of 1st order)
Global activation energy, E[a]	105–180 kJ/mol (many: 130–150 kJ/mol)	105–180 kJ/mol

a) Excluding pure, highly heat treated carbons.

In order to explain the data of Table 2.12 and the fact that at higher temperatures, i.e. above 1700 K, the observed reaction order increases again to 1 (since the reaction becomes controlled by adsorption) [91], Hurt and Calo use the following reactions:

$$C + O_2 \rightarrow 2C(O) \quad \text{(R1)}$$

$$C(O) + O_2 \rightarrow CO_2 + C(O) \quad \text{(R2)}$$

$$C(O) \rightarrow CO \quad \text{(R3)}$$

In this model, which does not try to give a detailed description of the elementary processes of char oxidation, R2 may not only represent the direct interaction between gaseous oxygen and a surface complex, but also the attack of sites adjacent to an existing complex resulting in complex destabilisation and rapid desorption of CO_2 (which makes R2 first order in gaseous O_2).

The unbalanced stoichiometry of R1-R3 is a consequence of the choice of not describing all the elementary steps involved [91]. Hurt and Calo [91] assume that both R1 and R2 are first order in free active sites, although, depending of the elementary steps, they could be either first or second

order in free surface sites; they consider this assumption not critical for the purpose of getting a semi-global kinetics that can be used in combustion models.

The resulting rate laws and the parameters values used by Hurt and Calo [91] are presented in Table 2.13.

Table 2.13 Rate laws for the mechanism proposed by Hurt and Calo [91].

	Rate Laws	*Model Parametres*
R1	$r_1 = k_1 \cdot P_{O2} \cdot (1-\theta^a)$	$A_1 = 3.3 \cdot 10^{-4}$ bar^{-1}, $E_1 = 35$ kJ/mol.
R2	$r_2 = k_2 \cdot P_{O2} \cdot \theta$	$A_2 = 5.7 \cdot 10^{-4}$ bar^{-1}, $E_2 = 130$ kJ/mol
R3	$r_3 = k_3 \cdot \theta$	$A_3 = 1.0$, $E_3 = 180$ kJ/mol

a) θ is the fraction of sites occupied by complex.

The laws in Table 2.13 can be combined to yield the steady state expression for overall gasification rate and primary CO/CO_2 ratio:

$$r_{gas} = \frac{k_1 \cdot k_2 \cdot P_{O_2}^2 + k_1 \cdot k_3 \cdot P_{O_2}}{k_1 \cdot P_{o_2} + k_3 / 2} \tag{2.6}$$

$$CO/CO_2 = \frac{k_3}{k_2 \cdot P_{O_2}} \tag{2.7}$$

The ratio of the produced CO to the produced CO_2 is an important parameter to be considered when predicting the burnout time. Unfortunately, the empirical expressions for determining the ratio CO/CO_2 give significantly different results, as can be inferred from Table 2.14 and Figure 2.34. The parameters in Table 2.14 and the curves in Figure 2.34 refer to equation (2.8), which is the usual way of representing the dependence of the ratio CO/CO_2 on the particle temperature (A is a pre-exponential factor independent of temperature):

$$\frac{CO}{CO_2} = A P_{O_{2,s}}^n \exp\left(-\frac{B}{T}\right) \tag{2.8}$$

The ratio CO/CO_2 at the surface of a burning char particle can differ several orders of magnitude (see Figure 2.34). According to Zeng and Fu [65] the wide gap existing among these values may partly result from the fact that all these parameters are in fact averages of values of CO and CO_2 measured in a discrete time interval. Since the oxygen concentration at the surface of a particle varies during combustion, changes in the ratio CO/CO_2 occur as well; they suggest that in order to

Table 2.14 Summary of results for the ratio CO/CO_2. (see equation (2.8))

Ref.	*Material*	*System*	*Temperature (K)*	P_{O2} *(bar)*	*A* (bar^{-n})	*B (K)*	*n (-)*
[66]	Highly pure carbon	Pressurised thermobalance	900-1600	0.4-4	600	8000	-0.24
[66]	Natural graphite coal char	Flow system + $POCL_3$	730-1170	0.05-0.25	2500	6240	0
[67]	Spherocarb	EDB	670-1670	0.05-1.0	0.02	3000	-0.21
[68]	Vitreous carbon	Flow system	770-920	0.25-0.15		2000	-0.18
[69]	Graphon	Static system	800-950	$0.013 \cdot 10^{-3}$- $0.26 \cdot 10^{-3}$		3200	-0.22
[70]	Coal char	Laminar-flow reactor	1500-2000	0.06-0.12	$4 \cdot 10^4$	30000	0
[71]	Bass-wood char	Flow system	1050-1350	0.21	4.3	3390	0
[72]	Almond shell char	Laminar flow reactor	1200	0.06-0.12	$10^{4.4}$	8020	0

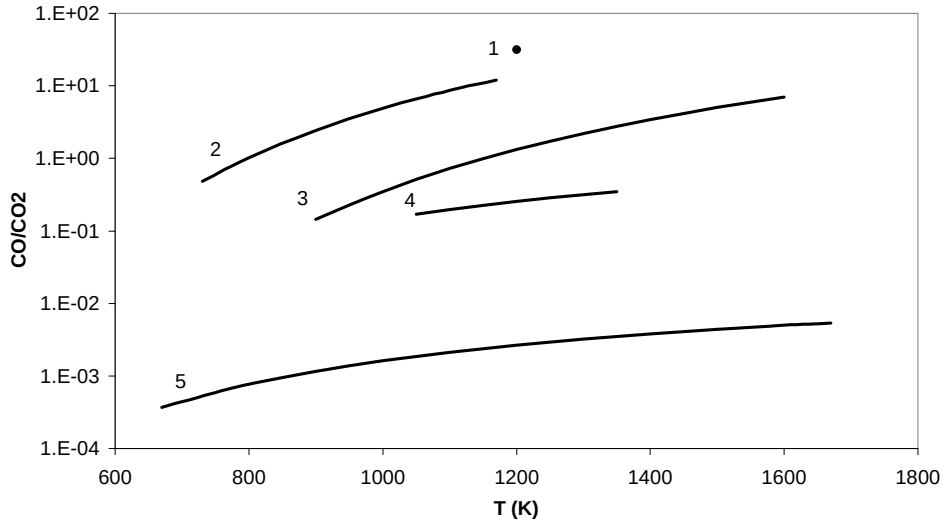

Figure 2.34 Comparison of literature data on CO/CO_2 ratio during combustion of different chars. The curves are obtained by using data of Table 2.14 in equation 2.8. Point 1, almond shell char [73]; curves: 2, natural graphite coal char [67]; 3, highly pure carbon [66]; 4, bass-wood char [72]; 5, Spherocarb [68].

have a more precise assessment of the ratio CO/CO2 at the surface of a burning particle the concentrations should be determined instantaneously [66]. The difficulty in measuring these gas concentrations at the surface of a burning particle is also related to the occurrence of homogeneous gas phase oxidation of CO to CO_2.

As can be seen, most of the results in Table 2.14 refer to either pure carbon particles or coal chars. Only very few expressions for the production ratio of CO to CO_2 from a biomass were found in literature [71,72].

2.5.3 INTRINSIC REACTIVITY AND ACTIVE SURFACE AREA

The expression "intrinsic reactivity" refers to the rate of reaction based on the internal surface area of the char particle in the absence of transport limitations. It has already been mentioned that the internal surface area of the char is much greater than its external surface area, because of its porous structure. The structure and dimensions of the pores determine, together with the total porosity, the Total Surface Area (TSA) of the particle. As the carbon is consumed by the reaction with oxygen, the pores tend to become larger and, initially, the TSA increases. At higher conversions, though, the TSA eventually reaches a maximum value [34], after which some of the pores merge so that some of the area is lost.

Not all of the surface area will react in the same way with oxygen: the reaction will preferentially occur on active sites such as defects and edge carbon atoms. A measure of the concentration of the active sites on the internal surface of the particle is given by the ratio between Active Surface Area (ASA) and TSA.

Models of char conversion need to take the development of the available surface area during conversion into account. The description of the changes in available surface area will depend on the assumed pore model; different pore structures evolve differently during char conversion and it is the behaviour of the pores which brings about the changes in available surface area. Table 2.15 shows how the variation in available surface area is expressed depending on the choice of pore model for some pore models found in literature. In Table 2.15, X is the conversion, S(X) the available surface area at a certain conversion and S_0 the available surface area of the original char prior to oxidation.

As previously mentioned, some of the metals present in the char catalyze the oxidation reaction. Changes in appearance, total concentration and distribution of the catalysts during conversion will obviously affect the intrinsic rate of reaction.

Table 2.15 Pore models. After Janse *et al.* [37].

Pore Model	*Model Equation*	*Parameters*
Power-law (grain) model [73]	$\frac{S(X)}{S_0} = (1-X)^n$	*n*: no physical meaning
Pore tree model [74]	$\frac{S(X)}{S_0} = (1-X)\sqrt{\frac{X}{\varepsilon_0} + (1-X)}$	ε_0: initial porosity
Random pore model [75, 76]	$\frac{S(X)}{S_0} = (1-X)\sqrt{1-\varphi \ln(1-X)}$	$\varphi = \frac{B_0}{2\pi B_1^2}$ B_0: total pore length per unit volume. B_1: total pore surface per unit volume.
Bifurcated pore model [77]	$\frac{S(X)}{S_0} = (1-X)\sqrt{1-\frac{1}{\ln(\frac{1}{1-\varepsilon_{micropore,0}})}\ln(1-X)}$	$\varepsilon_{micropore,0}$: initial micropore porosity

2.5.4 KINETICS OF THERMAL DEACTIVATION

Char reactivity decreases as the char is subjected to increasing temperatures; this is known as thermal deactivation.

One of the available models of thermal deactivation is that proposed by Hurt *et al.* [78]. In this model the sites on the surface of the char deactivate according to a first order thermal process:

$$\frac{dN}{dt} = -A_d N \exp(-E_d / RT) \qquad (2.9)$$

The actual number of sites at a given time is unknown, and the deactivation is expressed as the ratio N/N_0 of the total number of sites (N) to the number of sites at time zero (N_0). A_d is the pre-exponential factor (s^{-1}), E_d the activation energy for annealing (kJ/mol), R the gas constant and T the absolute temperature. The sites are assumed to deactivate with a common pre-exponential factor and a distribution of activation energies:

$$N / N_0 = \int_0^\infty F(t, E_d) dE_d \qquad (2.10)$$

$F(E_d)$ is the frequency function and in the model of Hurt *et al.* [78] it represents a log-normal distribution of activation energies.

Zolin *et al.* [79] applied this model to their data obtained by oxidation of char in a TGA apparatus. They modify the model slightly by using a Γ distribution (instead of a log-normal) for the activation energies of the annealing reaction; also, they introduced a lower bound for the activation energy in order to describe the fact that deactivation of the char does not start until a temperature of about 400ºC (for coal chars) is reached. This lower limit is expressed by shifting the Γ distribution of activation energies [79]:

$$f(E_d) = \frac{(E_d - \delta)^{(\alpha-1)}}{\Gamma(\alpha)\beta^{\alpha}} \exp(-\frac{(E_d - \delta)}{\beta}) \qquad (2.11)$$

where δ is a shift parameter indicating the origin of $f(E_d)$. The mean activation energy and variance are simple functions of α and β ($E_{d,m} = \delta + \alpha\beta$ and $\boldsymbol{\sigma}_d^2 = \alpha\beta^2$). Zolin *et al.* [79] introduced in their model a lower limit for char reactivity corresponding to the reactivity of commercial graphite: indeed, the active sites of a char are deactivated, not destroyed, and in theory as the char deactivates it approaches the structure and reactivity of graphite.

The model used by Zolin *et al.* [79] provided good agreement with experimental data for oxidation of chars from coal and from leached straw. Zolin *et al.* used char produced in a TGA to assess the values of the parameters in the model; they then showed that the model with these parameters could predict with reasonable accuracy the thermal deactivation of chars produced in other reactors at much higher heating rates and temperatures.

This model could be tested for wood char, provided that the lower limit for the reactivity is not set (as for coals) equal to the reactivity of graphite, since wood char would not attain such levels of order (i.e. such low reactivity) even at very high conversion.

Another model that describes thermal annealing was developed by Salatino *et al.* [80]: this model takes into account the dependence of thermal deactivation on the length of the time interval of heat treatment. The model was applied to the study of the reactivity of a bituminous coal char relative to gasification reaction with carbon dioxide [80]. It is assumed that the reactivity of the char at any moment during heat treatment can be expressed as a linear combination of the reactivity of the non deactivated char and the reactivity of the completely deactivated char. The parameter ξ, which represents the fraction of annealed char, assumes the values ξ=0 for the fresh char and ξ=1 for the totally annealed char:

$$R = R_0(1-\xi) + R_\infty \xi \tag{2.12}$$

where R is the gasification reactivity, R_0 the reactivity of the fresh char and R_∞ is the reactivity of the fully annealed char. The model further assumes that $R_\infty << R_0$. At the temperature T_{HT} the rate at which ξ changes with time is expressed by the following nonlinear kinetic equation:

$$\frac{d\xi}{dt} = k(T_{HT})(1-\xi)^n \tag{2.13}$$

The rate constant k follows an Arrhenius dependency on temperature:

$$k(T_{HT}) = k_0 \exp\left(-\frac{E_a}{RT_{HT}}\right) \tag{2.14}$$

Integrating between time 0 and the time of heat treatment t_{HT} and assuming that the reaction occurs at constant temperature the model gives the following expression for the deactivation ratio:

$$\frac{R(T_R)}{R_0(T_R)} = 1^{-\frac{1}{(n-1)}} + \left([(n-1)k(T_{HT})]^{-\frac{1}{(n-1)}}\right) t_{HT}^{-\frac{1}{(n-1)}} \tag{2.15}$$

2.6 CONCLUSIONS

Wood is a very heterogeneous fuel. Hardwood and softwood have different structures and, more importantly with respect to combustion, different compositions (the higher content of lignin in softwood will be shown to have an impact on wood char formation in Chapter 4).

The main relevant features of wood as a fuel are its high volatile fraction, the high content of O_2 and the low amount of ash, which is usually below 1 wt%.

Wood pyrolysis yields a varying amount of char depending on pyrolysis conditions and wood type. Both higher pyrolysis temperature and higher heating rate lead to a lower char yield. Another factor that influences the pyrolysis process is the amount and composition of mineral matter in the wood, which can catalyze tar cracking and repolymerisation, thereby increasing the yield of char. Various models that describe wood pyrolysis have been presented.

The morphology of wood char is influenced by pyrolysis conditions as well as parent wood type. Generally, wood char is considered to retain the structure of the wood fuel; this is certainly true when pyrolysis is carried out at low temperatures and heating rates; however, few authors suggest

that as pyrolysis becomes more severe the structure of the char deviates from the one of wood, possibly going through plastic deformation during pyrolysis at conditions similar to those found in a pulverised fuel boiler. More detailed knowledge about pulverised fuel char morphology may allow a better understanding and modelling of the pulverised wood combustion process.

As far as char reactivity is concerned, the available data show that wood char is more reactive than coal char, due to its higher oxygen content and possibly its less ordered structure. Nevertheless, there is poor agreement among biomass char reactivity data, the majority of which were assessed for char produced at much milder conditions than those of pulverised combustion.

A semi-global mechanism for the char oxidation reaction was presented, as well as various models describing the evolution of char surface area during combustion and char thermal deactivation.

The role of oxidation reactivity, gas film diffusion and pore diffusion during char combustion was presented; a particle combustion model must take them all into account since at different stages one or more of them can control the particle burning rate. A more detailed review of combustion models is given in Chapter 5.

REFERENCES

1. Kramer P. J. and Kozlowski T. T., Physiology of woody plants, Academic Press, 1979
2. Pedersen R. S., Residual ash formation during combustion of woody biomass, M. Sc. Thesis, DTU, 2003
3. Pacific Union College, www.puc.edu/Faculty/Gilbert_Muth/botlec04.htm
4. Siau J. F., Transport processes in wood, Springer-Verlag Series in Wood Science, 1984
5. Butterfield, B. G. and Meyland, B. A., Three dimensional structure of wood, an ultrastructure approach, Chapman and Hall, 1980
6. Ehrburger, P. and Lahaye, J., Effect of carbonization on the porosity of beechwood, Carbon, 1982, 20, 433
7. Grønli M., A theoretical and experimental study of the thermal degradation of biomass, Ph.D. thesis, NTNU, 1996
8. Wenzel H.F.J., The chemical Technology of wood, Academic Press, New York, 1970, pp 92-101
9. Skorupska N.M., Coal specifications – impact on power station performance, IEACR/52, IEA Coal Research, London, 1993
10. Skodras G., Grammelis P., Kakaras E. and Sakellaropoulos G.P., Evaluation of the environmental impact of waste wood co-utilization for energy production, Energy, 2004, 29, 2181
11. Öhman M., Boman C., Hedman H., Nordin A. and Boström D., Slagging tendencies of wood pellet ash during combustion in residential pellet burners, Biomass and Bioenergy, 2004, 27, 585
12. Chen Y., Charpenay S., Jensen A., Wójtowicz M.A. and Serio M.A., Modeling of biomass pyrolysis kinetics, Twenty-Seventh Symposium (International) on Combustion, The Combustion Institute, 1998, 1327
13. Bridgwater A.V., Principles and practice of biomass fast pyrolysis processes for liquids, Journal of Analytical and Applied Pyrolysis, 1999, 51, 3
14. Svenson J., Pettersson J.B.C. and Davidsson K.O., Fast pyrolysis of the main components of birch wood, Combustion Science and Technology, 2004, 176, 977
15. Biagini E., Fantozzi C. and Tognotti L., Characterization of devolatilization of secondary fuels in different conditions, Combustion Science and Technology, 2004, 176, 685
16. Rath J., Wolfinger M.G., Steiner G., Krammer G., Barontini F. and Cozzani V., Heat of wood pyrolysis, Fuel, 2003, 82, 81
17. Stenseng M., Jensen A. and Dam-Johansen K., Investigation of biomass pyrolysis by thermogravimetric analysis and differential scanning calorimetry, Journal of Analytical and Applied Pyrolysis, 2001, 58-59, 765
18. Milosavljevic I., Oja V. and Suuberg E.M., Thermal effects in cellulose pyrolysis: relationship to char formation proceses, Ind. Eng. Chem. Res., 1996, 35, 653
19. Grønli M., Antal M.J. and Várhegyi G., A Round-Robin study of cellulose pyrolysis kinetics by thermogravimetry, 1999, Ind. Eng. Chem. Res., 38, 2238
20. Nik-Azar M., Hajaligol M.R., Sohrabi M. and Dabir B., Mineral matter effects in rapid pyrolysis of beech wood, Fuel Processing Technology, 1997, 51, 7
21. Zanzi R., Sjöström K. and Björnbom E., Rapid high-temperature pyrolysis of biomass in a free-fall reactor, Fuel, 1996, 75, 545
22. Müller-Hagedorn M., Bockhorn H., Krebbs L. and Müller U., Investigation of thermal degradation of three wood species as initial step in combustion of biomass, Twenty-Ninth Symposium (International) on Combustion, The Combustion Institute, 2002, 399
23. Di Blasi C. and Branca C., Kinetics of primary product formation from wood pyrolysis, Ind. Eng. Che. Res., 2001, 40, 5547
24. Cordero T., García F. and Rodríguez J.J., 1989, A kinetic study of holm oak wood pyrolysis from dynamic and isothermal TG experiments, Termochimica Acta, 149, 225
25. Cozzani V., Lucchesi A., Stoppato G. and Maschio G., 1997, A new method to determine the composition of biomass by thermogravimetric analysis, The Canadian Journal of Chemical Engineering, 75, 127
26. Nik-Azar M., Hajaligol M.R., Sohrabi M., Dabir B., 1996, Effects of heating rate and particle size on the product yields from rapid pyrolysis of beech wood, Fuel Science and Technology Int'l, 14, 479
27. Chan W.-C.R. and Krieger B.B., Analysis of chemical and physical processes during devolatilization of a single, large particle of wood, 1982, ACS Symposium Series 196, 459
28. Chan W.-C.R., Kelbon M. and Krieger B.B., Modelling and experimental verification of physical and chemical processes during pyrolysis of a large biomass particle, Fuel, 1985, 64, 1505
29. Stenseng M., Pyrolysis and Combustion of Biomass, 2001, Ph. D. Thesis, Department of Chemical Engineering, Technical University of Denmark
30. Grønli M. G. and Melaaen M. C., Mathematical model for wood pyrolysis-comparison of experimental measurements with model predictions, Energy and Fuels, 2000, 14, 791

31. Hastaoglu M. A. and Al-Khalid T.T., Treatment of wood pyrolysis data via a multiple gas-solid reaction model, Ind. Eng. Chem. Res., 2001, 40, 1845
32. Senneca O., Chirone R., Masi S. and Salatino P., A thermogravimetric study of nonfossil solid fuels.1, Energu & Fuels, 2002, 16, 653
33. Órfão J. J. M., Antunes F.J.A. and Figueiredo J.L., Pyrolysis kinetics of lignocellulosic materials- three independent reactions model, Fuel, 1999, 78, 349
34. Smith I. W., The combustion rates of coal chars: a review, Nineteenth Symposium (International) on Combustion, The Combustion Institute, 1982, pp 1045-1065
35. Wornat, M. J., Hurt R.H., Davis K.A. and Yang N.Y.C., Single-particle combustion of two biomass chars, Twenty-Sixth Symposium (International) on Combustion, The Combustion Institute, 1996, 3075
36. Branca C. and Di Blasi C., Global kinetics of wood char devolatilization and combustion, Energy & Fuels, 2003, 17, 1609
37. Janse A. M. C., de Jonge H.G., Prins W. and van Swaaij W.P.M., Combustion kinetics of char obtained by flash pyrolysis of pine wood, Industrial and Engineering Chemistry Research, 1998, 37, 3909
38. IUPAC Manual of Symbols and Terminology, 1972
39. Wildman J. and Derbyshire F., Origins and functions of macroporosity in activated carbons from coal and wood precursors, Fuel, 1991, 70, 655
40. Cetin E., Moghtaderi B., Gupta R. and Wall T.F., Influence of pyrolysis conditions on the structure and gasification reactivity of biomass chars, Fuel, 2004, 83, 2139
41. Jensen A., Dam-Johansen K. , Wjtowicz M. A. and Serio M. A., TG-FTIR Study of the Influence of Potassium Chloride on Wheat Straw Pyrolysis, Energy Fuels, 1998, 12 (5), 929
42. Davidsson K.O. and Pettersson J.B.C., Birch wood particle shrinkage during rapid pyrolysis, Fuel, 2002, 81, 263
43. Klose W. and Schinkel A., Measurement and modeling of the development of pore size distribution of wood during pyrolysis, Fuel Processing Technology, 2002, 77-78, 459
44. Pastor-Villegas J., Durán-Valle C.J., Valenzuela-Calahorro C. and Gómez-Serrano V., Organic chemical structure and structural shrinkage of chars prepared from rockrose, Carbon, 1998, 36 (9), 1251
45. Byrne C. E. and Nagle D. C., Carbonized wood monolith-characterization, Carbon, 1997, 35(2), 267
46. Kumar M. and Gupta R. C., Scanning electron microscopic study of acacia and eucalyptus wood chars, Journal of Material Science, 1995, 30, 544
47. Gergova K., Petrov N. and Eser S., Adsorption properties and microstructure of activated carbons produced from agricultural by-products by steam pyrolysis, Carbon, 1993, 32(4), 693
48. Wan Daud W. M. A. and Wan Ali W. S., Comparison on pore development of activated carbon produced from palm shell and coconut shell, Bioresource Technology, 2004, 93, 63
49. Pastor Villegas J., Valenzuela-Calahorro C., Bernalte-Garcia A. and Gomez-Serrano V., Characterization study of char and activated carbon prepared from raw and extracted rockrose, Carbon, 1993, 31, 1061
50. Bailey J. G., Tate A., Diessel C.F.K. and Wall T.F., A char morphology system with applications to coal combustion, Fuel, 1990, 69, 225
51. Zolin A., Reactivity of solid fuels, 2001, Ph.D. Thesis, Department of Chemical Engineering, Technical University of Denmark
52. Davis K. A., Hurt R.H., Yang N.Y.C. and Headley T.J., Evolution of char chemistry, cristallinity, and ultrafine structure during pulverized-coal combustion, Combustion and Flame, 1995, 100, 31
53. Zhang X., Dukhan A., Kantorovich I.I., Bar-Ziv E., Kandas A. and Sarofim A.F., Structural changes of char particles during chemically controlled oxidation, Twenty-Sixth Symposium (International) on Combustion, The combustion Institute, 1996, 3111
54. Beeley T., Crelling J., Gibbins J., Hurt R.H., Lunden M., Man C., Williamson J. and Yang N., Transient high-temperature thermal deactivation of monomaceral-rich coal chars, Twenty-Sixth Symposium (International) on Combustion, The combustion Institute, 1996, 3103
55. Senneca O., Russo P., Salatino P. and Masi S., The relevance of thermal amnnealing to the evolution of coal char gasification reactivity, Carbon, 1997, 35, 141
56. Mitchell R. E. and Akanetuk A. E. J., The impact of fragmentation on char conversion during pulverized coal combustion, Twenty-Sixth Symposium (International) on Combustion, The combustion Institute, 1996, 3137
57. Wornat M. J., Hurt R.H., Yang N.Y.C. and Headley T.J., Structural and compositional transformations of biomass chars during combustion, Combustion and Flame, 1995, 100, 131
58. Frandsen F.J., Moiraghi L and van Lith S., 1st Annual Report, EU project SES6-CT-2003-502679, Ash and aerosol related problems in biomass combustion and co-firing, 2005
59. Marsh H., Introcution to carbon science, 1989, Butterworths & Co

60. Feng B. and Bhatia S. K., Percolative fragmentation of char particles during gasification, Energy and Fuels, 2000, 14, 297
61. Hurt R. H., Structure, properties and reactivity of solid fuels, Twenty-Seventh Symposium (International) on Combustion, The combustion Institute, 1998, 2887
62. Haynes B. S. and Newbury T. G., Oxyreactivity of carbon surface oxides, Twenty-Eighth Symposium (International) on Combustion, The combustion Institute, 2000, 2197
63. Haynes B. S., A turnover model for carbon reactivity I. Development, Combustion and Flame, 2001, 126, 1421
64. Laurendau N. M., Heterogeneous kinetics of coal char gasification and combustion, Prog. Energy Combust. Sci., 1978, 4, 221
65. Zeng T. and Fu W.B., The ratio CO/CO2 of oxidation on a burning carbon surface, 1996, Combustion and Flame, 107, 197
66. Arthur J., 1951, Trans.Faraday Soc., 47, 164
67. Tognotti L., Longwell J.P. and Sarofim A.F., The products of the high temperature oxidation of a single char particle in an electrodynamic balance, Twenty-Third Symposium (International) on Combustion, The combustion Institute, 1990, 1207
68. Otterbein M. and Bonnetain C., Combustion d'un carbone vitreux sous basses pressions d'oxygene, 1968, Carbon, 6, 877
69. Philips R., Vastola F.J. and Walker P.L. Jr, The effect of oxygen pressure and carbon burn-off on the product ratio of the carbon-oxygen reaction, 1970, Carbon, 7, 479
70. Hurt R. and Mitchell R. E., Unified high-temperature char combustion kinetics for a suite of coals of various rank, Twenty-Fourth Symposium (International) on Combustion, The combustion Institute, 1992, 1243
71. Evans D.D. and Emmons H.W., Combustion of wood charcoal, 1977, Fire Research, 1, 57
72. Campbell P.A., Mitchell R.E. and Ma L:, Characterization of coal char and biomass char reactivities to oxygen, Twenty-Nineth Symposium (International) on Combustion, The combustion Institute, 2002, 519
73. Kristiansen A., Understanding coal gasification, 1995, IEA Coal Research, London
74. Simons G.A. and Finson M.L., The structure of coal char: Part I. Pore branching,1979, Combustion Science and Technology, 19,217
75. Bhatia S.K. and Perlmutter D.D., A random pore model for fluid-solid reactions: I.isothermal, kinetic control.,1980, AIChE J, 26, 379
76. Gavalas G.R., A random capillary model with application to char gasification at chemically controlled rates. AIChE J, 1980, 26, 577
77. Tseng H.P. and Edgar T.F., The change of physical properties of coal char during reaction, 1989, Fuel, 68, 114
78. Hurt R., Sun J.-K and Lunden M., A kinetic model of carbon burnout in pulverized coal combustion, 1998, Combustion and Flame, 113, 181
79. Zolin A., Jensen A. and Dam-Johansen K., Kinetic analysis of char thermal deactivation, Twenty-Eighth Symposium (International) on Combustion, The combustion Institute, 2000, 2181
80. Salatno P., Senneca O. and Masi S., Assessment of thermodeactivation during gasification of a bituminous coal char, 1999, Fuel, 13, 1154
82. Mc Carthy D.J., Changes in oxyreactivity of carbons due to heat treatment and prehydrogenation, 1981, Carbon, 19, 297
83. Burggraaf R. And Prins W., Reaction kinetics of graphite and wood char, Unpublished results, Twente University, 1983
84. Magnaterra M.R., Cukierman A.L., Lemcoff N.O., Kinetic study of combustion of cellulose and a hardwood species char, 1989, Latin Amarican Applied Research, 19, 61
85. Magnaterra M.R., Fusco J.R., Ochoa J., Cukierman A.L., Kinetic study of the reaction of different hardwood sawdust char with oxygen. Chemical and structural characterization of the samples. In *Proceedings in Advances in thermochemical biomass conversion*, Bridgwater A.V., 1992, Blackie Academic and Professional, London
86. Kashiwagi T. and Nambu H., Global kinetic constants for thermal oxidative degradation of a cellulosic paper, 1992, Combustion and Flame, 88, 345
87. Zolin A., Jensen D.A., Dam-Johanden K., Coupling thermal deactivation with oxidation for predicting the combustion of a solid fuel, Combustion and Flame, 2001, 125, 1341
88. Hayhurst A.N. and Parmar M.S., Does solid carbon burn in oxyfen to give the gaseous intermediate CO or produce CO_2 directly? Some experiments in a hot bed of sand fluidized by air, Chemical Engineering Science, 1998, 53, 427
89. Hurt R.H. and Haynes B.S., On the origin of power-law kinetics in carbon oxidation, Thirtieth Symposium (International) on Combustion, 2005, The combustion Institute, 2161

90. Campbell P.A. and Mitchell R.E., The impact of the distributions of surface oxides and their migration on characterization of the heterogeneous carbon-oxygen reaction, 2008, Combustion and Flame, 154, 47
91. Hurt R.H. and Calo J.M., Semi-global intrinsic kinetics for char combustion modeling, 2001, Combustion and Flame, 125, 1138

CHAPTER 3

FULL SCALE PULVERISED WOOD COMBUSTION

3.1 INTRODUCTION

An extensive measurement campaign was carried out, in cooperation with DONG Energy A/S, at Avedøreværket's Boiler Unit AVV2 to investigate wood suspension combustion characteristics in a full size boiler. The boiler is a 800 MWth, once through suspension fired boiler where oil, pulverised wood and natural gas are co-fired, with a net electrical efficiency of up to 49% [1]. Wood pellets can be pulverised by up to 3 mills. The maximum feed rate for the wood pellets is equivalent to 70 % of the full load of the boiler [2]. A short description of the unit is given in Chapter 1.

Measurements on the following parameters were performed: emission of NO_x, SO_2 and CO; deposit formation and ash composition; influence of wood pellet mills on obtained particle size; burnout of the wood fuel; flame temperatures. Different combinations of fuels were tested under different operating conditions, as shown in Table 3.1. During the last day of the campaign coal ash was added to the fuels in order to test its effect on deposit formation and deposits composition (coal ash can act as absorbent for KCl).

Table 3.1 Combinations of fuels during the campaign.

	DAY 1	*DAY 2*	*DAY 3*	*DAY 4*	*DAY 5*
Fuel shares (%, thermal basis)	Wood: 51.3 Oil: 48.7	Wood: 49.6 Gas: 50.4	Wood: 51.7 Gas: 48.3	A) Wood: 46.8 Gas: 53.2 B) Wood: 23.5 Gas: 76.5	A) Wood: 49.4 Gas: 50.6 Coal fly ash B) Wood: 49.3 Oil: 50.7 Coal fly ash
Boiler load (%)	89	89	95	A)87 B)86	86

This chapter presents the results of the wood fuel characterisation (composition and size distribution) as well as particle burnout calculations and CO level at combustion chamber outlet. A comprehensive report on the measuring campaign is found in reference [3].

3.2 WOOD FUEL CHARACTERISATION

3.2.1 WOOD SAMPLING METHODS

The main boiler of Avedøre Unit AVV2 is a once-through suspension fired boiler (see Chapter 1). Four rows of corner multi-fuel burners (oil, gas, and wood fuel) deliver the fuel to the furnace (wood can be fed through the three lowest burners' levels). Wood arrives at the power plant in the form of pellets; typical pellets' dimensions are a diameter of about 8 mm and a length of 25 to 40 mm [4]. The wood pellets are opened by milling before the fuel is transported by hot air to the burners. Samples of wood were withdrawn at two different stages of the process, i.e. before and after a mill.

Wood pellets are fed to the mills through a feeder silo, a conveyor belt and a hopper. Figure 3.1 shows a sketch of the pellets sampling technique used before the mill; samples were withdrawn as the pellets left the conveyor belt and fell through the hopper towards the mill. Each sample consisted of approximately 3 kg of pellets. During the campaign two wood mills were in operation.

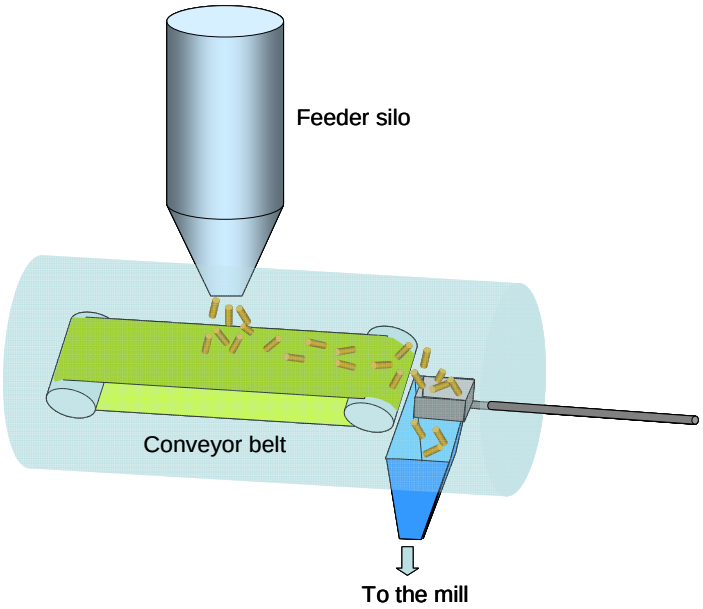

Figure 3.1 Sampling method for wood pellets before the mill.

During the five days of investigation, a total of 26 samples were collected (6 samples on each of Day 1, 4 and 5; 5 samples on Day 2 and 3 samples on Day 3).

In principle, as explained above, the wood appears in pellets before the mill; however, the samples collected showed a varying and at times major presence of wood powder already at this stage. The opening of the pellets may be caused by the handling process, for example by attrition in the feeder silos.

For each of the samples before the mill a corresponding sample after the mill was collected. These samples were taken isokinetically from the pipe through which preheated air transports the pulverised wood to the burners. Figure 3.2 shows the sampling method for the wood fuel: a probe was inserted in the pipe through a window in the pipe wall; the probe was connected at its end to a pump. Each sampling lasted 3 minutes, and in an attempt to get a more representative sample the probe was held at three different positions (one minute in each position, see Figure 3.2-b).

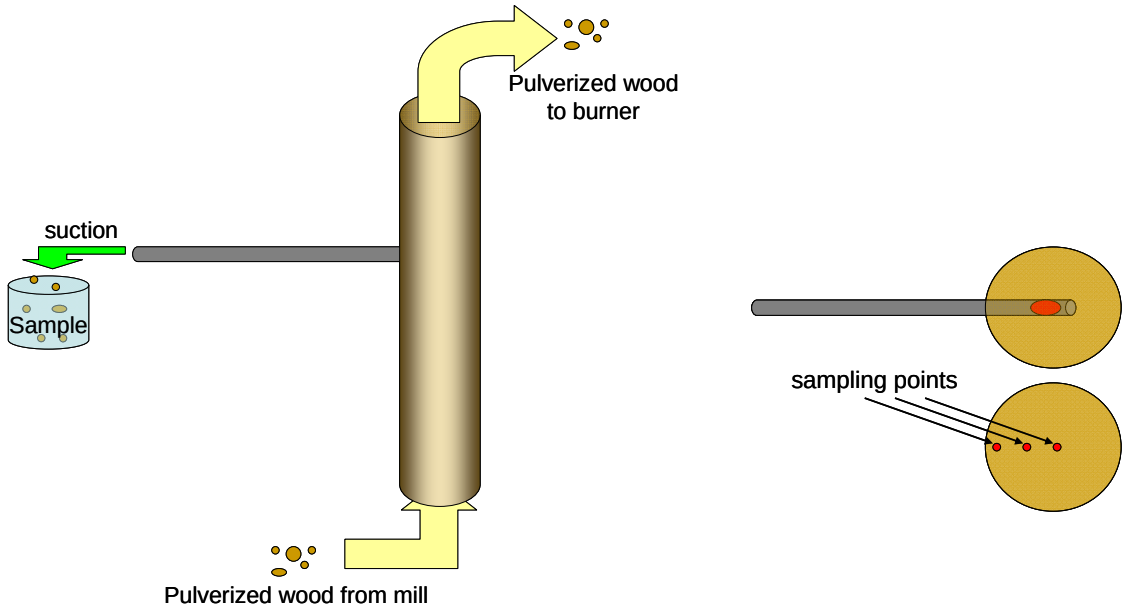

Figure 3.2 Sampling method for pulverised wood after the mill (a) and view from below (b).

Ten average samples (one from the samples before and one from the samples after the mill, for each campaign day) were prepared from the single samples and further analyzed with respect to composition and particle size distribution. The labelling of the samples is described in Table 3.2.

Table 3.2 Labeling of average samples.

	DAY 1	*DAY 2*	*DAY 3*	*DAY 4*	*DAY 5*
Samples before mill	Average_1_before	Average_2_before	Average_3_before	Average_4_before	Average_5_before
Samples after mill	Average_1_after	Average_2_after	Average_3_after	Average_4_after	Average_5_after

3.2.2 WOOD COMPOSITION

Samples Average_1_after to Average_5_after were analyzed at Enstedværket's laboratory. The results of the proximate and ultimate analysis are shown in Table 3.3.

Table 3.3 Proximate and ultimate analyses of the wood fuel.

	Units	Average 1 After	Average 2 After	Average 3 After	Average 4 After	Average 5 After
Total water	% as received	5.6 ± 0.2	5.8 ± 0.2	5.8 ± 0.2	5.8 ± 0.2	6.0 ± 0.2
Ash	%, d.b.[a]	0.9 ± 0.2	0.6 ± 0.2	0.6 ± 0.2	1.2 ± 0.2	1.0 ± 0.2
Volatile matter	%, d.b.	83.0 ± 1.7	83.3 ± 1.7	83.5 ± 1.7	82.8 ± 1.7	82.8 ± 1.7
Higher Heating Value	MJ/kg, d.b.	20.39 ± 0.12	20.45 ± 0.12	20.37 ± 0.12	20.32 ± 0.12	20.33 ± 0.12
Effective Heating Value	MJ/kg, d.b.	19.06 ± 0.12	19.11 ± 0.12	19.05 ± 0.12	19.00 ± 0.12	18.99 ± 0.12
C	%, d.b.	49.61 ± 0.25	50.49 ± 1.10	49.675 ± 0.04	49.11 ± 0.01	49.74 ± 0.20
H	%, d.b.	6.25 ± 0.05	6.32 ± 0.21	6.23 ± 0.01	6.25 ± 0.01	6.33 ± 0.07
N	%, d.b.	0.093 ± 0.001	0.082 ± 0.003	0.091 ± 0.002	0.104 ± 0.001	0.101 ± 0.003
S	%, d.b.	0.0143 ± 0.0008	0.00845 ± 0.0001	0.00835 ± 0.0011	0.0086 ± 0.0001	0.0078 ± 0.0003
Cl	%, d.b.	0.0043 ± 0.0004	0.0040 ± 0.0003	0.00405± 0.0004	0.00565 ± 0.0004	0.00575± 0.0001
Al	%, d.b.	0.014 ± 0.001	0.0090 ± 0.0009	0.010 ± 0.001	0.025 ± 0.003	0.020 ± 0.002
Ca	%, d.b.	0.14 ± 0.01	0.12 ± 0.01	0.12 ± 0.01	0.18 ± 0.01	0.16 ± 0.01
Fe	%, d.b.	0.013 ± 0.001	0.0085 ± 0.0009	0.0093 ± 0.0009	0.022 ± 0.002	0.016 ± 0.002
K	%, d.b.	0.048 ± 0.003	0.043 ± 0.003	0.044 ± 0.003	0.054 ± 0.003	0.049 ± 0.003
Mg	%, d.b.	0.024 ± 0.001	0.020 ± 0.001	0.021 ± 0.001	0.035 ± 0.002	0.030 ± 0.002
Na	%, d.b.	0.0045 ± 0.0005	0.0034 ± 0.0005	0.0034 ± 0.0005	0.0077 ± 0.0008	0.0071 ± 0.0007
P	%, d.b.	0.0058 ± 0.0008	0.0052 ± 0.0008	0.0052 ± 0.0008	0.0066 ± 0.0008	0.0053 ± 0.0008
Si	%, d.b.	0.17 ± 0.02	0.11 ± 0.01	0.10 ± 0.01	0.28 ± 0.03	0.20 ± 0.02
Ti	%, d.b.	0.00075±0.00038	<0.00053	<0.00053	0.0018 ± 0.0004	0.0012 ± 0.0004
Zn	mg/kg, d.b.	14 ± 1	13 ± 1	12 ± 1	14 ± 1	12 ± 1

a) Dry basis

As can be seen in Table 3.3 the composition of the wood was quite constant during the campaign; no large variations in composition were found among the different samples. The fuel composition was used to estimate the degree of burnout of the particles, as will be illustrated later.

Table 3.3 shows that the ash content of the fuel was between 0.6 and 1.2%, typical values for wood. The most abundant ash elements were Ca (0.12 - 0.18 % on a dry basis), Si (0.10 - 0.28 %), K (0.043 - 0.054 %), and Mg (0.020 - 0.035 %). The Cl content of the wood fuels was relatively low: if all of it was assumed to be present in the ashes, then the ashes would contain 0.5 to 0.7 wt% Cl. This element is important to be considered when analyzing power plant fuel because of its corrosive potential. However, no KCl was found in the deposits collected during the campaign [1].

3.2.3 PARTICLE SIZE DISTRIBUTION

The particle size distribution of the ten average samples in Table 3.2 was obtained by sieving.

To determine the distribution of the wood particles that made up the pellets before milling, samples Average_#_before were soaked in water. By doing this, the pellets disaggregated into their constituting wood particles. The particles were then dried in oven prior to sieving. One may think that dissolving the pellets in water could make the wood fibres swell. In order to assess the effect of the handling process, a sample of pulverised (after mill) wood was first sieved, then processed following the same procedure applied to the pellets, i.e. dissolved in water and dried in oven. The sample was then re-sieved. The results are shown in Figure 3.3; very little swelling seems to happen when water is added and its extent does not cause a significant shift in the distribution obtained by sieving. Moreover, by visual observation it was possible to exclude that aggregates were formed during the sieving of the wood.

Figure 3.4 to Figure 3.6 show the results of the sieving. Figure 3.4 shows that the samples before the mill contained a significant fraction of large wood particles (size interval 0.7 – 2 mm). Although this is a general feature, there are differences among the samples; for example, particles of nominal size between 1 and 2 mm make up about 33 % of the mass in sample Average_2_before and 23.5 % in samples Average_4_before and Average_5_before. The pellets fed to the mill during days 2 and 3 of the campaign seem to have had a higher mass fraction of particles larger than 1 mm (38.5 % compared to 26.5 - 29 %) and a significantly lower mass fraction of particles with nominal size smaller than 355 μm (16 % vs. 24 – 30 %).

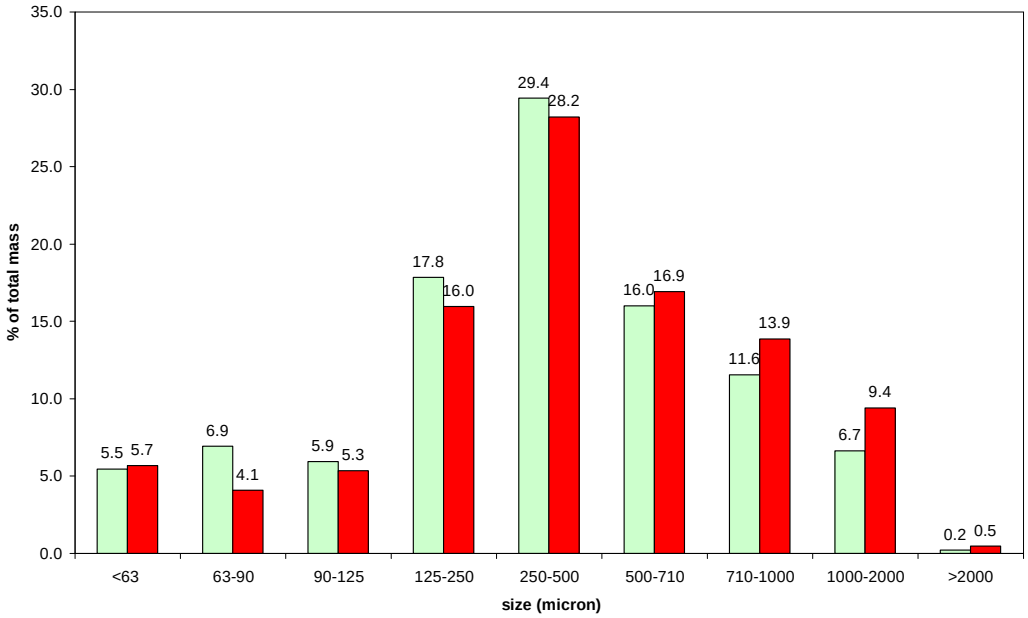

Figure 3.3 Effect of the handling method for opening the pellets (dissolution in water and subsequent drying in an oven). Green: untreated sample; red: re-sieved sample after handling.

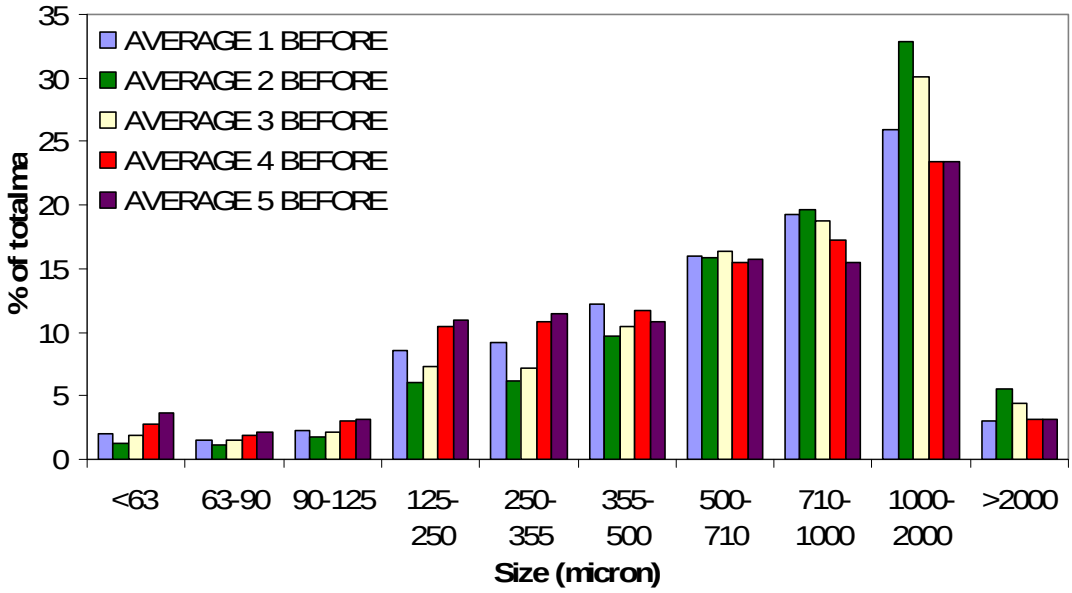

Figure 3.4 Particle size distributions of wood pellets before the mill obtained by sieving.

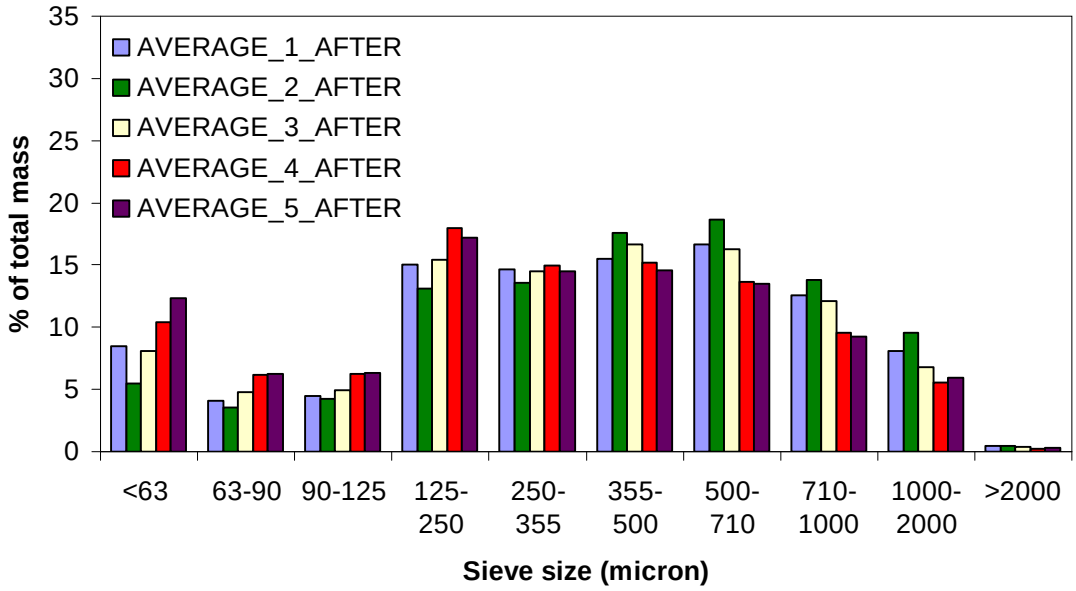

Figure 3.5 Particle size distributions of pulverised wood after the mill obtained by sieving.

In Figure 3.5 it is seen that some differences in particle size distribution were also present among the wood fuel samples (after milling). For instance, Average_2_after had a greater amount of larger particles than the rest of the samples, which is in accordance with the mass distribution of Average_2_before relative to the other pellets samples (Figure 3.4). Moreover, the fraction of mass made up by particles with nominal size below 90 micron varied from 9 % (Average_2_after) to about 19 % (Average_5_after).

The distribution of the wood fuel after the mill was different from that of the pellets: this is clearly seen in Figure 3.6, where the cumulative mass distributions for the pellets and the wood fuels are shown. It is important to highlight that the data relative to the finest fractions are somewhat less reliable than the rest, due to the fact that during the handling of the samples some of these particles may be lost. In fact, the cumulative mass curves of wood fuel samples (after mill) in Figure 3.6 follow very much the same trend, but with different starting points (mass% of particles smaller than 63μm).

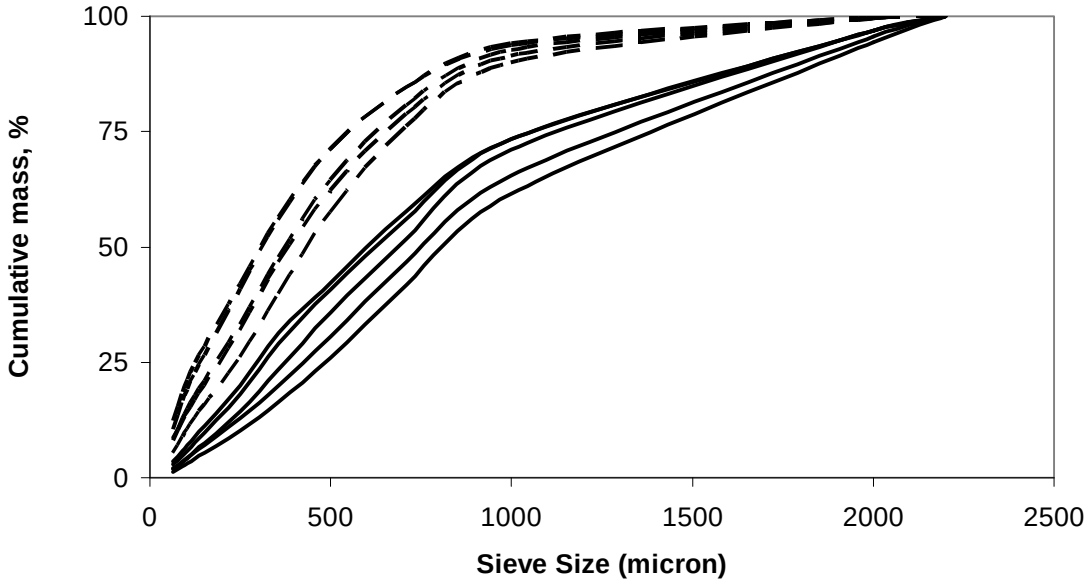

Figure 3.6 Cumulative particle size distributions of wood pellets before the mill (solid line) and pulverised wood after the mill (dashed line) obtained by sieving.

From Figure 3.6 it seems that the mills in operation at Avedøreværket have a significant effect on the wood fuel, reducing the particle size. In particular, the mill reduced drastically the fraction of wood particles larger than 1 mm and moderately the fraction between 710 micron and 1 mm; the fraction of particles below 355 micron increased significantly as a result of the grinding. The particles with sieve size larger than 1 mm made up 27 – 38 % of the mass of wood pellets before the mill, whereas they represented only 6 – 10 % of the milled wood. Half of the sample mass was made up of particles with sizes below 600 - 800 μm before the mill; the same mass fraction corresponded to particles with sizes below 300-430 μm after the mill (see Figure 3.6).

In order to investigate whether these results were affected by the sampling method, a new set of pulverised wood samples (after mill) were collected several months after the campaign. The pulverised wood samples were withdrawn at the same location as during the first campaign. Three sets of samples were collected: each set consisted of four samples withdrawn at four different points on the cross section of the pipe, as illustrated in Figure 3.7.

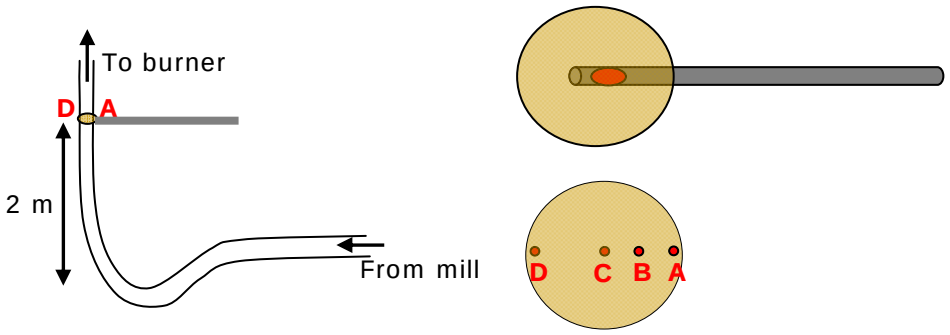

Figure 3.7 Sampling of pulverised wood at Avedørevæket Boiler Unit AVV2, new measurements. Isokinetic sampling for the same time interval at each of the points A-D.

Figure 3.8 shows the particle size distribution, obtained by sieving, of the first set of wood samples (run 1); A - D refer to the point along the cross section where the sampling was carried out, according to Figure 3.7.

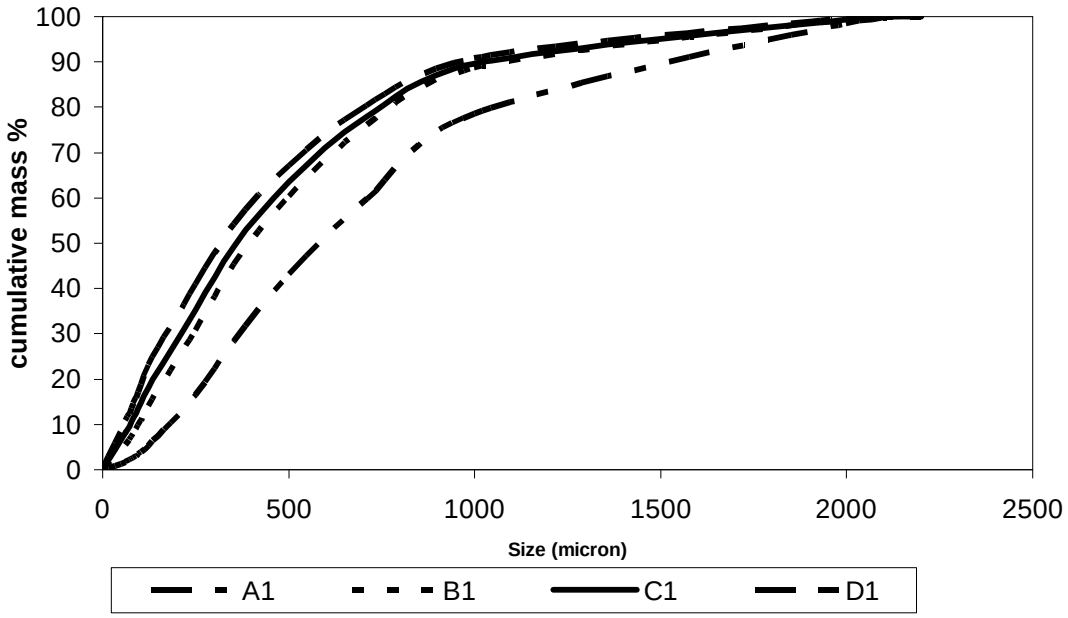

Figure 3.8 Representative example of the obtained cumulative mass distribution of pulverised wood samples; A-D refer to the sampling points in Figure 3.7.

As can be seen in Figure 3.8, the size distribution of pulverised wood was found to vary across the pipe cross area. Moving from point A to point D, a higher fraction of smaller particles was found. It is not surprising that the particles are distributed unevenly on the cross section of the pipe; the fact that the sampling window is located just 2 m after a bend of the pipe is expected to be one of the causes. Not only did the particle size distribution differ at points A-D, but also the amount of collected wood was quite different, as seen in Table 3.4. Data in Table 3.4 was used to calculate a

total weighted particle distribution curve for each of the three runs. These three distributions were practically identical and Figure 3.9 shows a comparison between one of them and the previously obtained results (Figure 3.6).

Table 3.4 Wood fuel collected at points A-D during the three sets of sampling. The sampling time was 3 minutes at each point for Run 1, and 2 minutes at each point for Run 2 and Run 3.

Point	*Run 1 (g/min)*	*Run 2 (g/min)*	*Run 3 (g/min)*
A	512	767	451
B	382	339	375
C	227	169	227
D	290	272	264
Total	1411	1546	1317

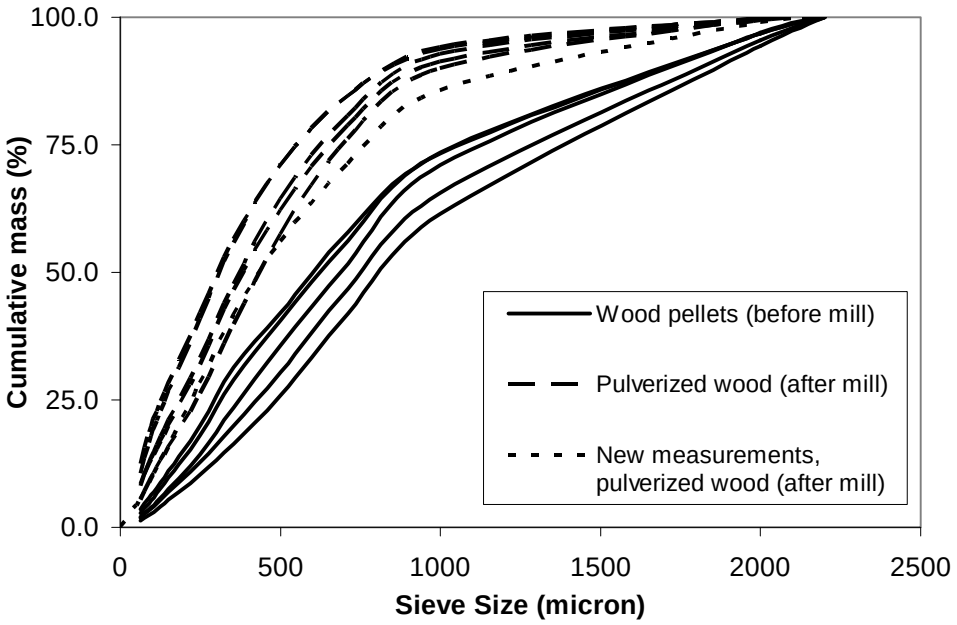

Figure 3.9 Cumulative particle distributions: comparison of the result of the new sampling sets with the results of the main experimental campaign (Figure 3.6).

The curves in Figure 3.9 indicate that the particle size distribution of wood fuel during the new measurements was very similar to the ones previously obtained for wood fuel (after mill). Assuming that the wood pellets used during the new measurements had a similar distribution to the ones in Figure 3.4 (before mill), this result seems to confirm that the effect of the mills is not only to open the wood pellets, but they also reduce the wood particles size.

It is therefore important not to assume that the size distribution of the wood fuel corresponds to that of the wood pellets, when aiming at describing wood combustion in this plant. As discussed in this thesis, a difference in particle size can affect significantly the mode of particle combustion and thereby the burnout time and the overall plant operation.

3.3 BURNOUT

During the measurement campaign fly ash particles were withdrawn from the furnace chamber just below the superheaters, at the top of the combustion chamber, i.e. 25 m above the upper row of wood fuel burners. Gas sampling was also carried out at the same position.

3.3.1 FLY ASH PARTICLE SAMPLING

The particles were collected by a particle sampling system sketched in Figure 3.10 [3]. The system consists of an approximately Ø50 mm x 3 m water cooled probe with several inner tubes for sampling. Particles were sampled through an Ø6 mm tube. The probe was cooled with water heated to 60°C to avoid any water condensation. A sintered metal filter with pore size of 1 µm was housed in a metal shell, which was directly connected to the probe and heated to a temperature above 100°C. The particle sample was drawn by an ejector pump. The sampling time was set from 1 to 4 hours. The particle samples were collected only from the metal filter. The tube was inspected several times, and no significant amount of particles appeared to be held in the piping system. At one occasion a 0.3µm metal filter was installed downstream the 1µm filter. But nothing was collected on the 0.3µm filter and this filter was not used any further.

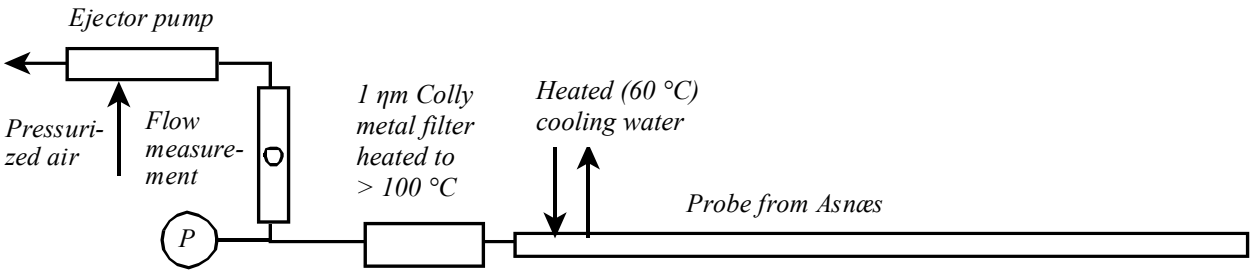

Figure 3.10 Illustration of the applied particle sampling method [3].

3.3.2 GAS SAMPLING

The gas sampling system used in the measurements is illustrated in Figure 3.11 [3]. The system consisted of a water cooled (60°C) gas sample probe with a cooled filter tip, a heated (150°C) sample line, a coarse filter, a condenser (2-5°C) for drying, an aerosol filter, a pump, a flow control and two Fisher-Rosemount MLT4 gas analyzers based on paramagnetism (O_2), IR-absorption (CO_2, CO, NO) and UV-absorption (SO_2), arranged in series. The water cooled gas probe was 2 m long and was inserted as deep as possible into the boiler chamber; thus, the sampling position was approximately 1.5 m from the boiler wall.

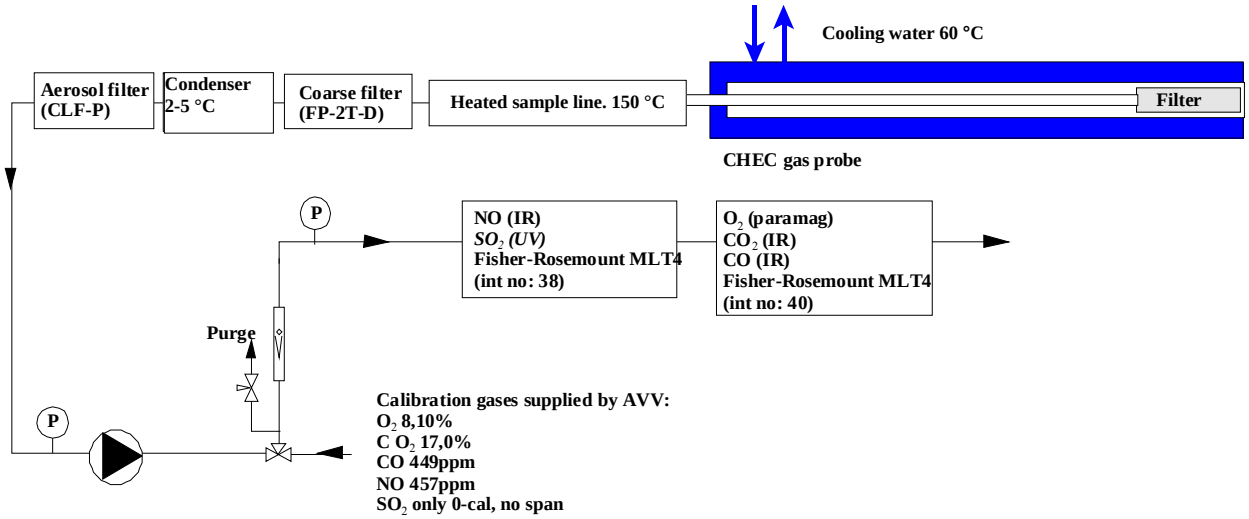

Figure 3.11 Sketch of the gas sampling system [3].

3.3.3 CHAR BURNOUT

Table 3.5 shows the applied experimental conditions (fuels, measured O_2, CO_2 and CO content in the gas at the sampling point and CO and O_2 concentration in the flue gas after the boiler) under which each ash particle sample was collected, together with the relevant wood fuel composition data (fixed carbon, volatile matter (VM), ash content and elemental carbon). The total organic carbon (TOC) content of the fly ash particles is also shown in Table 3.5. The column "Fuel burnout" in Table 3.5 shows the calculated degree of burnout with respect to the initial elemental carbon content of the wood. The degree of burnout was calculated according to the assumption that all the ash forming matter contained in the original fuel was present in the fly ash.

Further assumptions were made for the calculation of the degree of char burnout (also reported in Table 3.5), i.e. that the wood particles had first undergone pyrolysis in a non oxidizing atmosphere and that after pyrolysis the carbon content of the wood char was equal to the fuel fixed carbon. Both of these assumptions are obviously very radical. As illustrated by the results of our work which will be discussed in Chapter 4, pyrolysis at severe conditions can yield a significantly lower amount of char than suggested by the fixed carbon value. In this regard, the calculated value for char burnout probably underestimates the true value. On the other hand, the conditions in the boiler and the feeding method favour the overlap of the pyrolysis and combustion processes.

According to these assumptions, the burnout has been calculated as follows:

$$FuelBurnout = 1 - \frac{TOC \cdot Ash}{C_{fuel} \cdot (1 - TOC)} \tag{3.1}$$

$$CharBurnout = 1 - \frac{TOC \cdot Ash}{FixedC \cdot (1 - TOC)} \tag{3.2}$$

Considering that the char burnout values in Table 3.5, for the above mentioned assumptions, are minimum values for the actual char burnout, we can conclude that a very high degree of wood fuel and char burnout was achieved for all the applied combinations of fuels and all conditions tested during the measuring campaign. This result is confirmed by the low level of CO measured at the top of the combustion chamber.

The burnout of wood particles was not estimated for the last two experiments, since the composition of coal fly ash used was unknown. In these two measurements, the very low TOC content of the particles suggests that what we sampled was probably coal fly ash that had undergone further oxidation and thus lost much of its residual carbon.

Table 3.5 Gas temperature and composition at suction point. Burnout calculations from fuel and fly ash composition data.

Date	*Sample*	*Fuel*	*Ash (dry basis)*	*VM (dry basis)*	*Fixed C (dry basis)*	*Elemental C (weight fraction)*	*Tgas at suction point (°C)*	*O_2 at suction point (vol%)*	*O_2 after boiler*	*CO_2 at suction point (vol%)*	*CO at suction point (ppm)*	*CO after boiler (ppm)*	*NO at suction point*	*TOC in fly ash (%)*	*Fuel burnout (%)*	*Char burnout (%)*
Day 1	1 (*)	wood + oil	0.009	0.830	0.161	0.496	n.a.	3.1(*)	3.36	14.8	255	3	n.a.	0.1209	99.751	99.232
	2	wood + oil	0.009	0.830	0.161	0.496	n.a.	2.8	2.39	14.7	5	3	n.a.	0.0306	99.943	99.824
Day 2	3	wood + gas	0.006	0.833	0.161	0.505	958	1.4	1.58	14.1	433	1	72	0.0812	99.895	99.671
	4	wood + gas	0.006	0.833	0.161	0.505	923	3.7	2.77	13	6	1	96	0.0305	99.963	99.883
Day 3	5	wood + gas	0.006	0.835	0.159	0.497	947	2.9	2.35	13.8	17	5	119	0.0556	99.929	99.778
	6	wood + gas	0.006	0.835	0.159	0.497	925	2.9	2.63	13.9	44	5	73	0.0244	99.970	99.906
	7	wood + gas	0.006	0.835	0.159	0.497	933	4.0	3.87	11.8	4	4	93	0.0205	99.975	99.921
Day 4	8	wood + gas	0.012	0.828	0.160	0.491	918	3.2	3.73	12.8	6	1	87	0.0176	99.956	99.866
	9	wood + gas	0.012	0.828	0.160	0.491	929	2.6	2.37	11.8	14	1	105	0.0062	99.985	99.954
Day 5	10	wood + coal flyash	0.010	0.828	0.162	0.497	938	3.7	2.53	12.6	19	2	96	0.0073	-	-
	11	wood + oil + coal flyash	0.010	0.828	0.162	0.497	955	3.1	2.65	14.9	13	3	140	0.0067	-	-

(*): boiler conditions and thus gas concentrations varied during the sampling; at the sampling point O_2 concentration varied between 0.1 and 5.8 %.

Figure 3.12 shows that it is not possible to establish any clear correlation between the concentration of oxygen in the gas and the burnout of the particles. As far as sample 1 is concerned, from Figure 3.12 and Table 3.5 it is easy to see the exception of this measurement; in this case, despite a high O_2 content in the gas, the residual carbon made up 12% of the sampled particles. One may think that co-combustion of wood and oil may cause this, but this is not confirmed by the second sample, that was taken with the same combination of fuels. On the other hand, the fact that conditions were changed during the sampling may partly explain this result. The oxygen concentration was gradually decreased after the first half of the sampling and adjusted to a much lower value than before (4.8 to 1%); the varying conditions have caused a significant increase in CO (from 3 ppm to several hundreds ppm); this is in accordance with Figure 3.13 where it is shown that in connection with high CO concentrations the burnout decreased.

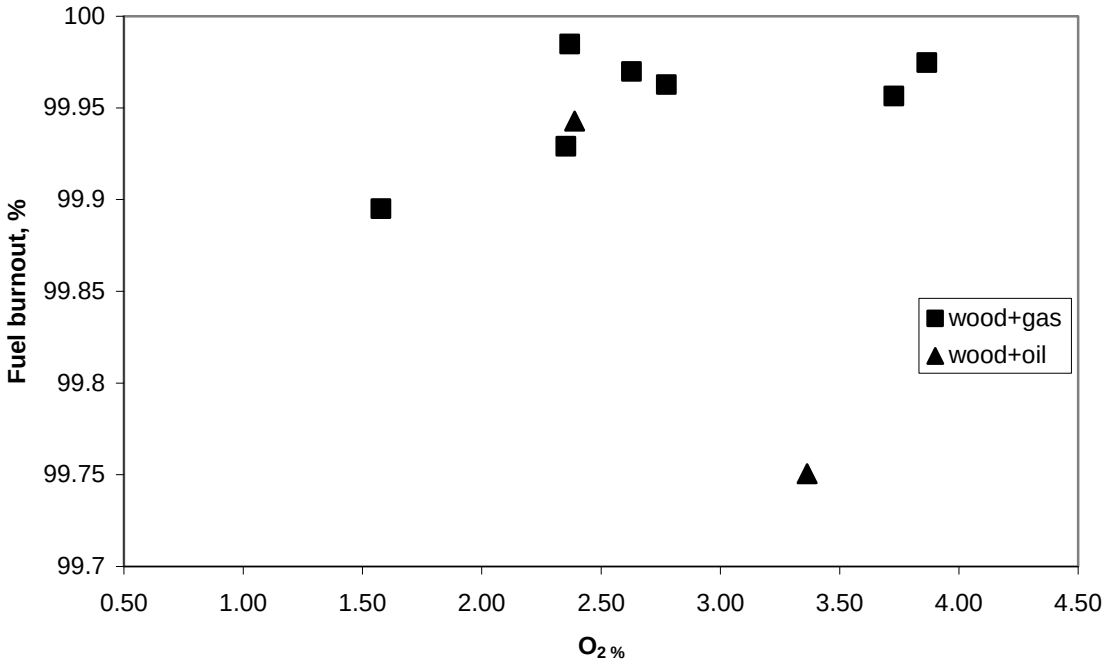

Figure 3.12 Wood burnout as a function of oxygen concentration, sampling below the superheaters. Fuels: ■, wood and gas; ▲, wood and oil. During the sampling corresponding to the point with burnout 99.75 the O_2 content at the sampling point varied between 0.1 and 5.8%.

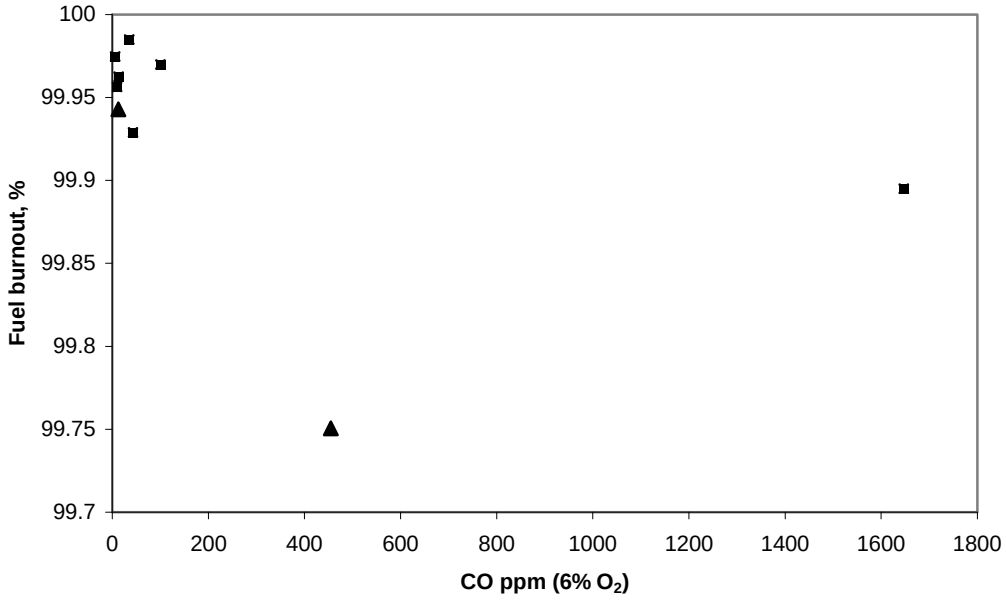

Figure 3.13 Wood burnout as a function of CO gas concentration. Fuels: ■, wood and gas; ▲, wood and oil.

3.4 CO AT THE TOP OF THE COMBUSTION CHAMBER

Figure 3.14 shows the relation between CO and O_2 concentration at the top of the combustion chamber. In general, the production of CO was very low. Two exceptions are experiments 1 and 3 (see also Table 3.5); in both cases, the concentration of O_2 at the sampling point was below 1.5% (in the case of sample 1, as explained before, O_2 concentration varied widely) and this explains the results. This is in agreement with an extensive analysis of plant operation data which covered a whole year of operation of the plant and showed that CO production increased drastically when excess O_2 at boiler exit was less than 1.5 % [3].

Figure 3.14 also shows the effect of varying the over fire air (OFA) on CO emissions. Over fire air is used to achieve staged combustion, mainly to reduce NO_x emissions; the plant normally operates with 10 % of combustion air introduced as OFA. During the campaign the effect of varying OFA between 0 and 20% of the combustion air was investigated: indeed, as seen in Figure 3.14, there does not seem to

be a clear effect on CO production, whereas it was found that the use of OFA led to a strong reduction of NO_x emission [3].

From Table 3.5 it can be seen that the measured CO concentrations after the boiler never exceeded 5 ppm; all in all, the changes of the combustion conditions did not affect the CO emissions at the chimney of the plant.

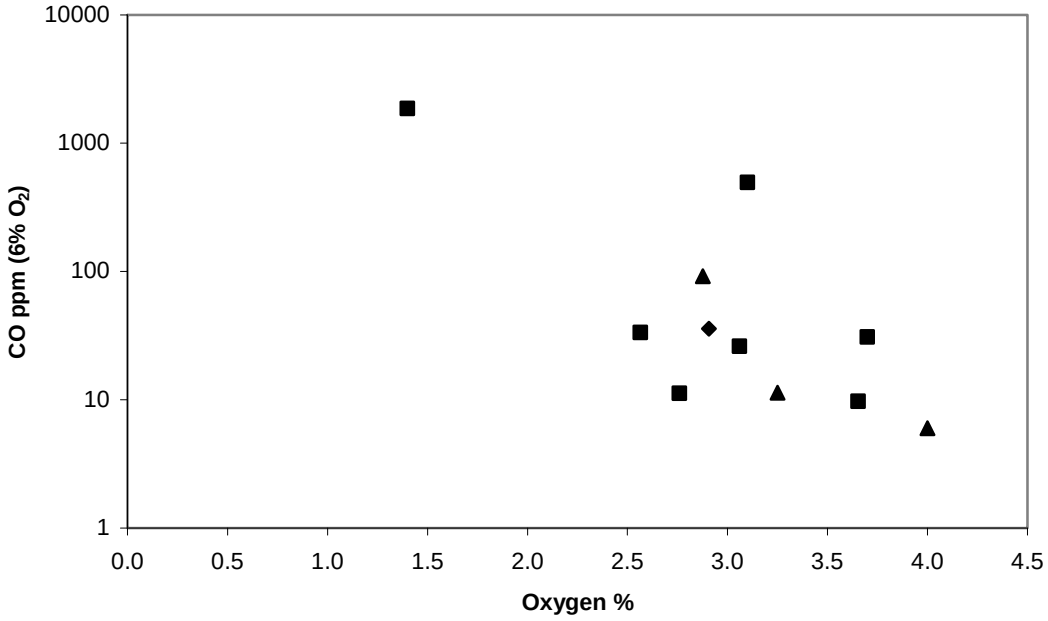

Figure 3.14 CO concentration vs O_2 below the superheaters. ♦, no over fire air (OFA); ■, 10% OFA; ▲, 20% OFA.

3.5 CONCLUSION

A measurement campaign was carried out at Avedøreværket's Unit 2, a 800 MWth, once through suspension fired boiler where oil, pulverised wood and natural gas are co-fired.

As far as wood fuel size distribution is concerned, sieving of the collected samples showed that the mills in operation at the plant ground the wood particles to smaller sizes than those of the received wood pellets. In particular, wood pellets contained 27 – 38 wt % of particles with sieve size larger than

1 mm, whereas after milling this fraction was reduced to 6 – 10 wt %. Half of the sample mass was made up of particles with sizes below 600 - 800 μm before the mill; the same mass fraction corresponded to particles with sizes below 300 - 430 μm after milling. These results were confirmed at a later stage by a second wood sampling campaign.

Different operating conditions and fuel combinations were tested. Gas sampling at the top of the combustion chamber showed that the CO level was very low and increased only when the excess oxygen concentration was as low as 1.5 %. No relation between CO and O_2 concentration was found, as far as the latter was above 1.5%. The excess oxygen was varied during the campaign from about 1.5 to about 4.5% O_2 after the boiler; in all cases the measured emission of CO (CO concentration after the boiler) was extremely low, namely below 5 ppm.

The use of over fire air had no apparent effect on CO production, while it reduced significantly the NO_x concentration.

Finally, under all of the applied conditions the wood fuel was found to have reached a very high degree of burnout of at least 99.7%.

REFERENCES

1. www.dongenergy.com
2. Jensen J.P. and Ottosen P., Anvendelse af træ- og halmpiller i store kraftvarmeanlæg, Internal report, DONG Energy.
3. Energinet.DK research PSO Project 6526, Co-firing of biomass and natural gas and NO_x emission from pulverized biomass firing, Final Report, 2008.
4. Gjernes E., Poulsen H.H., and kristensen N., Large Scale Utilisation of Biomass in Fossil Fired Boilers, presented at Powergen Europe 2007

CHAPTER 4

WOOD CHAR FORMATION AND CHARACTERISATION

4.1 INTRODUCTION

In suspension firing wood particles are heated up fast to high temperatures as they enter the furnace and thereby pyrolyse and leave a solid residue called char. The subsequent oxidation of the char is the slowest step in the conversion of wood and thus determines the degree of burnout of the fuel as well as the heat release profile in the boiler, affecting the operation and efficiency of the plant.

As explained in chapter 2.5.1, the overall reaction rate between char and oxygen can be controlled by different phenomena depending on the conditions at which oxidation takes place, char characteristics and degree of conversion. Three different situations may occur that are commonly referred to as regime I (or zone I), regime II and regime III [1,2]: in regime I the overall burning rate is controlled by the chemical heterogeneous reaction between O_2 and the carbon of the char particle; in regime II the rate is determined by the chemical reaction as well as by internal diffusion of O_2 in the char pores; finally, in regime III external diffusion of O_2 from the bulk phase to the particle surface controls the burning rate. In suspension fired boilers it is likely that pulverised wood particles burn under regime II and III at the beginning of the conversion, whereas they may burn under regime I at higher conversion, when both the particle size and temperature have decreased. Therefore, in order to describe the burning of wood char in such plants it is necessary to investigate parameters that affect transport phenomena such as char porosity and particle size as well as char density and the intrinsic reactivity of char [2].

It is well known that both the yield of char and its properties, including size, morphology, composition and reactivity depend strongly on the pyrolysis conditions at which the char is formed [2]. The available literature about characterisation of wood char produced at suspension boiler conditions is not extensive, although some recent works address the topic [3-11].

As regards char reactivity, there is a well established awareness that chars from wood are more reactive than chars from coal [7]; this is due to several reasons, including a less ordered structure of the char carbon matrix due to the high content of oxygen in biomass chars and the high amount of

volatiles in wood [2]. The dependence of char properties on pyrolysis conditions together with the heterogeneity of wood, result in a relatively poor agreement among the few published kinetic data for the oxidation of wood char generated by fast pyrolysis [7,12,13]. Janse *et al.* [7] compared their combustion kinetics data derived for wood char generated by fast pyrolysis (up to 300 K/s in their study) with available slow pyrolysis (1-20 K/min) char reactivities and observed that the high heating rate char was considerably more reactive than the other; Guerrero et al. [9] came to similar conclusions by studying low and high heating rate Eucalyptus char reactivity. The oxidation kinetics of several wood chars studied by Branca and Di Blasi [12] seemed to be more influenced by a change of pyrolysis conditions (pyrolysis temperature and heating rate) than by the difference among the wood species. Mermoud et al. [8] noticed that the steam gasification reactivity of chars produced at high heating rates was not much affected by changes in pyrolysis soaking time. They also observed that char reactivity could be correlated better to char ash content than to char surface area.

In this chapter an investigation on the relation between pyrolysis of wood and wood char properties is presented: the main focus is on fast pyrolysis whereas slow pyrolysis, which is relatively easier to study and on which literature is more extensive, serves mainly as a reference case.

4.2 EXPERIMENTAL

4.2.1 FUELS

Two fuels have been used in this study: pine wood (softwood) and beech sawdust (hardwood). The fuels were sieved and fractions with a nominal size of 90-125 μm and 250-355 μm were used in the experiments. The proximate analysis of the fuels together with the main ash-forming elements contents are reported in Table 4.1.

As can be seen in Table 4.1, the main difference between the compositions of the two fuels is the ash content, which is higher (0.9 %, dry basis) in beech than in pine (0.5 % dry basis). The ash composition is also different; beech sawdust contains 50 % more calcium and three times more potassium than pine does. Both these elements are known for having an influence on char yield and char properties [8].

Table 4.1 Proximate analysis and chemical composition of the fuels.

	Pine	*Beech sawdust*
	Proximate analysis	
Moisture (wt %, as delivered)	7.1	7.4
Volatiles (wt %, dry basis)	85	84.2
Ash (wt %, d.b.)	0.5	0.9
Fixed C (by difference, wt %, d.b.)	14.5	14.9
	Ultimate analysis	
C (wt %, d.b.)	49.7	49.5
H (wt %, d.b.)	6.3	6.1
N (wt %, d.b.)	0.1	0.13
Cl (wt %, d.b.)	0.011	< 0.0021
S (wt %, d.b.)	0.022	0.011
O (by difference) (wt %, d.b.)	43.5	43.4
Ca (wt%, d.b.)	0.125	0.190
K (wt%, d.b.)	0.033	0.095
Mg (wt%, d.b.)	0.027	0.029
Si (wt%, d.b.)	0.065	0.063

4.2.2 PYROLYSIS IN ENTRAINED FLOW REACTOR (EFR)

Fast pyrolysis of the fuels was carried out in an entrained flow reactor. The reactor had been previously used for similar studies on coal pyrolysis and combustion [14]. The EFR facility includes equipment for data acquisition, gas supply, fuel particle feeding and gas preheating. The fuel is fed into the reactor by a water-cooled injection probe that passes through the gas preheater. The fuel and preheated gas are then mixed in the top of the reactor. The gas and particles react as they flow down the central ceramic reactor tube. The reactor has a length of 2 m, an inner diameter of 8 cm and a maximum fuel feed rate corresponding to a thermal input of about 5 kW (net heating value). The maximum temperature is about 1773 K. Particle residence times are in the range 0.05 – 2.0 s with 1.5 – 2.0 s being used in this work. A metal probe can be inserted in the bottom of the

reactor, so that the gas and the particles can be conveyed to a cyclone. A scheme of the setup is shown in Figure 4.1.

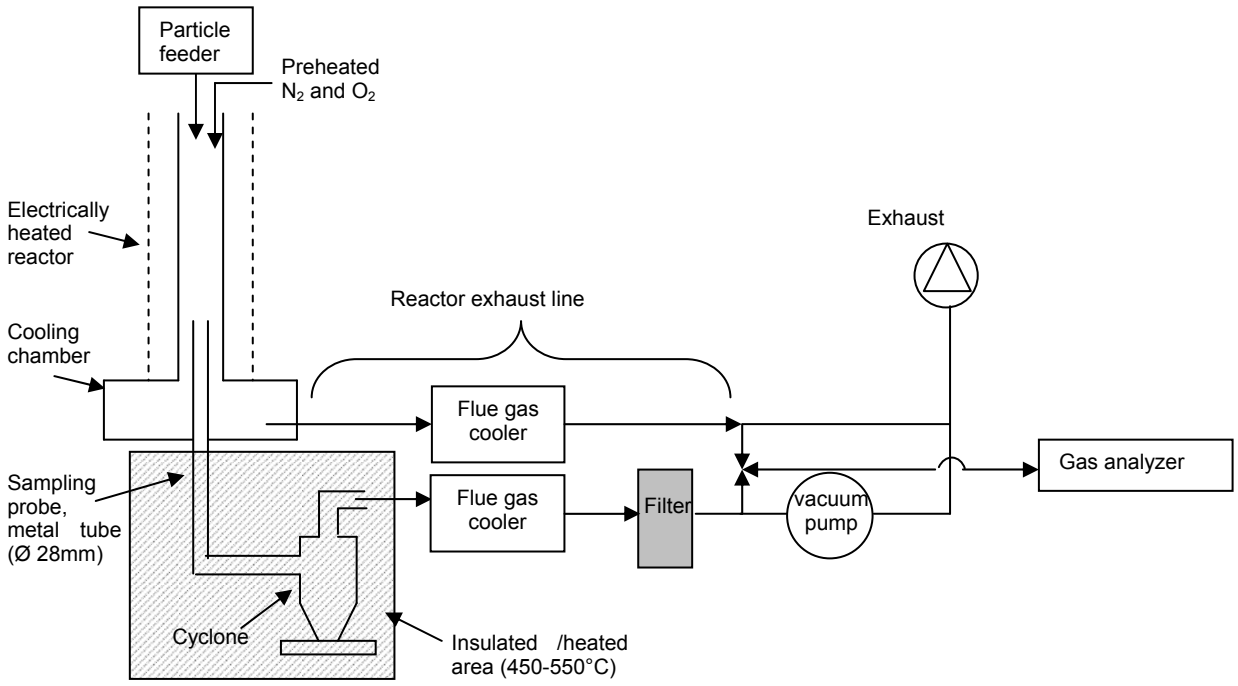

Figure 4.1 Entrained Flow Reactor (EFR) setup used for fast pyrolysis of wood fuels.

The sieved fuel was fed at a rate of 0.35 kg/h to the reactor by a stream of 10 l/min of nitrogen. The rest of the inlet gas was pre-heated before entering the top of the reactor. The total gas flow to the reactor was 57 Nl/min and contained about 2.2% oxygen in nitrogen. It was estimated that the amount of oxygen introduced in the reactor would be sufficient to burn about 30 % of the released volatiles, assuming that the char yield would be 10 % on an ash free basis. The average residence time of the particles in the reactor was 1.5 - 2 s and the estimated initial heating rate was between 2×10^4 and 4×10^5 K/s depending on wood particle size and reactor temperature. A metal sampling probe through which a suction flow was established was used to extract the exhaust pyrolysis gas and the pyrolysed particles. Char particles were then separated from the gas stream by means of a cyclone. The sampling probe and the cyclone were kept at sufficiently high temperature (723-823 K) to avoid tar condensation on the walls and tar deposition on char. After going through the cyclone the gas entered a gas cooler and a metal filter cartridge that served the purpose of removing any residual tar and solid particles before the gas was sent to gas analyzers to measure the exit gas O_2, CO and CO_2 content.

Each pyrolysis test in the EFR was done at 1273 and 1573 K. For pine, fast pyrolysis experiments were carried out for two size fractions (90-125 μm and 250-355 μm), whereas only the largest size fraction (250-355 μm) was used for beech sawdust.

4.2.3 PYROLYSIS IN SIMULTANEOUS THERMAL AND GRAVIMETRIC ANALYZER (STA)

Slow pyrolysis was carried out in a Netzsch STA 409C analyzer. Sieved fractions of nominal size 90-125 μm and 250-355 μm were used for pine wood and beech sawdust respectively. Samples of about 7 to 10 mg were heated in nitrogen at 20 K/min to the final pyrolysis temperature and held at this temperature for 20 min. Pyrolysis temperatures were varied in the interval 673 - 1673 K. After 20 min at the pyrolysis temperature, the char samples were cooled to 473 K, held at this temperature for 40 min, and subsequently oxidised as explained in the next section.

Pine wood of nominal size 90-125 μm was also pyrolysed in the STA by heating a sample to 1373 K at 10 K/min and holding it at this temperature for 30 min.

Chars produced in both the STA and in the EFR were analyzed by Scanning Electron Microscopy (SEM) as illustrated later.

4.2.4 CHAR OXIDATION REACTIVITY

The oxidation reactivity of wood chars was derived by thermogravimetry. Chars were oxidised in the STA analyzer in 4% O_2 – 96% N_2 atmosphere, during non-isothermal runs. Preliminary oxidation tests were run in order to insure that no transport limitations affected the samples' mass loss and thereby the derived oxidation kinetics. It was found that by applying a heating rate as low as 2 K/min to a char sample of about 5 to 7 mg all transport effects were eliminated.

The oxidation kinetics of the chars was derived from the experimental mass loss data according to a volumetric reaction model assuming a single first order reaction (SFOR) based on the instantaneous char weight, as follows:

$$X = 1 - m/m_0 \qquad (4.1)$$

$$\text{Rate} = -1/m\ dm/dt = 1/(1 - X)\ dX/dt = k_0\ e^{-Ea/RT} \qquad (4.2)$$

Where m and m_0 are the dry ash-free mass of the wood char at a certain time t and before oxidation starts respectively, X is the conversion of the dry ash-free char and R is the ideal gas constant. To ease the comparison of different chars' reactivity, the activation energy E_a was assumed to be common for all chars and its value was set at 166 kJ/mol (E_a/R = 20,000 K) and the pre-exponential factor was thus the only parameter to be derived. The use of a common value of activation energy for the chars was previously proved useful by Zolin et al. [14] who studied the reactivity of chars from different coals and straw.

As shown in Figure 4.2, reasonable agreement was generally found between experimental STA data and curves generated with the derived SFOR kinetic parameters.

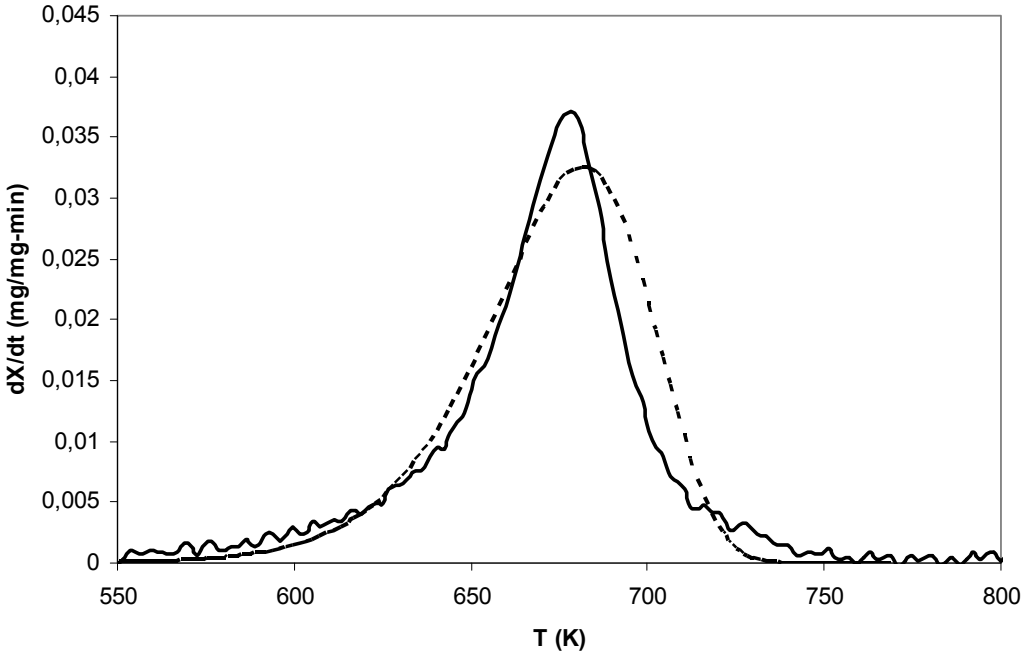

Figure 4.2 Differential thermogravimetric (DTG) curves of oxidation of pine char produced in the EFR reactor at 1273 K in 2.2% O_2. Continuous line: experimental data; dashed line: computed data. Oxidation in STA was carried out at 2 K/min in 4% O_2.

4.3 RESULTS

4.3.1 CHAR YIELD

The yield of char from pyrolysis at different temperatures was calculated by the ash tracer method on the basis of STA data; Figure 4.3 shows the results. As the pyrolysis temperature increases, char

yield decreases; in fact, STA chars seem to reach a rather constant yield of about 15-17% on a dry ash free basis (daf) above about 1200 K. At any temperature in the applied interval the char yield from fast pyrolysis in EFR was extremely low, ranging between 1% and 2.6% for pine wood and between 4.7% and 6.1% daf for beech sawdust.

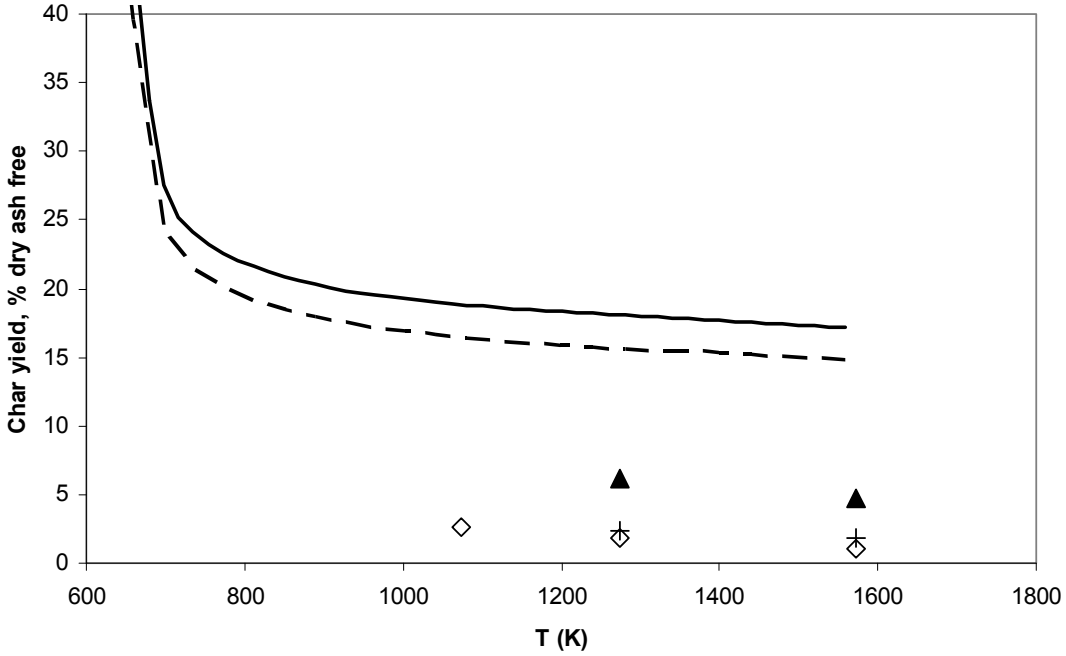

Figure 4.3 Wood char yield as a function of pyrolysis temperature. Lines correspond to pyrolysis in STA at a heating rate of 20 K/min, symbols to fast pyrolysis in EFR. Continuous line: pine wood of nominal size 90-125 μm; dashed line: beech sawdust of nominal size 250-355 μm; ◊: pine wood 90-125 μm; +: pine wood 250-355 μm; ▲ beech sawdust 250-355 μm.

4.3.2 CHAR MORPHOLOGY

Figure 4.4 shows a SEM picture of pine wood char pyrolysed at low heating rate (10 K/min) in the STA at maximum temperature of 1373 K. The particles are needle-like, as the original fuel particles; moreover, the fibrous structure of the wood is unaltered. This observation is in accordance with previous studies of wood char from STA pyrolysis [15-17].

Chars in Figure 4.5 are produced at a similar temperature (1273 K) as those of Figure 4.4 but at a much higher heating rate in the EFR. These pine char particles have lost any trace of the original wood structure and must have gone through a liquid phase; they are spherical, porous, have a smooth surface and large internal cavities. Probably the particles melted as they were heated during fast pyrolysis and the simultaneous release of a large volume of volatiles gave rise to the pores. This mechanism for biomass char formation during fast pyrolysis at high temperatures agrees, though to

different extents, with studies by Cetin *et al.* [5], Biagini *et al.* [6], Biagini *et al.* [10] and Zolin *et al.* [11]. Cetin *et al.* [5] noticed that char produced at very high heating rate (~10^5 K/s) consisted mainly of macropores. The chars shown in Figure 4.5 seem to be consistent with this observation. The open particle in Figure 4.5b has large internal cavities and pores; the outer surface of the particles is smooth.

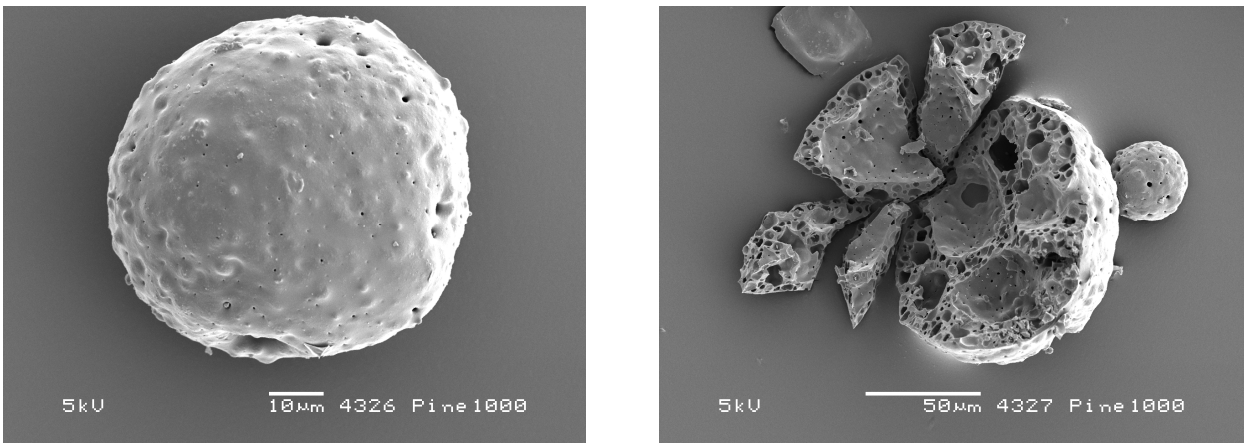

(a) (b)

Figure 4.5 SEM picture of pine wood char. Pine particles of nominal size of 90-125 µm were pyrolised at 1273 K by fast pyrolysis in N_2 in the EFR reactor. (a) A typical spherical char particle with smooth outer surfaces and (b) a broken particle where the large internal voids and pores can be observed.

Figure 4.6 compares chars obtained from pine wood and beech sawdust of the same size. As can be seen the appearance of pine char from particles of nominal size 250-355 µm in Figure 4.6 does not differ from that of char from smaller pine particles (90-125 µm) of Figure 4.5. Indeed, pine char morphology was similar for all the applied pyrolysis temperatures (1073, 1273 and 1573 K) and fuel sizes during fast pyrolysis tests in the EFR; almost all the particles had the same spherical shape. The only noticeable difference between the pine char samples was that their particle size decreased as pyrolysis temperature increased, as reported in Table 4.2. This observation is in agreement with the fact that at 1573 K the char yield was lower; wood particles released a higher fraction of volatiles giving therefore rise to smaller char particles. When considering the data in Table 4.2 it is important to remember that the reported size of the original needle-like wood particles is in fact the size of the meshes used to sieve the fuel, i.e. the longer dimension of the particles was up to several times greater than the mesh size. Having that in mind, Table 4.2 shows that pine particles shrank considerably during pyrolysis. The very low yield of char from the

pyrolysis tests is surely the most obvious and clear explanation of the observed shrinkage of the particles.

Char from beech sawdust had a different morphology from that of pine char, as seen in Figure 4.6; beech particles did not seem to have melted completely during pyrolysis, although the char particle surface was smooth, indicating that some plasticity was attained. In some beech char particles produced at 1273 K the wood structure was still recognizable (see the lowest picture in Figure 4.6); in particular, the channels typical of hardwood were seen.

	Parent fuel (sieved 250-355 μm)	EFR 1273 K	EFR 1573 K
pine	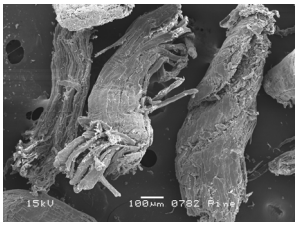	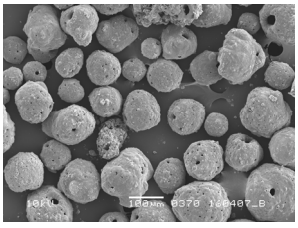 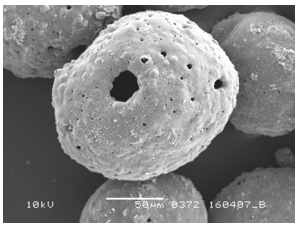	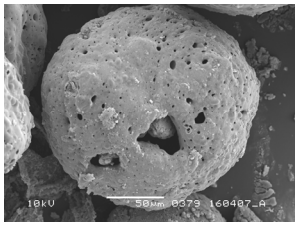
beech		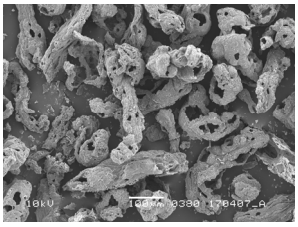 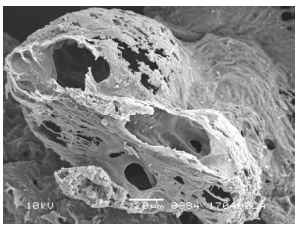	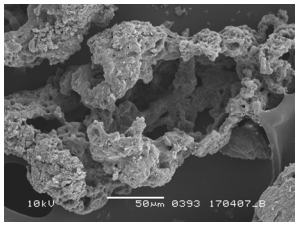

Figure 4.6 SEM images of the parent fuels used in the experiments and the collected chars. All these chars were produced by fast pyrolysis in EFR at the indicated temperature. Both the nature of the parent material and the pyrolysis temperature determine size and morphology of the char particles.

Table 4.2 Char particle size of fast pyrolysis chars produced in EFR. The pyrolysis gas was 2.2% O_2 in N_2. The numbers in parenthesis indicate the range in which particle size varied.

Pyrolysis T (K)	*Fuel particle size (μm)*	*Char particle size(μm)*
Pine		
1073	90-125	20-50
1273	90-125	30 (15-70)
1273	250-355	70-200
1573	90-125	20 (10-35)
1573	250-355	60-130
Beech sawdust		
1273	250-355	Round shape 100-130; needle-like 200
1573	250-355	Round shape 100-130 (more than in beech 1273 K); needle-like 200

In the studied temperature range, pyrolysis temperature had a stronger influence on beech char than on pine char: Figure 4.6 shows that the beech char particles produced at 1573 K in the EFR had undergone a more severe transformation than char particles produced at 1273 K. Not only had the higher temperature beech char a smoother surface, but larger cavities also appeared which brought about a more spherical particle shape. In fact, some of the beech char particles had a more spherical shape than others and the fraction of these particles, as reported in Table 4.2, was higher when pyrolysis had been carried out at 1573 K. As far as particle size is concerned, Table 4.2 shows that a more severe transformation of the beech particles morphology (i.e. smoother and more spherical char particles) was accompanied by greater shrinkage. It should also be noted that beech char particles were generally larger in size than pine char particles, this being in agreement with the observed higher char yield of beech.

4.3.3 CHAR OXIDATION REACTIVITY

Figure 4.7 and Figure 4.8 show the calculated rate constants for pine chars and beech chars respectively.

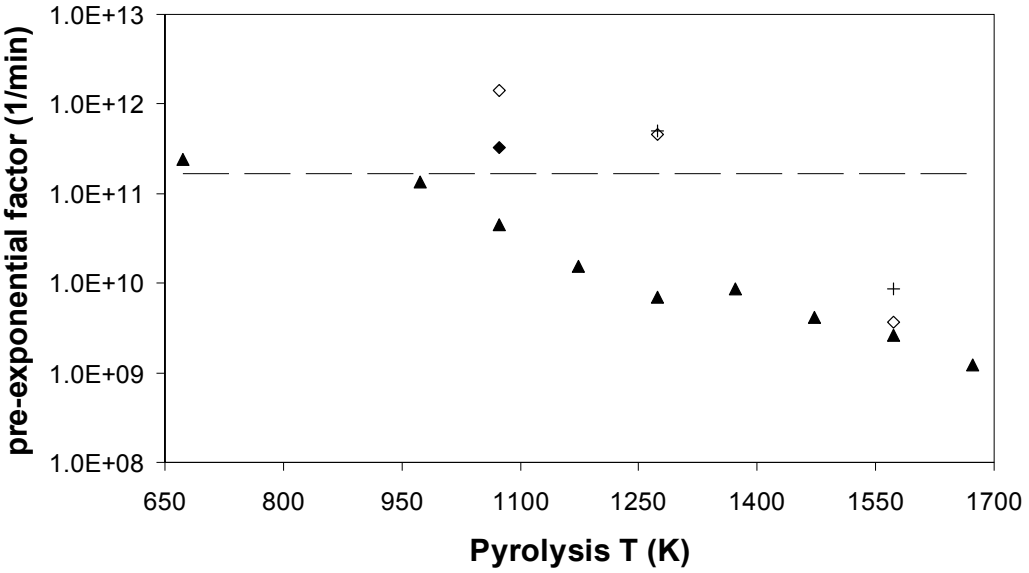

Figure 4.7 Oxidation reactivity (pre-exponential factor) of pine char. Activation energy was set to 166 kJ/mol. Dashed line: fresh pine (not pyrolysed) burned in STA; ▲: chars produced in STA, pine particles of nominal size 90-125 μm ; ◊: chars produced in EFR from pine particles of nominal size 90-125 μm; +: chars produced in EFR from pine particles of nominal size 250-355 μm; ♦ char produced in EFR (at 1073 K) from pine particles of nominal size 90-125 μm that prior to oxidation in STA (2 K/min in 4% O_2) was heated in N_2 in the STA at 20 K/min up to 1073K and kept at this temperature for 20 min.

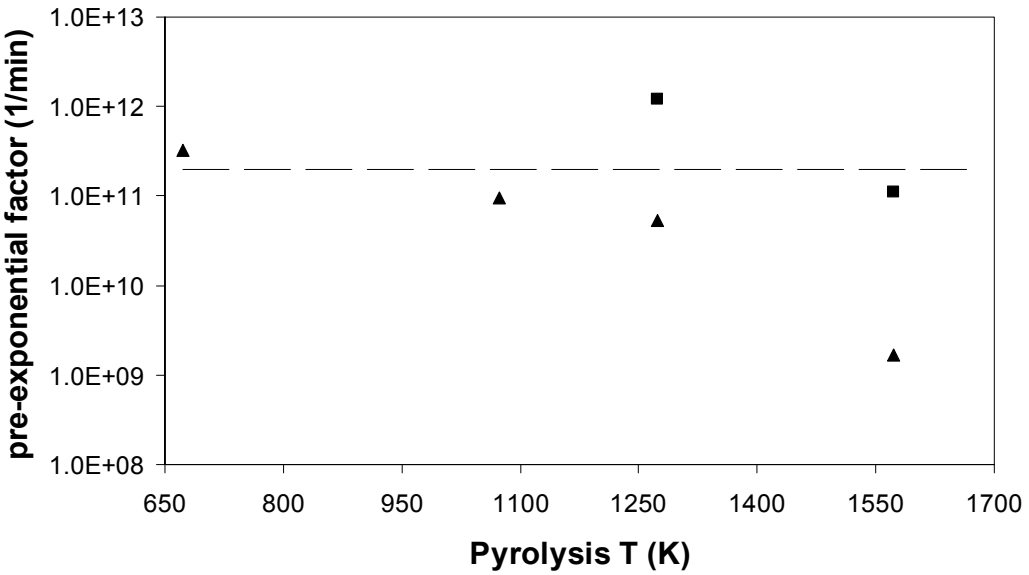

Figure 4.8 Oxidation reactivity (pre-exponential factor) of beech char. Activation energy was set to 166 kJ/mol. Dashed line: fresh beech (not pyrolysed) burned in STA; ▲: chars produced in STA; ■: chars produced in EFR from beech particles of nominal size 250-355 μm.

A general observation, valid for both fuels, is that char reactivity decreases as pyrolysis temperature increases. This well known phenomenon is usually called thermal deactivation [18]. At higher temperatures the carbon matrix of the char can attain a more ordered structure approaching the structure of graphite and thereby loses active sites.

For char produced in the STA, there exists a pyrolysis temperature interval (1173K – 1373K for pine char, 973-1273 for beech char) where char reactivity does not vary significantly; a similar behavior was observed for straw char by Zolin [18].

As can be seen in Figure 4.7 and Figure 4.8, all the chars produced in the EFR under boiler-like conditions have higher reactivity than those produced in the STA.

Samples of chars generated in the EFR have been subjected to further heat treatment in the STA (20 K/min up to 1073 K, in nitrogen, soaking time 20 min). The char samples were subsequently cooled down to 473 K and after a holding time of 40 min at this temperature the oxidation test started at the same conditions as for the samples directly oxidised in the STA, i.e. 2 K/min in 4 % oxygen. The reactivity of one of these further treated EFR char samples is shown in Figure 4.7, where it is seen that even when post-treated in the STA the char produced at high heating rates in the EFR preserved a higher reactivity than the STA char produced at the same pyrolysis temperature.

For pine char the difference in reactivity between fast pyrolysis char and slow pyrolysis char decreases considerably when the pyrolysis temperature is as high as 1573 K, whereas fast pyrolysis beech char preserved a very high reactivity in all the investigated temperature range. It is worth noticing, for instance, that the estimated pre-exponential factor for the oxidation of beech char produced by fast pyrolysis in the EFR at 1573 K (1.12×10^{11} min^{-1}) is only slightly lower than that of beech sawdust directly oxidised without prior pyrolysis (1.96×10^{11} min^{-1}).

When produced at the same conditions, beech char was more reactive than pine char; this is evident for EFR chars, where beech char was 2.5 and 13 times as reactive as pine char when produced at 1273 and 1573 K respectively.

The size of the parent pine particles does not seem to have influenced the char reactivity much; as seen in Figure 4.7, the two size intervals of pine particles produced chars of similar reactivity.

4.4 DISCUSSION

SEM pictures showed no traces of soot in the char samples included in this study; in fact, soot was collected on the metal filter, downstream the cyclone (Figure 4.1). Zhang et al. [4] recently showed that a high amount of soot can be formed during wood pyrolysis. For cypress sawdust pyrolysed at 1273 K they measured a yield of 4.0% char and 6.6% soot respectively; when the pyrolysis temperature was risen to 1473 K the yield of char and soot were 2.4% and 14.7% respectively. A similar behaviour was observed in this study, although only qualitatively. No soot was collected on the metal filter during experiments at 1273 K, both with pine and beech; on the other hand, all experiments at 1573 K led to soot formation and soot collection on the filter. The experimental conditions used in this study (presence of a small fraction of oxygen in pyrolysis gas) may have hindered the formation of soot in as high quantities as the ones measured by Zhang et al. [4]. The material collected on the filter was found to have a very low ash content (below 1 %), which supports the assumption that it was soot. Thus, it seems that the experimental system used in this study (hot cyclone, gas cooler, filter) provided a good separation of char from the rest of the pyrolysis products and the char yield results are therefore expected to be accurate.

From Figure 4.3 it is seen that the heating rate has a crucial influence on the pyrolysis char yield. The effect of heating rate on char yield has been studied by a number of authors and our results are in agreement with their work [6,19]. The char yields of white quebracho and birch wood were found to decrease from 15 and 20 % respectively for slow pyrolysis to 5.5 and 8.2 respectively for fast pyrolysis in a free-fall reactor by Zanzi et al. [19]. Similar results were obtained by Biagini et al. [6] who studied various biomass fuels. A low char yield of fast pyrolysis in EFR, which in this study was 1 to 6 % daf, was therefore expected. Theoretically the presence of oxygen during pyrolysis in the EFR might have contributed to the low char yield by partly oxidizing the chars; nevertheless the O_2 content was estimated to be sufficient to burn at most 30 % of the released volatiles and is therefore not expected to have initiated char combustion.

We pointed out earlier that pine char morphology did not vary in the applied range of temperature and particle sizes; it is expected, though, that when the fuel particle size increases the particles might not experience such a uniform rapid heating to high temperature and this could perhaps limit the extent of melting leaving a char more similar to the original wood particle. Further investigation would be needed on this topic.

The fuels' ash content seems to have an important role during EFR pyrolysis, both with regard to char yield, char morphology and char reactivity. Jensen et al. [20] studied wheat straw pyrolysis and found that water-washed straw had a much lower char yield (12.3%) than raw straw (22.1%); when the washed straw was impregnated with KCl, the char yield increased to similar levels as the raw fuel (20.6%). They concluded that the presence and amount of mineral matter (in their specific case KCl) in biomass affects the pyrolysis of biomass macrocomponents (lignin, hemicelluloses, cellulose). Similar observations were made by Sharma et al. [21] who studied lignin pyrolysis. In our case, beech sawdust contains almost twice as much ash and three times as much potassium as pine wood (see Table 4.1). The higher char yield from beech sawdust during fast pyrolysis in the EFR could thus be due to the higher ash content of this type of wood; more specifically, from Table 4.1 it can be observed that the main elements that are more abundant in beech than in pine are calcium and potassium, both known for having an effect on biomass devolatilisation rate and char oxidation rate [22].

As seen in Figure 4.3, pine wood pyrolysed in the STA yielded more char than beech sawdust. This seems to be in contrast with the behaviour under boiler-like pyrolysis described above, but might be explained by the higher lignin content of softwoods (pine) with respect to hardwoods (beech); in fact, lignin was found to have a high char yield when pyrolysed at low heating rates [21].

Jones et al. [22] have shown that mineral matter in wood affects char morphology as well as char yield. They burned different willow samples at ~1500 K: raw, water-washed, demineralised and K-impregnated. Of these samples, only the demineralised willow melted during devolatilisation, suggesting that minerals are determining to a great extent the kind and degree of structural changes of wood during pyrolysis. The higher ash and potassium content of beech sawdust may thus be one of the reasons for beech particles not to have melted like pine particles during fast pyrolysis in the EFR.

Some models describing the pyrolysis of coal [23-25] can be helpful in the interpretation of the results of this study. Solomon et al. [23] developed the FG-DVC model (Functional Group – Depolymerisation, Vaporisation and Crosslinking model). The model assumes that during pyrolysis the following phenomena occur: depolymerisation; repolymerisation, i.e. cross linking of metaplast fragments; transport of lighter molecules away from the particle surface; internal transport of lighter molecules by gas bubbles. These phenomena are simultaneous at low heating rate, but consecutive at high heating rates, i.e. repolymerisation starts after depolymerisation [24], leading to the formation of a highly molten particle during pyrolysis. It was also found that small differences in

the cross linking rate affects drastically the fluidity of the resulting char [23] and that oxygen favours cross linking thereby preventing fluidity of the char [25].

It is thus clear that the course of these phenomena during fast pyrolysis can be much affected by the ash content and the ash composition of the fuel, especially as regards catalytic elements like Ca and K. If Ca and K catalyze cross linking, both the higher yield of beech char and its less severe morphological changes may be explained. It is worth noticing that cross linking leading to final formation of wood char seems to happen in a way that preserves a certain degree of disorder in the carbon structure of the char, since the reactivity of chars from high heating rate pyrolysis was high in all cases.

As far as char oxidation reactivity is concerned, it is known that some minerals contained in ash, like K, may act as catalysts [20,22]. Moreover, Mermoud et al. [8] found that the ash content (mainly the elements Ca and K) in beech char was proportional to its steam gasification reactivity. These observations can explain the fact that beech char, being the fuel with the highest ash and K content, is more reactive than pine char, as shown in Figure 4.7 and Figure 4.8.

As seen before, chars experiencing fast pyrolysis in the EFR, have higher reactivity than those produced in the STA. This could be due to the major transformation of the particle structure during fast pyrolysis; rearrangement of both the carbon and the mineral structure can affect very much char reactivity, for example by varying the number of active sites, a measure of which can be the oxygen content of the char [9]. Guerrero et al. [9] found that char from eucalyptus wood produced in a fluidised bed reactor at high heating rate contained more hydrogen and oxygen than the one produced at low heating rate; they therefore consider the higher number of active sites to be the cause of the higher reactivity of the high heating rate chars. This observation might be affected by the fact that the low heating rate char was kept for 1 h at the final pyrolysis temperature, whereas the high heating rate pyrolysis tests were much faster [9].

Our study, however, indicates that the time of exposure at pyrolysis temperature does not influence char reactivity as much as the pyrolysis heating rate. As discussed before, Figure 4.7 shows that a further heat treatment step in the STA at 1073 K had a minor effect on the reactivity of the EFR pine char produced at 1073 K. The same (in fact, generally smaller) effect was observed for all the char samples generated in the EFR, regardless of the EFR pyrolysis temperature. This shows that the properties (structure, degree of disorder) of the char attained during fast pyrolysis are preserved at least in the applied pyrolysis temperature range. We can therefore conclude that what makes chars from high heating rate pyrolysis more reactive is not being exposed to high temperatures for a

much shorter time than the STA char; during pyrolysis, the particle residence time has less influence on char reactivity than the final pyrolysis temperature and the heating rate.

The heating rate is thus a very important parameter to be considered when char reactivity is investigated. Generally, STA studies have given significantly different results than those in EFR and are therefore not recommended for studies of wood char related to pulverised fuel firing. As seen in Figure 4.7 and Figure 4.8, in only one of the applied combinations of fuels and conditions, i.e. pine particles pyrolysed at 1573 K, was the reactivity of fast pyrolysis char not much different from that of slow pyrolysis char. At 1573 K for pine wood of nominal size in the range 90-355μm it seems that the pyrolysis temperature is dominant over the general thermal history of the particle as regards the influence on char reactivity. It is expected that this would hold true for any temperature greater than 1573 K; the available data do not allow drawing any general conclusion on this issue and it is believed that further investigation could provide useful information for future research on wood char reactivity.

The kinetic data obtained in this study have been compared to kinetic data of char oxidation of boilerlike-generated wood chars found in literature, as shown in Figure 4.9. It can be seen that the reaction rates of most of the chars from this study are in agreement with previously available values. The data in Figure 4.9 were all obtained for oxidation of fast pyrolysis (i.e. high heating rate) chars, but the only char produced at a temperature as high as the ones used in this study is the straw char (1473 K) [11] , whereas the other ones were generated at maximum pyrolysis temperatures between 800 and 900 K. This explains why the rates of reaction of chars generated at 1573 K in this study are lower than values found in literature.

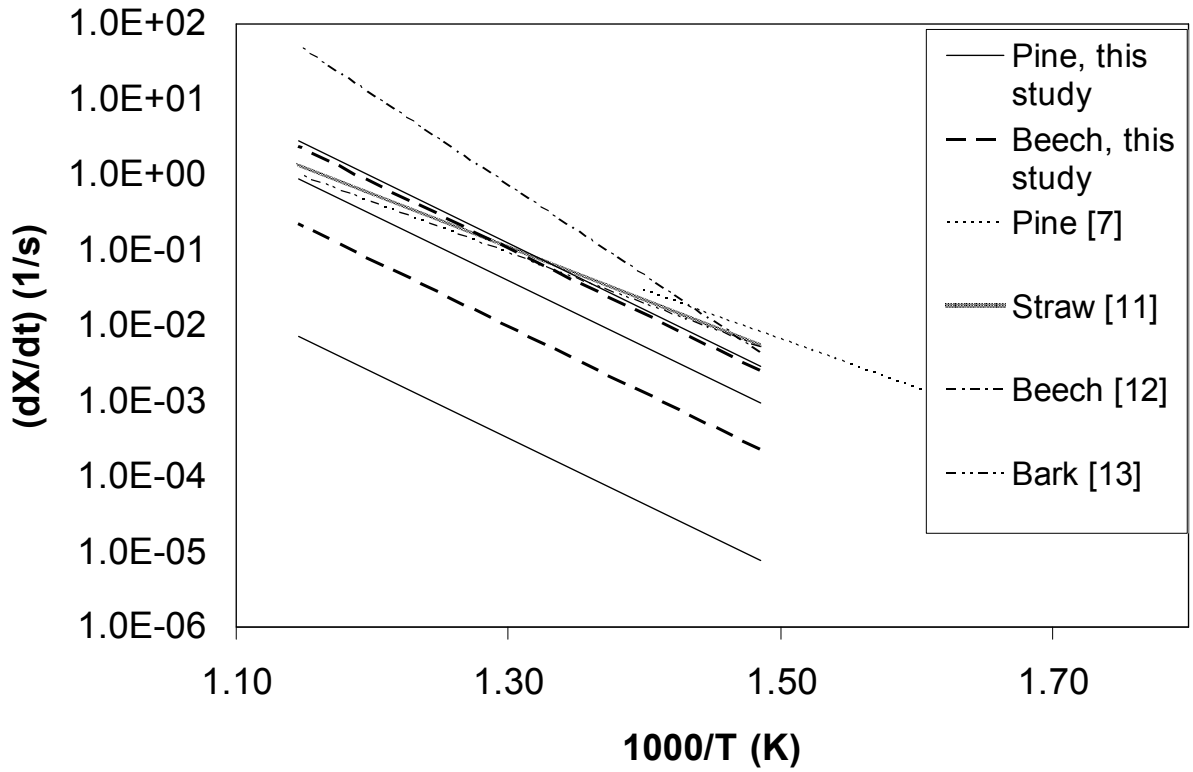

Figure 4.9 Arrhenius plot comparing reactivities of wood char from this study and several literature studies. All chars are obtained by fuel pyrolysis at high heating rates. In this study pine was pyrolysed at 1073, 1273 and 1573 K (three continuous lines), beech was pyrolysed at 1273 and 1573 K (two dashed lines). Straw [11] was pyrolysed at 1473 K, the other fuels were pyrolysed at temperatures between 800-900 K.

4.5 CONCLUSIONS

Pyrolysis experiments were carried out in an Entrained Flow Reactor (EFR) and in a thermo gravimetric analyzer (STA), to investigate how char morphology and reactivity depend on pyrolysis conditions. Pine wood and beech sawdust were used as fuels. The produced chars were analyzed by SEM microscopy and their reactivity to oxygen was assessed by thermogravimetry.

The yield of char from low heating rate (10 – 20 K/min) pyrolysis in the STA was 15-17 % daf and the char retained the original wood fibrous structure. On the other hand, rapid heating (10^4 – 10^5 K/s) to high temperatures in the EFR yielded much less char (1-6 % daf) and caused major transformation of the particles morphology.

Pine char particles from high heating rate pyrolysis were spherical with large internal cavities; this is considered the result of particle melting during this type of pyrolysis. Beech char particles were less spherical than pine char particles but still porous with a smooth surface, indicating that some plasticity was attained during high heating rate pyrolysis. It is believed that the higher ash content of beech sawdust (in particular higher Ca and K content) may be responsible for the difference in char particles morphology.

High heating rate pyrolysis chars produced in the EFR were more reactive than chars from the STA, indicating that the structure attained at high heating rates maintained a certain degree of disorder in spite of the high temperatures applied. The reactivity data obtained in this study by assuming a single first order char oxidation reaction are comparable with available literature data on wood chars from fast pyrolysis.

Pine and beech chars produced by low heating rate pyrolysis at 1573 K were about 20 and 50 times less reactive than those produced at 1073 K, respectively. Char thermal deactivation was also observed during high heating rate pyrolysis; the reactivity of EFR pine chars decreased by a factor of 3 when the pyrolysis temperature was risen from 1073 K to 1273 K and by 2 orders of magnitude with a further increase from 1273 K to 1573 K. In the same temperature interval (1273 – 1573 K), on the other hand, EFR beech chars deactivated only by a factor of 10.

This study has shown that pyrolysis time has little influence on char reactivity compared to pyrolysis temperature and pyrolysis heating rate.

The mineral matter content of the fuels was also related to the differences in char reactivity, in that the catalytic action of Ca and K may explain the higher reactivity of beech chars with respect to pine chars.

REFERENCES

1. Smith I.W., The combustion rates of coal chars: a review, Nineteenth Symposium (International) on Combustion, The Combustion Institute, 1982, pp 1045-1065.
2. Hurt R.H., Structure, properties and reactivity of solid fuels, Twenty-Seventh Symposium (International) on Combustion, The combustion Institute, 1998, 2887-2904.
3. Kang B., Lee K.H., Park H.J., Park Y. and Kim J., Fast pyrolysis of radiate pine in a bench scale plant with a fluidized bed: Influence of a char separation system and reaction conditions on the production of bio-oil, J. Anal. Appl. Pyrolysis, 2006, 76, 32-37.
4. Zhang Y., Kajitani S., Ashizawa M. and Miura K., Peculiarities of rapid pyrolysis of biomass covering medium- and high-temperature ranges, Energy Fuels, 2006, 20, 2705-2712.
5. Cetin E., Moghtaderi B., Gupta R. and Wall T.F., Influence of pyrolysis conditions on the structure and gasification reactivity of biomass chars, Fuel, 2004, 83, 2139-2150.
6. Biagini E., Fantozzi C. and Tognotti L., Characterization of devolatilization of secondary fuels in different conditions, Combustion Science and Technology, 2004, 176, 685-703.
7. Janse M.C.A., de Jonge H.G., Prins W. and van Swaaij W.P.M., Combustion kinetics of char obtained by flash pyrolysis of pine wood, Industrial and Engineering Chemistry Research, 1998, 37, 3909-3918.
8. Mermoud F., Salvador S., Van de Steene L. and Glofier F., Influence of the pyrolysis heating rate on the steam gasification rate of large wood char particles, Fuel, 2006, 85, 1473-1482.
9. Guerrero M., Ruiz M.P., Alzueta M.U., Bilbao R. and Millera A., Pyrolysis of eucalyptus at different heating rates: studies of char characterization and oxidative reactivity, J. Anal. Appl. Pyrolysis, 2005, 74, 307-314.
10. Biagini E., Narducci P. and Tognotti L., Size and structural characterization of ignin-cellulosic fuels after the rapid devolatilization, Fuel, 2008, 87, 177-186.
11. Zolin A., Jensen A., Jensen P.A., Frandsen F. and Dam-Johansen K., The influence of inorganic materials on the thermal deactivation of fuel chars, Energy Fuels, 2001, 15, 1110-1122.
12. Branca C. and Di Blasi C., Global kinetics of wood char devolatilization and combustion, Energy & Fuels, 2003, 17, 1609-1615.
13. Branca C., Iannace A. and Di Blasi C., Devolatilization and combustion kinetics of Quercus Cerris bark, Energy Fuels, 2007, 21, 1078-1084.
14. Zolin A., Jensen A.D., Jensen P.A. and Dam-Johansen K., Experimental study of char thermal deactivation, Fuel, 2002, 81, 1065-1075.
15. Grønli M., A theoretical and experimental study of the thermal degradation of biomass; Norwegian University of Science and Technology NTNU, 1996; Ph.D. Thesis.
16. Wildman J., Derbyshire F., Origins and functions of macroporosity in activated carbons from coal and wood precursors, Fuel, 1991, 70, 655-661.
17. Kumar M. and Gupta R.C., Scanning electron microscopic study of acacia and eucalyptus wood chars, Journal of Material Science, 1995, 30, 544-551.
18. Zolin A., Jensen A. and Dam-Johansen K., Kinetic analysis of char thermal deactivation, Twenty-Eighth Symposium (International) on Combustion, The combustion Institute, 2000, 2181-2188.

19. Zanzi R., Sjöström K. and Björnbom E., Rapid high-temperature pyrolysis of biomass in a free-fall reactor, Fuel, 1996,
75, 545-550.
20. Jensen A., Dam-Johansen K., Wójtowicz M.A. and Serio M.A., TG-FTIR Study of the Influence of Potassium Chloride on Wheat Straw Pyrolysis, Energy Fuels, 1998, 12 (5), 929-938.
21. Sharma R.K., Wooten J.B., Baliga V.L., Lin X., Chan W.G. and Hajaligol M.R., Characterization of chars from pyrolysis
of lignin, Fuel, 2004, 83, 1469-1482.
22. Jones J.M., Darvell L.I., Bridgeman T.G., Pourkashanian M. and Williams A., An investigation of the thermal and catalytic behaviour of potassium in biomass combustion, Proceedings of the Combustion Institute, 2007, 31, 1955-1963.
23. Solomon P.R., Fletcher T.H. and Pugmire R.J., Progress in coal pyrolysis, Fuel, 1993, 72, 587-597.

24. Niksa S. and Kerstein A.R., On the role of macromolecular configuration in rapid coal devolatilization, Fuel, 1987, 66,
1389-1399.
25. Marsh H., Introduction to carbon science; Butterworths; London, UK, 1989; pp 37 -71.

CHAPTER 5

WOOD CHAR COMBUSTION

5.1 INTRODUCTION

This chapter deals with the modelling of wood char combustion. Char oxidation is the slowest step in pulverised wood combustion and therefore determines the overall wood burnout; moreover, it influences the heat profile in the boiler, which in turn affects the efficiency of the plant and other important phenomena such as the formation of pollutants. Therefore, a good description of char combustion can be very useful for optimising the operation of pulverised wood plants.

In Chapter 2, the different kinetic regimes under which a char particle can burn are described; the actual burning rate of a particle depends on both heterogeneous reaction kinetics and transport processes.

Single-particle combustion models have been developed that can be used in combination with fluid dynamic models of reactors to simulate solid combustion processes and predict burnout and pollutants production [1,2]. Due to the complexity of the heterogeneous reaction and of the fluid dynamic conditions inside a boiler, models normally need strongly simplifying assumptions [3]. The use of empirical coefficients and correlations to describe some aspects of the particle combustion (e.g. the CO/CO_2 ratio) is also common.

Section 5.2 gives a short review of existing particle combustion models; section 5.3 describes the model used in this work. The results of the model are given in section 5.4, where comparison is also made with data obtained during the experimental campaign at Avedøreværket.

5.2 REVIEW OF PARTICLE CONVERSION MODELS

As far as suspension combustion of pulverised fuel is concerned, most of the available particle conversion models were derived for coal. In this section the focus is thus on how these models describe the combustion rather than on quantitative results obtained.

Hurt *et al.* [4] developed a model of char particles conversion (Carbon Burnout Kinetic Model, CBK) that aims at predicting the carbon burnout and ultimate fly ash carbon content for prescribed temperature/oxygen histories typical of pulverised coal combustion systems.

The CBK model consists of four sub-models accounting for:

- Single-film char oxidation
- Statistical variations in single particle reactivity and density
- Char thermal deactivation
- A physical property sub-model which describes swelling, diameter and density changes and ash inhibition

Ash inhibition refers to the effect in the latest stages of burnout, when the main components of the particles are inorganics that can act as additional resistance to the flow of oxygen to the carbon.

The CBK model does not include any pyrolysis sub-model; the starting point of the model is a distribution of char particles. Devolatilisation has to be accounted for in a comprehensive combustion model, as reported by Eaton *et al.* [5]: as seen in Chapter 4, particle pyrolysis occurs very rapidly during the early stages of the conversion of a pulverised fuel particle and determines size and characteristics of the char.

The main ideas of the CBK model are: the burning of a char particle at high temperature is controlled by transport phenomena (kinetic regime II and III) up to a certain conversion, whereas the final stage of conversion occurs under regime I, i.e. kinetic control; different factors contribute to the loss of reactivity of the char during its conversion. It is evident that since the latest stage of the conversion is governed by intrinsic oxidation kinetics (regime I), it is extremely important that the effect of char deactivation be accounted for. The CBK model by Hurt *et al.* [4] considers three main sources of deactivation:

- Preferential consumption of more reactive matter, which is described by a statistical formulation for kinetics and properties
- Thermal deactivation
- Ash inhibition

The submodel that accounts for char thermal deactivation was presented in Chapter 2, paragraph 2.5.4: thermal annealing follows a first order kinetics and the active sites anneal at different rates (this is described by a log normal distribution of the activation energy) [4].

The single-film char oxidation sub-model accounts for global zone II surface kinetics, radiative and conductive heat transfer, diffusive mass transfer with Stefan flow in the particle boundary layer, and a variable CO/CO_2 ratio in the primary products given by the empirical correlation:

$$\frac{CO}{CO_2} = A_c e^{\left(-\frac{E_c}{RT_p}\right)} \tag{5.1}$$

Where T_p is the particle temperature (assumed to be isothermal) and A_c and E_c are kinetic parameters.

In CBK the particle burning rate per unit external area ($k_{c,ext}$, in $\frac{kg}{m^2 s}$) is given by:

$$k_{c,ext} = A \cdot e^{\left(-\frac{E}{RT_p}\right)} \cdot P_{O_2}^n \tag{5.2}$$

where P_{O_2} is the oxygen partial pressure at the surface of the particle. A value of $n = 0.5$ was used by the authors when applying their model [4].

In order to account for the heterogeneity of properties and reactivity within the fuel, Hurt *et al.* have introduced a statistical kinetic sub-model. The user is requested to specify the size distribution of the char particles, their density distribution and their reactivity. The variation of the reactivity among the particles is described by a variation of the global pre-exponential factor A, modelled as a gamma distribution.

The sub-model describing the changes in physical properties during conversion is based on the introduction of an empirical parameter β, called mode of burning. This parameter relates the carbon density at a certain time (ρ) relative to the original carbon density of the particle (ρ_0) with the correspondening reduction of mass of carbon:

$$\left(\frac{\rho}{\rho_0}\right) = \left(\frac{m}{m_0}\right)^{\beta} \tag{5.3}$$

m_0 is the original carbon mass, m is the actual carbon mass. For β=0, the particle's conversion is controlled by external transport only and the particle combustion could be described by the

shrinking core model. For β=1 the particles burn under regime I, i.e. chemical kinetic control. Given the conditions in a pulverised fuel boiler, Hurt *et al.* [4] suggest using a value of 0.2 for β for an unknown coal. This value is consistent with the high probability of zone II oxidation under those conditions; similar values have been used by other authors in literature, see Cozzani *et al.* [6]. Once the carbon density is computed from the previous expression, the particle global density (the ash porosity is an input parameter in CBK and is allowed to vary with conversion) and the particle diameter (assuming spherical particles) can be estimated.

The value of the diameter is used in the ash inhibition code to calculate the thickness of the porous ash layer surrounding the carbon rich core; in fact, the burning is described by a shrinking carbon core surrounded by an ash layer. The changes of the thickness of the ash layer result from a monodisperse grains description of the mineral matter in the particle. As the carbon is consumed by the reaction with oxygen, the grains are liberated from the carbon matrix and accumulate at the external surface of the particle. As the first layer of grains is being formed, the thickness of the ash layer remains equal to the grain diameter, while the ash porosity constantly decreases to a critical value, when a monolayer of grains is completed. From this moment on, the porosity of the ash layer is kept at the critical value, while the thickness of the ash layer increases [4].

A different approach to coal particle combustion is that of Jensen [7]. The original model, later modified by Jensen [8] was developed to describe the combustion of coal particles in a fluidised bed. According to the first version of the model, particles shrank during combustion because they lost their external ash layer due to attrition with other particles in the bed. From the point of view of pulverised fuel combustion, inter particles attrition has no influence on the combustion process. On the other hand, peripheral fragmentation was found relevant to pulverised coal combustion by Feng and Bhatia [9]. This process can be described as follows: when the outer shell of a particle burning under transport limited regimes reaches a critical value of porosity, the shell percolates and the particle size decreases. The reduction of particle size due to peripheral fragmentation can thus be simulated in the same way as the original reduction due to attrition and the model can be applied to pulverised coal combustion.

Jensen [7] modelled the combustion of spherical coal particles; this model assumes that the sole primary product of oxidation is CO and the particles are considered isothermal, but it does consider over-shoot temperatures.

Jensen's model [7] integrates a quasi steady state solution with a dynamic part. The oxygen profile in the particle and the particle temperature are calculated assuming steady state. Once the steady state profile is solved, a discrete step in time is taken, during which the carbon is consumed according to the steady state oxygen profile and temperature. The model includes an upper limit to particle porosity, i.e., the outer shell of the particle with porosity higher than a certain value undergoes peripheral fragmentation. This critical value of porosity is chosen by the user and determines the extent of particle shrinkage during the simulation.

Few models have been developed for the combustion of wood particles and some of them describe the burning of particles that are much larger than those used in pulverised wood combustion [10,11,12]. Both Mukunda *et al.* [10] and Kuo and Hwang [11] describe the oxidation of large particles (10-50 mm). They consider a pyrolysis front moving towards the centre of the particle, which is an unrealistic description for pulverised wood combustion: for this type of combustion it is more appropriate to assume a uniform rate of devolatilisation. Likewise, in these models during the burning of the char a key role is that of the conduction of heat and it is assumed that the core shrinks along with the temperature wave front [11]; pulverised fuel combustion is often described by assuming that the burning particle is isothermal, with few exceptions [13,14].

Table 5.1 summarises some of the features of several single particle combustion models. Some of the models utilise statistical distributions to describe one or more properties of the particles [4,6,17,19]. These distributions are used to account not only for the heterogeneity of the char (reactivity, density, etc.), but also, implicitly, for the changes in char properties that occur during combustion. For example, models that do not include thermal deactivation may use a distribution of char reactivity [6,17,19]. Coda and Tognotti [6,17] use a semi-empirical approach in their model: they determine statistically a mean specific surface area (m^2/g) and a mean porosity of the char particles which are then used as constants in the model; as for reactivity, the model includes a particle-size dependent distribution of the pre-exponential factor. Mitchell *et al*. [19] use a six-step reaction mechanism with distributed activation energy.

As far as the burning kinetic regime is concerned, several models require one or two parameters as input describing the relative importance of intrinsic kinetics, pore diffusion, and external diffusion during particle oxidation, as proposed by Smith [15]:

$$\left(\frac{d}{d_0}\right) = U^{\alpha} \qquad (5.4)$$

$$\left(\frac{\rho}{\rho_0}\right) = U^{\beta} \tag{5.5}$$

Where 3α+β=1. U is the unburned carbon fraction, d the particle diameter and d_0 the original particle diameter. For particles that burn with steadily reducing size and constant density α=1/3 and β=0: this corresponds to an overall effectiveness factor η≈0 (see Chapter 2.5.1). For a particle of unchanging size and decreasing density, i.e. when the chemical reaction alone controls the burning rate, α=0 and β=1 (equivalent to η=1). Equations (5.4) and (5.5) have been used both unchanged [18] or slightly modified, in order to account for the presence of ash in the char (at full conversion, for U=0, the (ash) particle would not exist) [4,6,16,17]:

$$\left(\frac{d}{d_0}\right) = \left(\frac{m}{m_0}\right)^{\alpha} \tag{5.6}$$

$$\left(\frac{\rho}{\rho_0}\right) = \left(\frac{m}{m_0}\right)^{\beta} \tag{5.3}$$

As discussed in Chapter 2, the product of carbon oxidation can be CO or CO_2. Of the ones included in Table 5.1, only the model by Mitchell et al. [19] calculates the production of CO_2 considering the reaction mechanism. The common way to account for CO_2 production (either directly or by CO oxidation), is to use an empirical Arrhenius type correlation to express the CO to CO_2 ratio [4,6,17].

Due to the limited knowledge on particle fragmentation during combustion, most models do not account for it, with a few exceptions such as the model by Jensen described above [7]. For similar reasons, char thermal deactivation is rarely included in models [1,2,4]; the loss of reactivity of the char as it is exposed to higher temperatures is more commonly accounted for by means of a distribution of reactivity [6,17,19].

Finally, few of the models in Table 5.1 combine the pyrolysis of a fuel particle and char oxidation [12,16,18].

Table 5.1 Key features of some particle combustion models describing pulverised fuel combustion.

Ref.	*Heat transport*	*Pyrolysis*	*Kinetic regimes*	*CO/ CO_2*	*Oxidation Kinetics*	*Char reactivity based on*	*Thermal deactivation*	*Fragmentation*	*Ash*	*(semi-) Empirical input parameters*	*Statistical distributions*
[4]	Isothermal particle	No	I, II, III Eq (5.3)	$\frac{CO}{CO_2} = A_c e^{\left(-\frac{E_c}{RT_p}\right)}$	Eq. (4.2) with n = 0.5	External surface area	$\frac{dN}{dt} = -A_d N \exp(-E_d / RT)$	No	Shrinking core + ash layer	β in eq. (4.3) ash porosity,	A is a gamma dist, E_d log normal dist, size dist, density dist,
[7]	Isothermal particle	No	II, III	Only CO				Peripheral fragmentation		Critical porosity	
[6,17]	Isothermal particle	No	I, II, III Eq. (5.6) & (5.3)	$\frac{CO}{CO_2} = A_c e^{\left(-\frac{E_c}{RT_p}\right)}$	$k = Ae^{\left(-E/RT_p\right)} P_{O_2}^n$	Mass	No	No	Inert, same properties as char	Surface area, porosity α, β in Eq. (4.6) & (4.3)	Reactivity (A), based on particle size
[16]	Isothermal particle	Yes	I, II, III Eq. (5.6) & (5.3)	Only CO	Eq. (4.2) with n = 1	External surface area	No	Yes	No influence on mass transport	Reactivity (A and E) α, β in Eq. (4.6) & (4.3)	Particle size
[18]	Isothermal particle	Yes	I, II, III Eq (5.4) & (5.5)	Only CO	Eq. (4.2) with n = 1	External surface area	No	No	No influence on mass transport	Reactivity (A and E); α, β in Eq. (4.4) & (4.5)	Particle size

Ref.	*Heat transport*	*Pyrolysis*	*Kinetic regimes*	*CO/ CO_2*	*Oxidation Kinetics*	*Char reactivity based on*	*Thermal deactivation*	*Fragmentation*	*Ash*	*(semi-) Empirical input parameters*	*Statistical distributions*
[1,2]	Isothermal particle	Yes [a)]	I, II,III Eq (5.6)	Ratio not specified	$k = Ae^{(-E/RT_p)}P_{O_2}^n$	Internal surface area	Yes, using an annealing factor f_{ann}	No	Not considered	Spec int area, porosity, f_{ann}	Particle size
[13]	Allows intraparticle gradient	No	I,II,III	Only CO	$k = Ae^{(-E/RT_p)}P_{O_2}^n$ n=1	Internal surface area	No	Peripheral fragmentation	Not considered	Gas film thickness, pore size (bimodal distr.)	None
[19]	Isothermal particle	No	I,II,III	Both CO and CO_2. 6-step mechanism, each step described by power law kinetics		Internal surface area	No	No	Not considered	Structural parameter	Activation energy

[a)] Includes soot formation from tar

5.3 SINGLE CHAR PARTICLE OXIDATION MODEL

The general approach in this work is to use a simple model to test whether the wood conversion attained in Avedøre Unit 2 boiler can be predicted and to gain useful information on the behaviour of pulverised wood in such a boiler. The choice of using a simple model is partly due to the complexity of the char oxidation process and to the limited information available on char characteristics and their changes during combustion (e.g. surface area development and particle fragmentation). On the other hand, strongly simplifying assumptions are necessary to describe the conditions in the furnace.

The next section deals with the kinetics of the chemical reaction. Mass transport equations are then derived, which are combined with the kinetics in the mass balance. Similarly, heat transport is dealt with and used to set up a heat balance for the combustion of a single char particle. After the derivation of the model equations, the values of the char properties applied during modelling are presented. Finally, the assumptions made to describe the pulverised wood furnace of Avedøre Unit 2 are outlined.

5.3.1 CHEMICAL REACTION

The model assumes that the only product of char oxidation is CO, i.e. the only reaction considered for mass and heat balances is:

$$2C + O_2 \rightarrow 2CO \qquad \text{(R1)}$$

In Chapter 4, equation (4.2) expresses the rate of carbon consumption during char oxidation:

$$Rate = -\frac{dm}{dt} = k_0' e^{-\frac{E_a}{RT}} \cdot m \qquad (5.7)$$

where m is the dry ash-free mass of the wood char at a certain time t, k'_0 is the pre-exponential factor, E_a the activation energy and R is the gas constant.

The present model assumes that wood char particles consist only of ash and carbon; therefore the mass of dry, ash-free char is actually the mass of carbon in the char and the units of the pre-exponential factor k'_0 in equation (5.7) are $\left[kg_C / (kg_C \cdot s)\right]$.

The model assumes that reaction (R1) is of first order with respect to oxygen. As explained in Chapter 4, the concentration of oxygen was kept constant during the thermogravimetric (STA) runs from which k'_0 was determined. It is thereby possible to calculate a new pre-exponential factor k_0 independent of the concentration of O_2:

$$k_0 = \frac{k'_0}{C_{O_2,STA}} = k'_0 \cdot \frac{R \cdot T}{y_{O_2,STA} \cdot P} = k'_0 \cdot \frac{R \cdot T}{0.04 \cdot P} \qquad \left[\frac{m^3}{mol_{O_2} \cdot s}\right] \tag{5.8}$$

where $C_{O_2,STA}\ [mol/m^3]$ is the concentration of oxygen in the gas during the thermogravimetric runs. Thus, the rate of carbon consumption can be written as:

$$Rate = -\frac{dm}{dt} = k_0 \cdot e^{-\frac{E_a}{RT}} \cdot C_{O_2} \cdot m = k_r \cdot C_{O_2} \cdot m \tag{5.9}$$

where k_r, whose units are $\left[\frac{m^3}{mol_{O_2} \cdot s}\right]$, is the reaction rate constant.

5.3.2 MASS TRANSPORT

5.3.2.1 GAS FILM DIFFUSION

The char particle is assumed to be spherical in the model; this assumption is supported by the results illustrated earlier (see Figure 4.5 in Chapter 4). The mass transfer of oxygen from the bulk of the gas stream to the surface of the char particle is described by assuming that all the resistance is found within a stagnant gas film surrounding the char particle. Under this assumption, the molar flux of oxygen from the bulk gas to the surface is described by:

$$W_{O_2} = h_D \cdot (C_{O_2,b} - C_{O_2,s}) \qquad \left[\frac{mol}{m^2 \cdot s}\right] \tag{5.10}$$

where $C_{O_2,b}$ and $C_{O_2,s}$ are the concentrations of oxygen in the bulk gas and on the char surface, respectively, and h_D, whose units are [*m/s*], is the mass transfer coefficient. The mass transfer coefficient is defined as the ratio between the diffusion coefficient of oxygen in the gas, $D\ [m^2/s]$, and the thickness of the gas film. In this model it is assumed that the bulk gas consists of only oxygen and

nitrogen: D is thereby the binary O_2-N_2 diffusion coefficient and is estimated by the Chapman-Enskog kinetic theory [7]. In practice, the mass transfer coefficient h_D is calculated from the definition of the dimensionless Sherwood number, Sh:

$$h_D = \frac{Sh \cdot D}{2r_p} \quad \left[\frac{m}{s}\right] \tag{5.11}$$

where r_p is the radius of the spherical char particle. Empirical correlations are available for estimating the Sherwood number for flow around a spherical particle as a function of the Reynolds number (Re) and the Schmidt number (Sc) [20]:

$$Sh = 2.0 + 0.6 \cdot \mathrm{Re}^{\frac{1}{2}} \cdot Sc^{\frac{1}{3}} \tag{5.12}$$

$$\mathrm{Re} = \frac{u_t \cdot 2r_p}{\nu} \quad , \quad Sc = \frac{\nu}{D}$$

where $\nu \left[m^2/s\right]$ is the gas kinematic viscosity, approximated here by nitrogen kinematic viscosity calculated according to a correlation proposed by Danner and Daubert [21] and u_t is the particle terminal falling velocity in the gas. In the model it is assumed that the gas flows upwards along the furnace axial direction, and that the particle follows the same flow path: therefore, the velocity of the char particle relative to the gas stream is its terminal falling velocity. This is thereby the velocity that needs to be considered for mass and heat transfer between the gas and the particle. The particle terminal falling velocity is calculated by means of a correlation that utilises the dimensionless particle radius given by [22]:

$$r_p^* = r_p \cdot \left(\frac{g \cdot \left(\rho_{gas} - \rho_{char}\right)}{\rho_{gas} \cdot \nu^2} \right)^{\frac{1}{3}} \tag{5.13}$$

g is the gravitational acceleration, $\rho_{gas} = MW_{N_2} \cdot \frac{P}{R \cdot T}$ is the gas (here N_2) density at pressure P and temperature T, and ρ_{char} is the char density. The correlation that estimates the dimensionless terminal falling velocity of the char particle is the following [22]:

$$u_t^* = \left(\frac{18}{\left(2 \cdot r_p^*\right)^2} + \frac{0.591}{\sqrt{2 \cdot r_p^*}} \right)^{-1} \tag{5.14}$$

Thus, using the definition of dimensionless velocity given in reference 22:

$$u_t = u_t^* \cdot \left(\frac{\nu \cdot g \cdot \left(\rho_{char} - \rho_{gas} \right)}{\rho_{gas}} \right)^{\frac{1}{3}} \tag{5.15}$$

5.3.2.2 INTRAPARTICLE DIFFUSION

Depending on the combustion conditions, the oxygen that diffuses through the gas film to the outer surface of the char particle may either react on the outer surface or diffuse into the particle through the pores. In the char particle, the fraction of cross surface area available for oxygen diffusion is ε_{char}, i.e. the char porosity. Moreover, pores are not straight and may have restrictions: this is accounted for by the so called tortuosity factor, τ. If the char pores are very small, their size may be smaller than the mean free path of the oxygen molecules; the type of diffusion taking place in this case is called Knudsen diffusion. Molecular binary diffusion and Knudsen diffusion act as resistances in series and therefore, the effective diffusion coefficient for oxygen into the char particle is expressed by:

$$D_e = \frac{1}{\frac{\tau}{D \cdot \varepsilon_{char}} + \frac{\tau}{D_K \cdot \varepsilon_{char}}} \tag{5.16}$$

where D_K is the Knudsen diffusion coefficient. To apply equation (5.16) a detailed knowledge of the pores' geometry is required, in order to estimate the tortuosity factor. The pores' size distribution is needed as well, since a different value of D_K corresponds to each pore size. It is therefore very complicated to use the definition of effective diffusion (equation (5.16)) in practice.

The model presented here calculates the effective diffusion coefficient in the char by means of the following approximation, which was successfully applied in previous works [7]:

$$D_e = D \cdot \varepsilon_{char}^2 \tag{5.17}$$

5.3.2.3 COMBINING MASS TRANSPORT AND CHEMICAL REACTION

In order to combine the effects of external gas film diffusion, internal diffusion through the pores and heterogeneous chemical reaction some dimensionless parameters are used. A detailed description of how these parameters are derived can be found in Fogler [23]. For a first order reaction in a spherical porous char particle, we can estimate the relative importance of the surface reaction rate to the rate of diffusion through the pores as [23]:

$$\Phi^2 = \frac{\frac{k_r \cdot \rho_C \cdot r_p \cdot C_{O_2}}{2 \cdot MW_C}}{D_e \cdot \left(C_{O_2} - 0\right) / r_p} = r_p^{\,2} \frac{k_r \cdot \rho_C}{2 \cdot MW_C \cdot D_e} \tag{5.18}$$

Where $\rho_C = \frac{m_C}{m_{char}} \cdot \rho_{char} = \frac{m_{char} - m_{ash}}{m_{char}} \cdot \rho_{char} = \rho_{char} \cdot (1 - \xi_{ash})$ is the carbon density in the char, $\xi_{ash} = \frac{m_{ash}}{m_{char}}$ is the mass fraction of ash in char, MW_C is the molar weight of carbon [*kg/mol*] and 2 is the stoichiometric coefficient of C in reaction (R1). The square root of Φ^2, i.e. Φ, is the Thiele modulus:

$$\Phi = r_p \cdot \sqrt{\frac{k_r \cdot \rho_C}{2 \cdot MW_C \cdot D_e}} \tag{5.19}$$

A large Thiele modulus corresponds to a situation in which diffusion through pores is much slower than the surface reaction rate.

If we consider only chemical reaction and internal diffusion, the so called internal effectiveness factor η is an indication of how far the oxygen molecules can penetrate into the char particle before reacting with the carbon on surface of the pores. The internal effectiveness factor can be defined as the ratio between the actual rate of reaction and the rate of reaction that would exist if the entire internal surface was exposed to the external char surface conditions (i.e. no internal diffusion limitation). Neglecting external mass transfer from the bulk gas to the particle external surface, the actual rate of reaction is the rate at which oxygen diffuses into the char at the outer surface. For the first order reaction considered in this model, η is given by the following expression [23]:

$$\eta = \frac{3 \cdot (\Phi \cdot \coth(\Phi) - 1)}{\Phi^2} \tag{5.20}$$

In order to account for external mass transfer, i.e. for the fact that the concentration of oxygen at the char outer surface is not equal to the oxygen concentration in the bulk gas, the overall effectiveness factor Ω is used. The overall effectiveness factor enables to express the overall burning rate in terms of the oxygen bulk concentration, as will be illustrated later. The expression for Ω used in this model is given below [23]:

$$\Omega = \frac{1}{\frac{1}{\eta} + \frac{k_r \cdot \rho_C}{2 \cdot MW_C} \cdot \frac{r_p}{3 \cdot h_D}} \tag{5.21}$$

5.3.3 MASS BALANCE

If all the internal and external surface of the char were exposed to the bulk oxygen concentration, the overall burning rate of a char particle would be simply expressed by equation (5.9). As explained above, the overall effectiveness factor Ω accounts for both internal and external diffusion limitations. The particle burning rate is thus expressed by:

$$R_m = -\frac{dm}{dt} = k_r \cdot C_{O_2,b} \cdot m \cdot \Omega \quad \left[\frac{kg_C}{s}\right] \tag{5.22}$$

On the other hand, the particle mass loss can also be expressed by:

$$-\frac{dm}{dt} = \frac{d}{dt}\left(\frac{4}{3}\pi \cdot r_p^{\,3} \cdot \rho_C\right) \quad \left[\frac{kg_C}{s}\right] \tag{5.23}$$

The model assumes that all the reacted carbon at each point in time is consumed at the outer surface of the particle. It is further assumed that the ash formed during the combustion of a certain layer of carbon leaves the char particle by peripheral fragmentation. Therefore, the burning particle is described as a shrinking char particle and both the carbon density and the particle density of the char remain constant during combustion, i.e. ρ_C and ρ_{char} are not a function of time.

Combining equation (5.22) and (5.23) we thus obtain:

$$\frac{4}{3}\pi \cdot \rho_C \cdot 3r_p^{\,2} \cdot \frac{dr_p}{dt} = -k_r \cdot C_{O_2,b} \cdot (\frac{4}{3}\pi \cdot r_p^{\,3} \cdot \rho_C) \cdot \Omega \qquad (5.24)$$

Simplifying and re-arranging we find:

$$\frac{dr_p}{dt} = -\frac{k_r \cdot \Omega \cdot C_{O_2,b} \cdot r_p}{3} \qquad \left[\frac{m}{s}\right] \qquad (5.25)$$

5.3.4 HEAT TRANSPORT

The model assumes that the char particle is isothermal; therefore heat transport in the char is neglected. As regards convective heat transfer between the particle and the bulk gas, heat diffuses through the gas film surrounding the particle. The heat and mass transfer principles and correlations for a free falling sphere immersed in a gas are analogous. The Nusselt (Nu) and Prandtl (Pr) numbers correspond to the Sherwood and Schmidt number respectively [23]:

$$Nu = 2.0 + 0.6 \cdot \mathrm{Re}^{\frac{1}{2}} \cdot \mathrm{Pr}^{\frac{1}{3}} \qquad (5.26)$$

$$\mathrm{Pr} = \frac{\nu \cdot \rho_{gas} \cdot C_{P,gas}}{k_t} \qquad (5.27)$$

where $\rho_{gas}\ \left[kg/m^3\right]$ is the gas density, $C_{P,gas}\ \left[J/(kg \cdot K)\right]$ is the gas heat capacity and $k_t\ \left[J/(K \cdot m \cdot s)\right]$ is the gas thermal conductivity.

The heat transfer coefficient h is calculated from the definition of the dimensionless Nusselt number [23]:

$$h = \frac{Nu \cdot k_t}{2r_p} \qquad \left[\frac{J}{m^2 \cdot s \cdot K}\right] \qquad (5.28)$$

Thus, the convective heat flux between the particle and the surrounding gas is:

$$q_c = h \cdot (T_b - T_{char}) \quad \left[\frac{J}{m^2 \cdot s}\right] \qquad (5.29)$$

The model takes into account heat transfer by radiation from the char particle to the surroundings. The heat flux by radiation is expressed by [24]:

$$q_r = \varepsilon \cdot \sigma \cdot \left(T_{char}^4 - T_{wall}^4\right) \quad \left[\frac{J}{m^2 \cdot s}\right] \tag{5.30}$$

where ε is the char emissivity, here assumed to be 0.8 and σ is the Boltzmann constant.

5.3.5 HEAT BALANCE

Taking into consideration the heat flux by convection (equation (5.29)), the heat flux by radiation (equation (5.30)) and the heat released by the exothermic oxidation rate, the heat balance for the burning particle can be written as follows:

$$C_P \cdot \frac{4}{3}\pi \cdot r_p^{\,3} \cdot \rho_{char} \cdot \frac{dT_{char}}{dt} = 4\pi \cdot r_p^{\,2} \cdot h\left(T_b - T_{char}\right) + 4\pi \cdot r_p^{\,2} \cdot \varepsilon\sigma\left(T_{wall}^{\,4} - T_{char}^{\,4}\right) + \frac{R_m \cdot \left(-\Delta H_{reac}\right)}{MW_C} \tag{5.31}$$

where:

$\frac{dT_{char}}{dt}$ is the instantaneous variation of particle temperature,

ΔH_{reac} [J/mol] is the heat of reaction per mole of carbon reacted, from Jensen [7]:

$\Delta H_{reac} = 106.39 \cdot 10^3 + 3.4309 \cdot T_{char} + 1.3807 \cdot 10^{-3} \cdot T_{char}^2 + 8.9119 \cdot 10^5 \cdot T_{char}^{-1}$,

and C_P is the char heat capacity, here assumed to be 1000 $\frac{J}{kg \cdot K}$.

Rearranging equation (5.31) we obtain:

$$\frac{dT_{char}}{dt} = \frac{3}{\rho_{char} \cdot C_P \cdot r_p} \cdot \left[h \cdot \left(T_b - T_{char}\right) + \varepsilon \cdot \sigma \cdot \left(T_{wall}^{\,4} - T_{char}^{\,4}\right) + \frac{R_m \cdot \left(-\Delta H_{reac}\right)}{MW_C \cdot 4 \cdot \pi \cdot r_p^{\,2}}\right] \tag{5.32}$$

Equations (5.25) and (5.32) are the two coupled differential equations solved in this model.

5.3.6 APPLIED CHAR CHARACTERISTICS

Table 5.2 shows the values of wood char characteristics used in the model. The values were determined during the experimental work presented in Chapter 4, unless another reference is given.

Table 5.2 Char parameters used in the model.

	Units	*Values used in the model*
Radius, r_p	μm	15 - 350
Initial particle temperature	K	1100
Char Density, ρ_{char}	kg/m^3	220 [25]
Char porosity, ε_{char}	-	0.87 [25]
Ash fraction, ξ_{ash}	kg/kg	0.11
Char reactivity:		
E_a	kJ/mol	166
k_0	$\left[\frac{m^3}{mol_{O_2} \cdot s}\right]$	$8.85 \cdot 10^7$ – $3.39 \cdot 10^{10}$

The wood char particles are assumed to be spherical. In Chapter 4, Table 4.2, sizes of char particles depending on wood particle size are shown. As discussed there, the extent of particle shrinkage during pyrolysis seemed to increase with pyrolysis temperature and decrease with wood particle size. Due to the limited data set available, it was not possible to derive an expression of wood particle shrinkage as a function of particle size and pyrolysis temperature. The wood particle size shown in Table 4.2, as well as the wood particle size from the full scale campaign at Avedøre unit 2 (Figure 3.5) were obtained by sieving. According to the wood fuel particle size distribution from full scale measurements, 85% of the mass of the wood fuel is made up of particles with sieve size between 125 μm and 2000 μm, while the median (50 % of the mass of wood fuel is constituted by smaller particles) was 440 μm; therefore it was decided to primarily investigate the behaviour of wood fuel particles between 125 μm and 2000 μm. Two different approaches were followed to determine the range of char particle sizes to be used as input to the model. First, an average shrinkage was calculated from the results in Table 4.2, which correlates the wood particle sieve size (before pyrolysis) to the spherical char particle radius (after pyrolysis): the obtained char particle radius is shown in Table 5.3 (from EFR). On the other hand, the size of char particles was also calculated based on wood pyrolysis' yield. As discussed in Chapter 4, the char yield measured during the EFR pyrolysis experiments of 90-355 μm wood particles was 2-6

wt%, while a higher yield of char is expected for larger particles: therefore, the calculation of the size of the char assumes a 2 wt% yield for 125 μm wood particles, 6 wt% yield for 440 μm wood particles and 10 wt% yield for 2000 μm wood particles. It was further assumed that wood fuel particles are spherical (diameter equal to the sieve size), the wood density is 700 kg/m^3 and the char density 220 kg/m^3 (as in Table 5.2). The results of the yield-based calculation are shown in Table 5.3 (from yield).

Table 5.3 Char particle radius used in the model.

Fuel sieve size (μm)	*Char particle radius (μm)*		
	from EFR	from yield	*used in simulation*
125	20	13	*15*
440	71	67	*70*
2000	322	361	*350*

As already discussed, the temperature history of a wood particle inside a pulverised fuel boiler is not easy to describe and may vary significantly depending on the particle's route. The model assumes that the temperature of any particle at the end of pyrolysis, i.e. when char combustion begins, is 1100 K.

As far as char density and char porosity are concerned, the values used in the model are found in Mermoud *et al.* [25]: for beech char produced at high heating rate (900 K/min), they measured a char (apparent) density of 220 kg/m^3. They also measured the solid density of the char, which was 1700 kg/m^3 [25]. The corresponding char porosity is found by: $\varepsilon_{char} = 1 - (\rho_{char} / \rho_{solid}) = 0.87$.

The value of the mass fraction of ash in char was first extrapolated from STA oxidation runs (see Chapter 4) assuming that the char consisted solely of carbon and ash. This value was then confirmed by letting a larger amount of char (about 0.3 g) burn in air at 650 °C and weighing the remaining ash.

As for wood char reactivity, the lowest and the highest pre-exponential factors *k* obtained from char produced at boiler-like conditions in the EFR were used as reference cases for the simulations (pine char obtained at 1573 and 1073 K, respectively).

As explained in section 5.4, some of the parameters listed in Table 5.2 such as char porosity and char density were changed over certain ranges in order to test the influence of literature data on model results.

5.3.7 SIMULATION OF BOILER CONDITIONS

In Chapter 1 the Avedøre Unit 2 power plant was described. In order to model the combustion of a char particle in the suspension fired furnace, major simplifying assumptions were made.

The quantity (number of moles) of bulk gas at any level in the furnace is assumed to be constant and equal to the quantity of primary air that enters the furnace. Furthermore, the gas is assumed to flow upwards from the lowest level of burners at a constant velocity of 7.6 m/s; this value corresponds to assuming that the furnace is operated at full load (800 MW) with 100% wood fuel firing, at an average furnace temperature of about 1450 K [26]. The fact that wood and air may enter the furnace at three different burner levels is not taken into account; it is assumed that the fuel and combustion air enter the chamber at the lowest level. Under this assumption, the distance between the burner and the radiation shield located just below the superheaters is 35 m and the gas residence time in the furnace is about 4.6s.

Another approximation used during the modelling of the combustion of the char is that the gas temperature is uniform in the furnace, although in practice it is lower at superheater level than at burner level, where combustion of the volatiles released during pyrolysis occurs. This choice was made partly because of the lack of reliable flame temperature measurements during the combustion of pulverised wood in the furnace in question. Moreover, describing the actual temperature of the bulk gas surrounding a char particle during its combustion in such a furnace realistically would require a much more detailed description of the two-phase flow in the furnace; this is only possible when the particle combustion model is included in a CFD simulation of the combustion chamber.

The wall temperature is also assumed to be constant along the furnace; its value was varied in the interval 800 – 1100 K in order to investigate its influence on the achieved conversion of a char particle in the furnace.

The char particle's actual velocity in the furnace is calculated by considering the velocity of the gas (u_g) and the particle's terminal velocity in the gas (u_t, see equation (4.15)), as follows: $u_{char} = u_g - u_t$. The height at which the particle is in the furnace at any given moment during combustion is thus found by integration of the following:

$$\frac{dL}{dt} = u_{char} \tag{5.33}$$

where L is the height in the furnace (at the burner *L=0*).

Table 5.4 summarises the values of the main parameters used in the model to describe the furnace of the Avedøre Unit 2 power plant.

Table 5.4 Furnace parameters used in the model.

	Units	*Values used in the model*
Distance burner - radiation shield	m	35
Distance burner-bottom of the boiler	m	22
Bulk gas temperature (uniform)	K	1200 – 1700
Wall temperature	K	800 - 1100
Gas velocity	m/s	7.6
Oxygen in bulk gas	%	0.1 – 4 (constant profile)

5.4 RESULTS AND DISCUSSION

Figure 5.1 to Figure 5.4 show the results obtained for the combustion of a char particle with a radius of 70 μm in a gas containing 2% O_2; the bulk gas temperature is 1200 K, the wall temperature 950 K and initially the char particle temperature is 1100 K. The pre-exponential factor k used for this simulation was $3.39 \cdot 10^{10}$ $m^3 mol^{-1} s^{-1}$. For comparison, the dotted lines in Figure 5.1 to Figure 5.4 were obtained without taking the heat balance into consideration, i.e. isothermal particle combustion at the bulk gas temperature (1200 K). In Figure 5.1 it can be seen that, in these conditions, the time for full particle conversion is quite short compared with the gas residence time in the boiler (4.6 s) and that the

evolution of conversion is not significantly affected by the heat balance. Figure 5.2 and Figure 5.3 illustrate the evolution of the particle's radius and temperature, respectively.

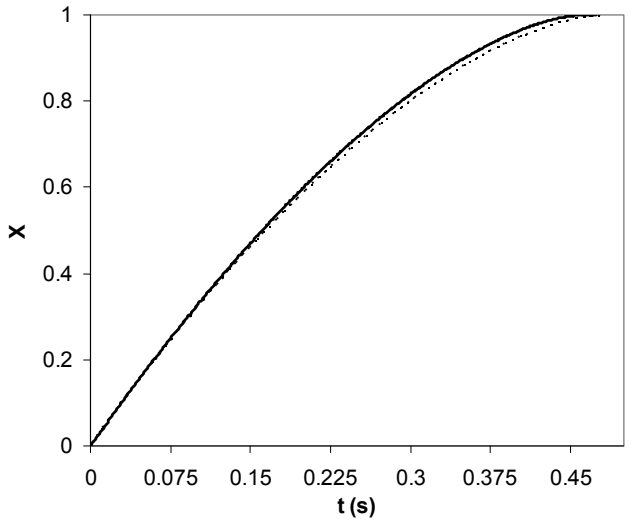

Figure 5.1 Char conversion during combustion. Bulk gas temperature: 1200K. Wall temperature: 950K. Initial char temperature: 1100K. O_2 in bulk gas: 2%. Reactivity: $k = 3.39 \cdot 10^{10}$. Initial char radius: 70µm. The dotted line illustrates the conversion when the heat balance is not included in the model, i.e. isothermal combustion (1200K).

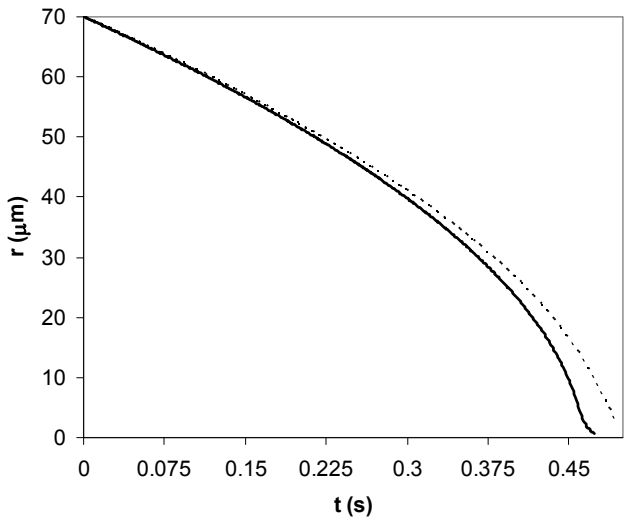

Figure 5.2 Char particle radius during combustion. Bulk gas temperature: 1200K. Wall temperature: 950K. Initial char temperature: 1100K. O_2 in bulk gas: 2%. Reactivity: $k = 3.39 \cdot 10^{10}$. Dotted line: isothermal combustion (1200K).

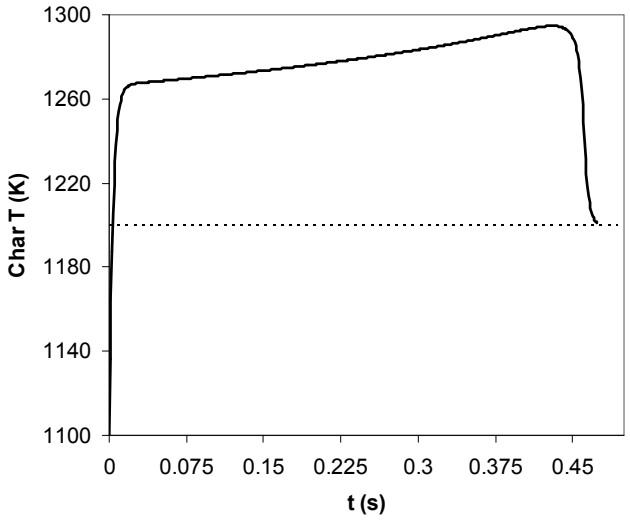

Figure 5.3 Char particle temperature during combustion. Bulk gas temperature: 1200K. Wall temperature: 950K. Initial char temperature: 1100K. O_2 in bulk gas: 2%. Reactivity: $k = 3.39 \cdot 10^{10}$. Initial char radius: 70µm. Dotted line: isothermal combustion (1200K).

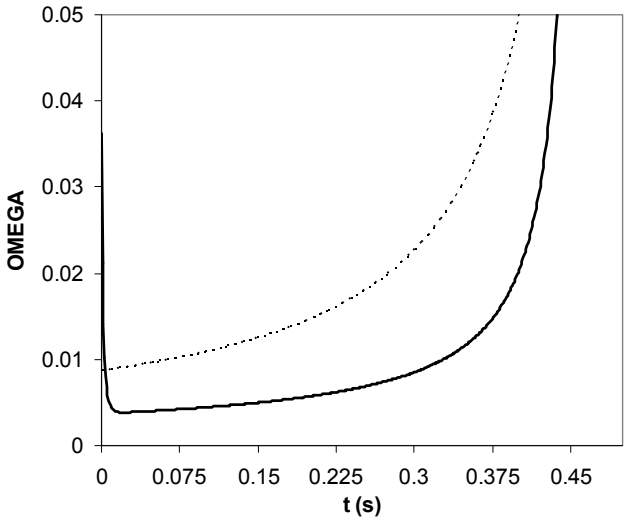

Figure 5.4 Overall efficiency factor (OMEGA) during char combustion. Bulk gas temperature: 1200K. Wall temperature: 950K. Initial char temperature: 1100K. O_2 in bulk gas: 2%. Reactivity: $k = 3.39 \cdot 10^{10}$. Initial char radius: 70µm. Dotted line: isothermal combustion (1200K).

As seen in Figure 5.3, the temperature of the particle increases rapidly to approximately 60 degrees above the surrounding gas temperature as a consequence of the heat released by the oxidation reaction. The higher temperature of the particle makes the rate of reaction increase; as a consequence, the overall effectiveness factor decreases, i.e. the rate of oxygen diffusion from the bulk gas to the inner surface of the particle relative to the rate of reaction becomes smaller, as can be seen by comparing Figure 5.3 with Figure 5.4. Moreover, Figure 5.4 shows that when the heat balance is excluded from the model no decrease of Ω is observed in the initial stages of conversion. The burning rate of the particle is controlled by external diffusion up to high conversion (regime III, $\Omega<0.1$). When the particle approaches full conversion the amount of carbon reacting at a certain time decreases and thereby the temperature of the particle decreases, causing the rate of reaction to fall; on the other hand, the particle has become smaller and this decreases internal and external resistances to mass transport. As a result, at high conversion Ω increases up to values close to unity and the particle burns in regime I, i.e. chemical reaction control.

Figure 5.5 to Figure 5.7 illustrate how char reactivity and bulk gas temperature influence the combustion of a 70 μm radius char particle. Dotted lines represent low reactivity chars ($k = 8.85 \cdot 10^{7}$ $m^3mol^{-1}s^{-1}$) while solid lines are used for high reactivity chars ($k = 3.39 \cdot 10^{10}$ $m^3mol^{-1}s^{-1}$); the temperature of the bulk gas was set to 1200 K (blue lines), 1500 K (red lines) and 1700 K (green lines); the bulk gas oxygen content was kept at 2% at all temperatures.

Figure 5.5 shows that the conversion time of a 70 μm radius low reactivity char in a gas at 1200 K (blue dotted line) is considerably longer than the conversion time in any of the other conditions. The time of conversion of low reactivity chars burning in a gas at 1500 K (red dotted line) and 1700 K (green dotted line) is much lower, due to the higher chemical reaction rate and diffusion rates at these temperatures. As regards high reactivity chars (solid lines in Figure 5.5), it can be seen that the time of conversion is always shorter for a char with higher reactivity, provided the other conditions remain unchanged. The lower the temperature of combustion, the larger the difference between conversion times for low and high reactivity char: for example, in Figure 5.5 the time for the char particle to achieve 99.80 % conversion in a gas at 1200 K is 7.56 s and 0.45 s for low and high reactivity respectively, while at 1500 K the corresponding times of 99.80% conversion are 0.73 s and 0.37 s. This is due to the fact that at higher temperatures the rate of combustion is less influenced by changes in

char reactivity. Both char chemical reaction rate and oxygen diffusion become greater at higher temperatures; yet, the reaction rate, which follows the Arrhenius law, increases more than the diffusion rate and therefore mass transport tends to become limiting.

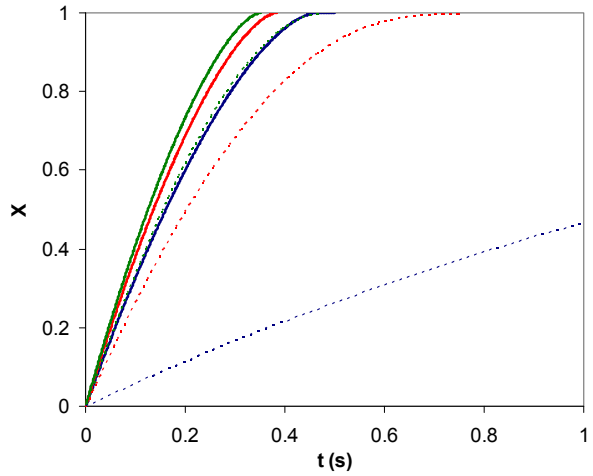

Figure 5.5 Char conversion. Initial char radius: 70μm. Wall temperature: 950K. Initial char temperature: 1100K. O_2 in bulk gas: 2%. Solid lines: $k = 3.39 \cdot 10^{10}$, dotted lines: $k = 8.85 \cdot 10^{7}$. Bulk gas temperature: blue, 1200K; red, 1500K; green, 1700K.

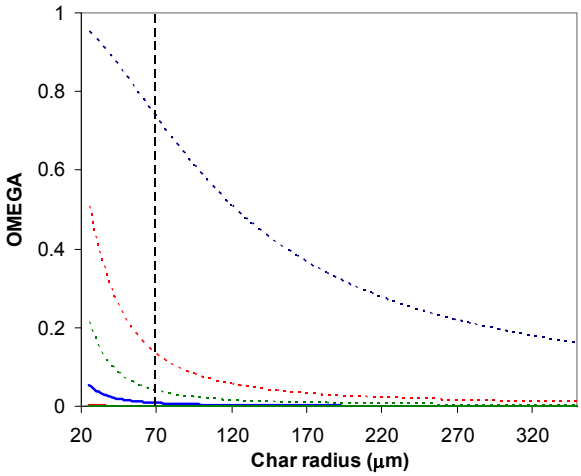

Figure 5.6 Initial overall efficiency factor (OMEGA) as a function of char radius. Wall temperature: 950K. Initial char temperature: 1100K. O_2 in bulk gas: 2%. Solid lines: $k = 3.39 \cdot 10^{10}$, dotted lines: $k = 8.85 \cdot 10^{7}$. Bulk gas temperature: blue, 1200K; red, 1500K; green, 1700K.

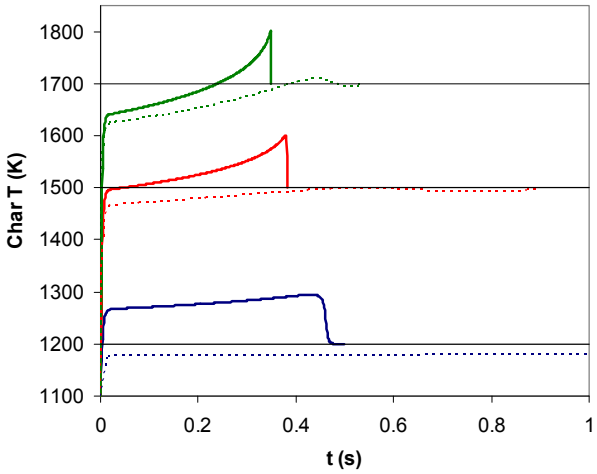

Figure 5.7 Char particle temperature during char combustion. Initial char radius: 70μm. Wall temperature: 950K. Initial char temperature: 1100K. O_2 in bulk gas: 2%. Solid lines: $k = 3.39 \cdot 10^{10}$, dotted lines: $k = 8.85 \cdot 10^{7}$. Bulk gas temperature: blue, 1200K; red, 1500K; green, 1700K. Horizontal lines indicate the bulk gas temperature.

Figure 5.6 illustrates the burning regime at the beginning of the combustion of char particles up to 350 μm radius. In agreement with the results in Figure 5.5, Figure 5.6 shows that the initial overall effectiveness factor Ω for 70 μm radius char particles is well below 0.1 (regime III) for high reactivity chars, regardless of the bulk gas temperature; for low reactive chars internal diffusion becomes more limiting as the bulk gas temperature decreases from 1700 K to 1500 K (regime II) and chemical reaction is the main controlling step at 1200 K, explaining why the conversion time in this condition is much longer. As far as char size is concerned, it can be seen in Figure 5.6 that the overall efficiency factor decreases with increasing particle size, in accordance with equation (5.21); as discussed above, the greater the particle radius, the greater the resistance to oxygen diffusion in the gas film surrounding the particle and in the pores. By comparing dotted lines with solid lines in Figure 5.6 it can be seen that an increase of the reactivity of the char of three orders of magnitude causes a major change in particle combustion regime for a given particle size; the conversion of highly reactive char particles with radius as small as 25 μm is controlled by external gas diffusion (regime III).

As regards the temperatures that char particles achieve during combustion, Figure 5.7 shows that the combustion temperature of high reactivity char particles is above the combustion temperature of low reactivity char particles, regardless of the bulk gas temperature. The difference is due to the higher heat of reaction released by the faster burning high reactivity chars. All the particles considered in Figure 5.7 are at 1100 K at the beginning of the combustion, according to the model assumptions. The temperature of the particles increases very fast in the early stages of combustion due to the heat released by the chemical reaction and to heat convection from the surrounding gas. As the particle temperature rises, the radiation heat from the particle to the cold walls of the furnace increases (see equation (5.30)); it is the radiation heat transfer that prevents low reactivity chars (dotted lines in Figure 5.7) from reaching the bulk gas temperature until the very end of combustion when, due to the very small size of the particle, the convection heat transfer coefficient becomes very high. Similar considerations can be done for high reactive particles (solid lines in Figure 5.7), as far as the effect of the cold walls is concerned. Nevertheless, high reactive particles do reach temperatures above that of the bulk gas. Although the peak temperatures for all the high reactivity chars are about 100 K above the gas temperature, the particle temperature evolution during combustion varies with the gas bulk temperature. Figure 5.7 shows that, after the common initial rise at the beginning of combustion, the particle temperature increases at a higher rate as the bulk gas temperature rises from 1200 K to 1700 K:

indeed, at higher temperatures both the reaction rate and the heat of reaction are higher, meaning that by reacting with oxygen the particle releases more heat in less time when the gas temperature is higher. At the late stages of combustion, when the mass of burning carbon becomes very small and the convective heat transfer from the particles to the bulk gas increases very fast, the highly reactive char particles cool down abruptly to the gas bulk temperature.

As discussed above, it is very difficult to describe the history of a particle in a suspension fired boiler realistically, as regards both its flow and the conditions (temperature, composition) of the surrounding gas. In this work it was chosen to use a constant oxygen fraction in bulk gas during the combustion of a particle, although in actual boilers a burning char particle may well go through zones with very different oxygen concentration in the gas, depending on its trajectory and on the boiler's operating conditions. The combustion of a 70 μm char particle in a gas at 1200 K was simulated for oxygen concentrations in the gas varying from 0.1 % to 4 %; the resulting evolution of char conversion with burning time, based on a pre-exponential factor of $8.85 \cdot 10^7$ $m^3 mol_{O2}^{-1} s^{-1}$, is shown in Figure 5.8. As seen in Figure 5.8 the fraction of oxygen in the gas has a large influence on the particle combustion. The time to attain 99.80 % particle conversion is shown in Figure 5.9. Changing the O_2 concentration from 0.1 % to 0.5 % causes the time for conversion to decrease from 165 s to 32 s. The reduction of combustion time is not only due to the higher availability of oxygen for the reaction, but also to the higher temperature that the particle attains as a consequence of the released heat of reaction, which in turn raises the chemical reaction rate, as can be inferred from Figure 5.10 and Figure 5.11. Figure 5.10 shows that for concentrations of up to 2 % oxygen in bulk gas the temperature of the particle increases by 60-80 degrees at the beginning of the combustion and then keeps increasing slowly during the rest of the conversion, approaching the bulk gas temperature (1200 K); both the initial increase in temperature and the subsequent rate of temperature increase become greater as the oxygen concentration in bulk gas increases. When the oxygen in bulk gas is 4 % (brown line in Figure 5.10), the particle attains an initial peak temperature greater than the bulk gas temperature; it then cools down due to radiation losses to the colder wall and convective heat transfer to the bulk gas, eventually attaining a temperature lower than the bulk gas temperature. Subsequently, the particle temperature starts to rise towards the bulk gas temperature again. As discussed for Figure 5.4, the initial decrease of the overall efficiency factor Ω observed in Figure 5.11 is due to the exponential increase of the chemical reaction rate with temperature. As the oxygen concentration in bulk gas increases, thereby

causing the particle temperature to increase, the internal pore diffusion resistance becomes more important.

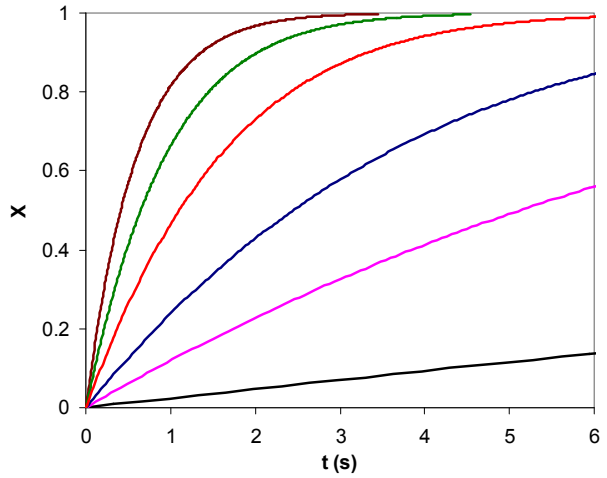

Figure 5.8 Influence of oxygen fraction in bulk gas on char conversion. Initial char radius: 70µm. Wall temperature: 950K. Initial char temperature: 1100K. $k = 8.85 \cdot 10^7$. Bulk gas temperature: 1200K. O_2 in bulk gas, vol %: 0.1, black; 0.5, pink; 1.0, blue; 2.0, red; 3.0, green; 4.0, brown.

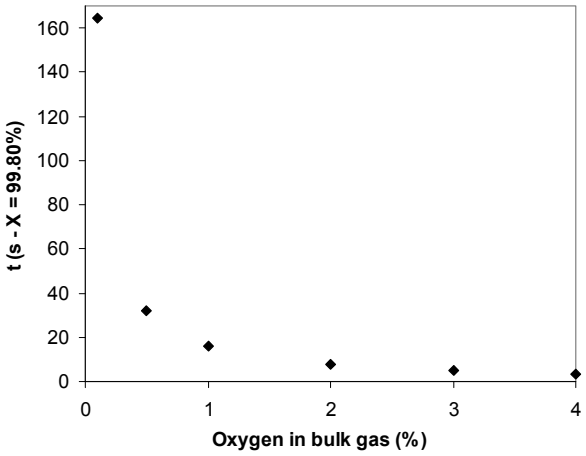

Figure 5.9 Influence of oxygen concentration in bulk gas on the time to achieve 99.80 % conversion. Initial char radius: 70µm. Wall temperature: 950K. Initial char temperature: 1100K. $k = 8.85 \cdot 10^7$. Bulk gas temperature: 1200K.

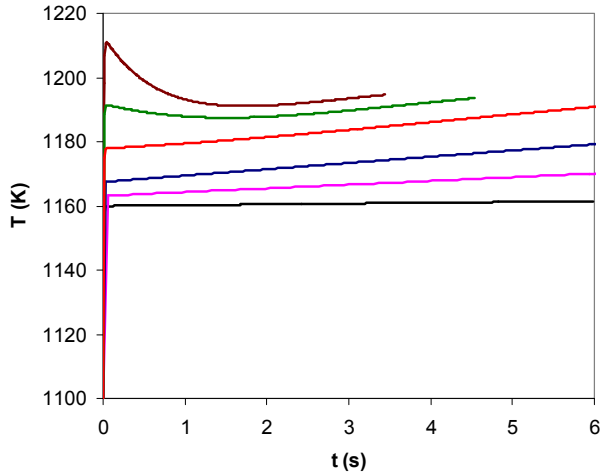

Figure 5.10 Influence of oxygen concentration in bulk gas on char temperature during combustion. Initial char radius: 70µm. Wall temperature: 950K. Initial char temperature: 1100K. $k = 8.85 \cdot 10^7$. Bulk gas temperature: 1200K. O_2 in bulk gas, vol %: 0.1, black; 0.5, pink; 1.0, blue; 2.0, red; 3.0, green; 4.0, brown.

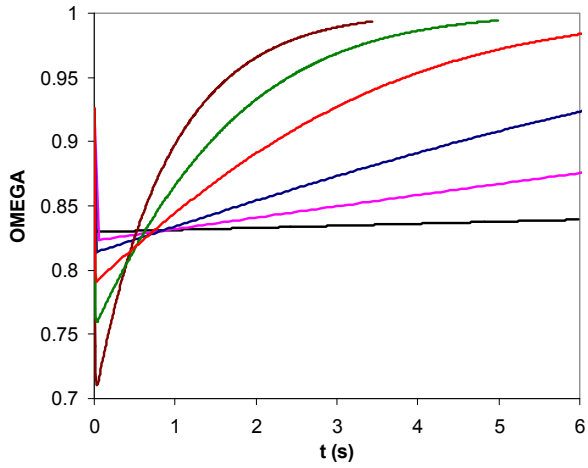

Figure 5.11 Influence of oxygen concentration in bulk gas on char combustion regime (overall efficiency factor). Initial char radius: 70µm. Wall temperature: 950K. Initial char temperature: 1100K. $k = 8.85 \cdot 10^7$. Bulk gas temperature: 1200K. O_2 in bulk gas, vol %: 0.1, black; 0.5, pink; 1.0, blue; 2.0, red; 3.0, green; 4.0, brown.

For all the oxygen concentrations considered in Figure 5.8 to Figure 5.11 char combustion occurs in regime II (combined chemical reaction and internal diffusion control) up to a certain particle conversion (about 70–80 %); having reached this conversion level, the size of the particle is reduced (39–47 μm; initial radius is 70 μm) and the particle burning rate is controlled only by the chemical reaction rate ($\Omega > 0.9$).

Char density is not an easy parameter to assess when simulating wood char combustion. First of all, the variety of wood species and the variation of wood characteristics in different parts of a plant make it difficult to choose the most appropriate literature data. Moreover, it is challenging to estimate the conditions at which the fuel is pyrolysed in the boiler, due to the complexity of the flow and temperature distributions in a pulverised fuel furnace. As reported earlier, in this work a char density of 220 kg/m^3 was used as reference case. Char density and char porosity were changed over certain ranges in order to test the sensitivity of the model to literature data. Both Mermoud *et al*. [25] and Senneca [27] found the solid density of wood chars to be 1700 kg/m^3 for chars originating from different fuels (pine wood chips and beech wood) produced at different pyrolysis conditions. In this study the value of the solid density of the char was kept constant at 1700 kg/m^3, so that the char density ρ_{char} and the char porosity ε_{char} are related as follows: $\varepsilon_{char} = 1 - (\rho_{char} / \rho_{solid})$. Based on the data found in Mermoud *et al*. [25] and in Senneca [27], combustion of a 250 μm char particle in a gas at 1200 K with 2 vol% O_2 was simulated for density values in the range 170 kg/m^3 to 493 kg/m^3, which correspond to porosities from 0.90 to 0.71. Figure 5.12 shows the obtained burning curves. As one would expect, the conversion of a particle with higher density takes longer time: when the particle density increases from 170 kg/m^3 (black line in Figure 5.12) to 493 kg/m^3 (blue line) the time to achieve 99.80% conversion rises from 13.6 s to 18.4 s. Indeed, the carbon mass to be oxidised increases linearly with char density for a given particle size; moreover, internal diffusion of oxygen is favoured by higher porosity, i.e. lower char density. The increase of burning time with particle density is more significant for larger particles; this is the reason that Figure 5.12 to Figure 5.14 are based on a particle radius of 250 μm rather than on a 70 μm radius particle as elsewhere in this work. Figure 5.13 illustrates the particle temperature during combustion: increasing the char density from 170 kg/m^3 to 340 kg/m^3 leads to an increase of about 20 K in the particle temperature during combustion. For large particles, a change of density may have a

significant effect on the particle's velocity relative to the gas, thereby changing the particle's residence time in the furnace. This effect is illustrated in Figure 5.14.

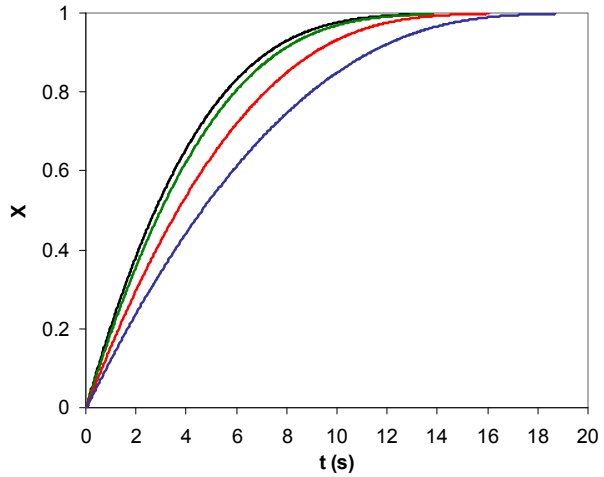

Figure 5.12 Influence of char density on particle conversion. Initial char radius: 250µm. Wall temperature: 950K. Initial char temperature: 1100K. $k = 8.85 \cdot 10^7$. Bulk gas temperature: 1200K. O_2 in bulk gas: 2%. Char density (kg/m^3): 170, black; 220, green; 340, red; 493, blue.

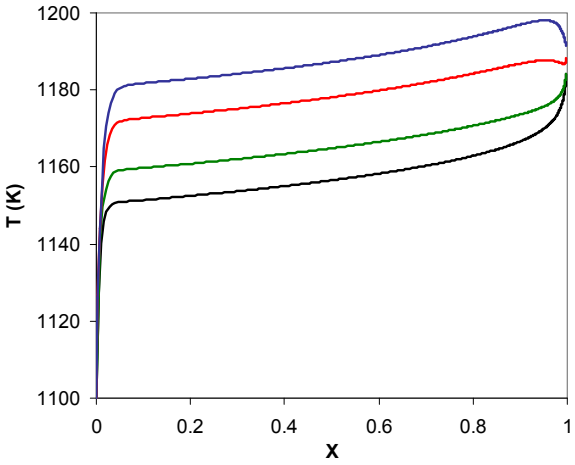

Figure 5.13 Influence of char density on particle temperature. Initial char radius: 250µm. Wall temperature: 950K. Initial char temperature: 1100K. $k = 8.85 \cdot 10^7$. Bulk gas temperature: 1200K. O_2 in bulk gas: 2%. Char density (kg/m^3): 170, black; 220, green; 340, red; 493, blue.

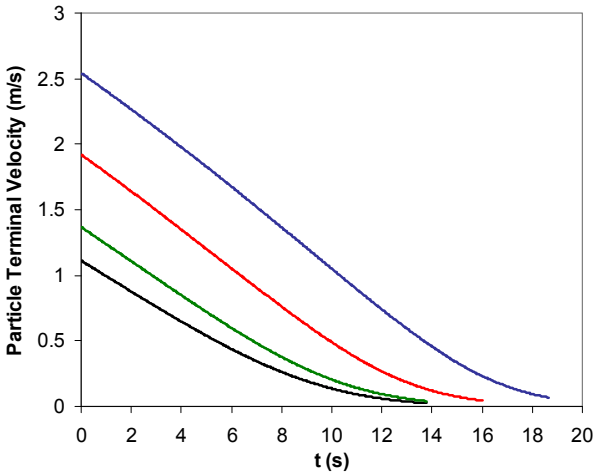

Figure 5.14 Influence of char density on particle terminal falling velocity during combustion. Initial char radius: 250µm. Wall temperature: 950K. Initial char temperature: 1100K. $k = 8.85 \cdot 10^7$. Bulk gas temperature: 1200K. O_2 in bulk gas: 2%. Char density (kg/m^3): 170, black; 220, green; 340, red; 493, blue.

It can be seen in Figure 5.14 that a particle of radius 250 μm can have a terminal falling velocity in the range 1-2.5 m/s at the beginning of combustion. These values are of the same order as the gas velocity (7.6 m/s) and imply that the particle does not follow the gas in the furnace. In fact, according to the assumptions the gas residence time in the furnace is 4.6 s, while the time for the particle in Figure 5.14 to reach the radiation shield below the superheaters is calculated by the model to be 5.2, 5.3, 5.7 and 6.4 s for char density of 170, 220, 340 and 493 kg/m^3 respectively. The increased residence time helps to increase char burnout in the furnace.

Figure 5.15 to Figure 5.17 show the height above the burners at which char particles with radius up to 350 μm reach 99.80% conversion, according to the model. As discussed before, the distance between the lowest burners' level and the radiation shield is 35 m. Both high and low reactivity chars are considered in Figure 5.15 to Figure 5.17, as well as three different bulk gas temperatures: 1200 K, 1500 K and 1700 K. In Figure 5.15 the wall temperature is assumed to be 800 K, whereas it is 950 K in Figure 5.16 and 1100 K in Figure 5.17.

The model predicts that low reactivity char particles burning in gas at 1200 K (blue dotted lines in Figure 5.15 to Figure 5.17) do not reach high conversion (99.80%) in the boiler, regardless of the wall temperature and the particle size. Moreover, it is seen that the temperature of the walls influences very much the conversion of these low reactive chars at 1200 K; for instance, a particle with a 100 μm radius would reach 99.80% conversion after 9.9 s (74 m above the burner's level) when the wall temperature is 800 K (Figure 5.15), compared with 6.9 s (52 m above the burner's level) when the wall is at 1100 K (Figure 5.17).This is due to the fact that in these conditions the radiation heat to the cold walls is of the same order as the heat of reaction. It can be seen that in all the other conditions considered in Figure 5.15 to Figure 5.17, for a given combination of char reactivity and gas temperature, the largest char size for which 99.80% conversion is attained in the boiler is not influenced by the wall temperature. In fact, as discussed in previous chapters, the reactivity of the chars is more likely to be lower at higher temperatures, because of thermal deactivation; the combination of gas temperature 1200 K and lower char reactivity might thus not be the most likely in practice and it seems therefore realistic to conclude that in most circumstances the temperature of the wall is not a key parameter for char burnout prediction in pulverised wood boilers.

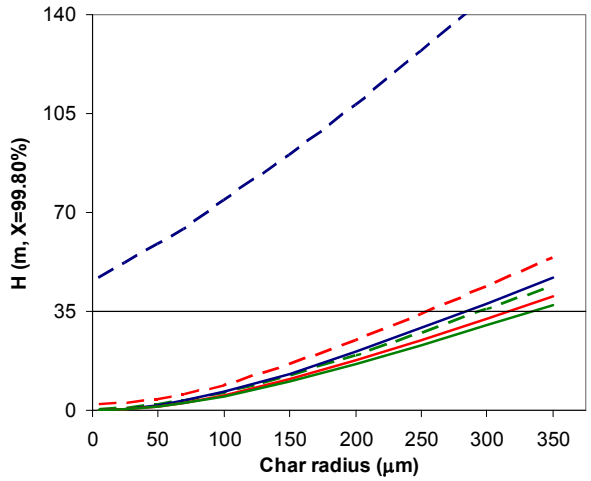

Figure 5.15 Height above burner for which char conversion is 99.80% as a function of particle radius. Wall temperature: 800K. Initial char temperature: 1100K. O_2 in bulk gas: 2%. Solid lines: $k = 3.39 \cdot 10^{10}$, dotted lines: $k = 8.85 \cdot 10^{7}$. Bulk gas temperature: blue, 1200K; red, 1500K; green, 1700K.

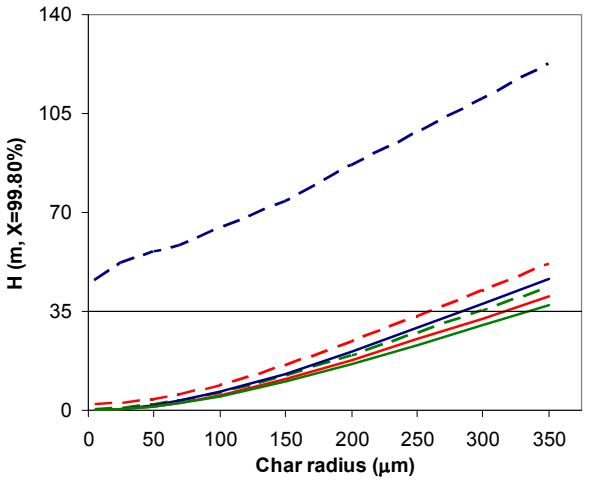

Figure 5.16 Height above burner for which char conversion is 99.80% as a function of particle radius. Wall temperature: 950K. Initial char temperature: 1100K. O_2 in bulk gas: 2%. Solid lines: $k = 3.39 \cdot 10^{10}$, dotted lines: $k = 8.85 \cdot 10^{7}$. Bulk gas temperature: blue, 1200K; red, 1500K; green, 1700K.

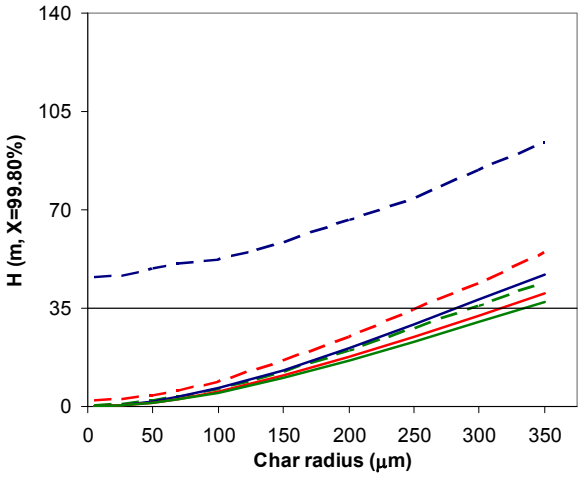

Figure 5.17 Height above burner for which char conversion is 99.80% as a function of particle radius. Wall temperature: 1100K. Initial char temperature: 1100K. O_2 in bulk gas: 2%. Solid lines: $k = 3.39 \cdot 10^{10}$, dotted lines: $k = 8.85 \cdot 10^{7}$. Bulk gas temperature: blue, 1200K; red, 1500K; green, 1700K.

As far as char reactivity is concerned, the results shown in Figure 5.15 to Figure 5.17 are in agreement with the observations made earlier in this section: the effect of reactivity is lower, yet significant, at higher temperatures. It can be seen in Figure 5.16 that at 1200 K (blue lines) a particle conversion of at least 99:80% is obtained for high reactive chars with radius up to 285 μm 35 m above the burners'

level; at 1500 K (red lines) low reactive particles with radius up to 260 μm reach 99.80% burnout, compared with 315 μm radius for highly reactive chars; at 1700 K (green lines) the maximum radius to achieve this conversion is 300 μm and 335 μm for low and high reactive chars, respectively. All in all, the model predicts that chars with radius up to 260 - 335 μm will attain 99.80 % conversion; these sizes correspond to wood fuel particles sieve sizes of 1450 - 1850 μm.

The results of the model can be compared with Table 5.5, which shows the char conversion of the samples collected during the full scale measuring campaign at the power plant. The full scale campaign is described in detail in Chapter 3; the samples were collected just below the superheaters, at the top of the combustion chamber.

Table 5.5 Char conversion at the top of the combustion chamber of Avedøre Unit 2 main boiler. Full scale data; the bulk gas temperature and oxygen concentration were measured below the superheaters.

Fuels	*Bulk gas T at the top of furnace (K)*	*O_2 at the top of furnace (vol%)*	*Char conversion (%)*
wood + oil	n.a.	n.a.	*99.23*
wood + oil	n.a.	2.8	*99.82*
wood + gas	1231	1.4	*99.67*
wood + gas	1196	3.7	*99.88*
wood + gas	1220	2.9	*99.78*
wood + gas	1198	2.9	*99.91*
wood + gas	1206	4.0	*99.92*
wood + gas	1191	3.2	*99.87*
wood + gas	1202	2.6	*99.95*

As seen in Table 5.5 during the full scale measurements the furnace was burning different combination of fuels; for all the test conditions, very high values of wood char conversion (at least 99.23 %) were obtained. When comparing model predictions with measured conversions it should be remembered that conversions in Table 5.5 are in fact average char conversions for a particle size distribution. As discussed in section 5.3.6, the median of the full scale wood size distribution was 440 μm (sieve size) and the maximum particle size 2000 μm (sieve size); due to shrinking during pyrolysis these sizes correspond to char particles of radius 70 μm and 350 μm, respectively. Moreover, it was found in Chapter 3 that only 6-10% of the mass of milled wood fuel at Avedøreværket was made up of particles with nominal sizes greater than 1000 μm, for which the corresponding char radius after pyrolysis is 150 μm. As discussed above, the model predicts that, with the exception of low reactivity chars burning in

gas at 1200 K, char particles with radiuses well above 150 μm (up to 260 - 335 μm depending on gas temperature and char reactivity) reach 99.80% burnout in the furnace, i.e. only a very little fraction of the wood char particles is not fully (99.80%) converted 35 m above the level of the burners. Indeed, these results agree qualitatively with the full scale data in Table 5.5 and it can be concluded that the model gives an acceptable prediction of the conversion achieved in the power plant in the investigated conditions.

The accuracy of the model's predictions may be improved in several ways. First of all, the very simplified modelling of gas and particle flow in the furnace may lead to misestimating the particles' residence time in the furnace. Moreover, the char particle sizes used in the model were calculated based on few measurements; a more systematic study of particle shrinkage during pyrolysis at boiler-like conditions would enable a more precise assessment of the char particle size distribution. The assumption of uniform gas temperature in the furnace is also limiting, since flame temperatures in the furnace can be several hundred degrees higher than average furnace temperature. On the other hand, the model does not consider char thermal deactivation which lowers the particle's reactivity and thus tends to decrease the achieved conversion.

5.5 CONCLUSION

The different approaches to single particle combustion modelling have been briefly reviewed. In order to cope with the complexity of the process various strategies are used: some authors include statistical distributions to describe the char particle's properties, such as reactivity to oxygen or density. Other models include empirical parameters as a so called mode of burning, which defines in which combustion regime the char is converted. Most advanced models include the effect of the formation of an outer ash layer in the mass transport calculations. Thermal deactivation and fragmentation are seldom added as a separate module, although a certain allowance is made by using statistical distributions of particle size and reactivity.

The model developed in this work combines the description of the char combustion with the characteristics of the Avedøre Unit 2 main boiler (suspension fired). The properties of the burning char were either determined experimentally (reactivity, size), as described in previous chapters, or taken from literature (density, porosity). The particle is assumed to burn in a bulk gas with constant temperature and constant oxygen fraction. The particle temperature is determined taking reaction heat, convection through boundary gas layer and radiation with furnace walls into account. As regards mass balance, the model accounts for external gas diffusion to the particle outer surface, internal diffusion in the pores and heterogeneous chemical reaction (CO is considered the only product). The model calculates an overall effectiveness factor for combustion, yet assumes that all the reacting carbon is consumed at the outer surface of the char. This results in a shrinking char particle with constant density and constant porosity.

The model predicts that the conversion of char particles in gas at 1200 K is very much affected by the reactivity of the char: for a particle with 70 μm radius increasing the reaction rate's pre-exponential factor by three orders of magnitude, as is possible depending on the char's thermal history as shown in Chapter 4, leads to a reduction of 94% of the time to achieve 99.80% conversion. The influence of the particle's reactivity is lower at higher temperatures: at a furnace temperature of 1500 K and 1700 K the combustion of the chars is mainly controlled by transport processes. It was shown that the combustion of highly reactive char particles with radius greater than 25 μm is solely controlled by external diffusion though the gas film, at any of the considered furnace temperatures. Due to radiation to the cold furnace wall low reactive char particles with radius 70 μm burn at temperatures lower than the surrounding gas, whereas highly reactive chars of the same size reach peak temperatures that are about 100 K above that of the bulk gas.

The effect of oxygen concentration in the bulk gas was investigated. For a particle with 70 μm radius, the time to achieve 99.80% conversion decreases from 165 s to 3.4 s when the oxygen concentration in the bulk gas increases from 0.1% to 4.0%; the corresponding temperature of the burning char particle was found to be about 50 K higher in the case of 4.0% oxygen with respect to 0.1% oxygen. In agreement with the increased particle temperature, it was also found that increasing oxygen concentration in bulk gas makes diffusion processes to become more limiting during combustion.

The char particle's density was varied in a range based on literature data (170 - 493 kg/m^3). Higher particle densities lead to a longer conversion time: for a low reactivity char with radius 250 μm burning in gas at 1200 K and 2% oxygen the time to achieve 99.80% conversion is 13.6 s and 18.4 s for particles with densities of 170 kg/m^3 and 493 kg/m^3 respectively. On the other hand, it was found that the residence time of larger particles in the furnace is longer than for the gas (up to 6.4 s for a 250 μm radius particle, 4.6 s for the gas), which helps to achieve higher particle conversion in the boiler.

Finally, the maximum radius that allows char particles to achieve 99.80% conversion at the top of the combustion chamber was estimated, considering different temperatures of the bulk gas and of the furnace walls and different values of char reactivity. The results show that low reactivity char particles burning in gas at 1200 K and 2% oxygen do not reach high conversion (99.80%) in the boiler, regardless of the wall temperature and the particle size. In these conditions the temperature of the walls influences very much the conversion of the particles: a particle with a 100 μm radius would reach 99.80% conversion 74 m above the burner's level when the wall temperature is 800 K, compared with 52 m when the wall is at 1100 K. On the other hand, it was shown that for gas temperatures of 1500 K and 1700 K and for high reactivity chars the particle's burnout at the top of the furnace is not influenced by the wall temperature. According to the model high reactive chars with radius up to 285 μm attain a conversion of at least 99.80% in the furnace when burning in gas at 1200 K and 2% oxygen; in order to obtain 99.80% conversion for gas temperatures of 1500 K and 1700 K low reactive particles should have radiuses no greater than 260 μm and 300 μm and highly reactive chars no greater than 315 μm and 335 μm, respectively. This corresponds to wood fuel particle sieve sizes of 1450 – 1850 μm.

The conversions measured at the top of the furnace of the main boiler of Avedøre Unit 2 were higher than 99.20% in all the tested conditions. The largest nominal particle size of milled wood fuel at the power plant was 2000 μm, which corresponds to an estimated char particle radius after pyrolysis of 350 μm. By comparing this value with the results of the single particle combustion model (99.80% or greater burnout for particles with radiuses up to 260 - 335 μm, depending on gas temperature and char reactivity) it can be concluded that the model predicts that only a very little fraction of the wood char particles is not fully (99.80%) converted 35 m above the level of the burners.

Low reactivity char particles burning in gas at 1200 K are an exception to these results; in this case the model predicts lower burnout than measured in the furnace. In fact, due to lower thermal deactivation, char reactivity is generally expected to be higher at lower temperatures and therefore the likelihood of low reactive chars burning at low temperature is low.

It is important to remember that the model includes some strongly simplifying assumptions, when comparing the results with full scale data. Nevertheless, it seems that it does provide a reasonable prediction of the conversion of wood char at the top of pulverised fuel boilers of the type considered in this work.

LIST OF SYMBOLS

$C_{O_{2,b}}$ = oxygen bulk concentration $\left[\frac{mol}{m^3}\right]$

$C_{O_2,s}$ = oxygen surface concentration $\left[\frac{mol}{m^3}\right]$

C_P = char particle heat capacity $\left[\frac{J}{kg \cdot K}\right]$

$C_{P,\,gas}$ = gas heat capacity $\left[\frac{J}{kg \cdot K}\right]$

D = O_2-N_2 diffusion coefficient $\left[\frac{m^2}{s}\right]$

D_e = effective diffusion coefficient $\left[\frac{m^2}{s}\right]$

D_K = Knudsen diffusion coefficient $\left[\frac{m^2}{s}\right]$

E_a = activation energy $\left[\frac{J}{mol}\right]$

g = gravitational acceleration $\left[\frac{m}{s^2}\right]$

h = heat exchange coefficient $\left[\frac{J}{m^2 \cdot s \cdot K}\right]$

h_D = mass transfer coefficient $\left[\frac{m}{s}\right]$

k_0 = reaction rate constant in Eq. 5.8 $\left[\frac{m^3}{mol_{O_2} \cdot s}\right]$

k_0' = pre-exponential factor in Eq. 5.7 $\left[\frac{kg_C}{kg_C \cdot s}\right]$

k_r = reaction rate constant $\left[\frac{m^3}{mol_{O_2} \cdot s}\right]$

k_t = gas thermal conductivity $\left[\frac{J}{m \cdot s \cdot K}\right]$

L = height $[m]$

m = mass of dry ash free char $[kg_C]$

MW = molar weight $\left[\frac{kg}{m^3}\right]$

Nu = Nusselt number = $\frac{h \cdot 2r}{k_t}$ [–]

P = pressure $[Pa]$

Pr = Prandtl number = $\frac{\nu \cdot \rho_{gas} \cdot C_{P,gas}}{k_t}$ [–]

q_c = convective heat flux $\left[\frac{J}{m^2 \cdot s}\right]$

q_r = heat flux by radiation $\left[\frac{J}{m^2 \cdot s}\right]$

r_p = radius of the char particle $[m]$

R = gas constant $\left[\frac{J}{mol \cdot K}\right]$

Re = Reynolds number = $\frac{u_t \cdot 2 \cdot r}{\nu}$ [–]

Sc = *Schmidt number* = $\frac{\nu}{D}$ $[-]$

Sh = *Sherwood number* = $\frac{h_D \cdot 2 \cdot r}{D}$ $[-]$

T_{char} = *char particle temperature* $[K]$

T_b = *bulk gas temperature* $[K]$

T_{wall} = *wall temperature* $[K]$

u_{char} = *char particle velocity* $\left[\frac{m}{s}\right]$

u_g = *gas linear velocity* $\left[\frac{m}{s}\right]$

u_t = *particle terminal falling velocity* $\left[\frac{m}{s}\right]$

W_{O_2} = *oxygen molar flux* $\left[\frac{mol}{m^2 \cdot s}\right]$

GREEK LETTERS

ΔH_{reac} = *heat of reaction* $\left[\frac{J}{mol}\right]$

ξ_{ash} = *mass fraction of ash in char* $[-]$

ε_{char} = *char particle porosity* $[-]$

Φ = *Thiele modulus* $[-]$

η = *internal effectiveness factor* $[-]$

ν = *gas kinematic viscosity* $\left[\frac{m^2}{s}\right]$

ρ_C = *carbon density in the char* $\left[\frac{kg}{m^3}\right]$

ρ_{char} = *char density* $\left[\frac{kg}{m^3}\right]$

ρ_{gas} = *gas density* $\left[\frac{kg}{m^3}\right]$

σ = *Stefan Boltzman constant* $\left[\frac{W}{m^2 \cdot K^4}\right]$

τ = *tortuosity factor* $\left[\frac{s}{m^2}\right]$

Ω = *overall effectiveness factor* $[-]$

REFERENCES

1. Backreedy R.I., Fletcher L.M., Ma L., Pourkashanian M., Williams A.. Modelling pulverised coal combustion using a detailed coal combustion model, Combustion Science and Technology, 2006, 178, 763.
2. Ma L., Jones J.M., Pourkashanian M. and Williams A., Modelling the combustion of pulverized biomass in an industrial combustion test furnace, Fuel, 2007, 1959
3. Żelkowski J., Some aspects of measurement, interpretation and practical use of results from solid fuel reactivity studies, 2001, Energy, 25, 1185.
4. Hurt R., Sun J.-K and Lunden M., A kinetic model of carbon burnout in pulverized coal combustion, Combustion and Flame, 1998, 113, 181.
5. Eaton A. M., Smoot L. D., Hill S. C. and Eatough C. N., Components, formulations, solutions, evaluation and application of comprehensive combustion models, Progress in Energy and Combustion Science, 1999, 25, 387.
6. Cozzani V., Petarca L., Pintus S. and Tognotti L., Ignition and combustion of single, levitated char particles, Combustion and Flame, 1995, 193, 103.
7. Jensen K. R., Dannelse af NOx ved forbrænding af kul, Master Thesis, Department of Chemical engineering, DTU, 1988.
8. Jensen A., Department of Chemical Engineering, DTU.
9. Feng B. and Bhatia S. K., Percolative fragmentation of char particles during gasification, Energy and Fuels, 2000, 14, 297.
10. Mukunda H.S., Paul P.J., Srinivasa U and Rajan N.K.S., Combustion of wooden spheres- experiments and model analysis, Twentieth Symposium (International) on Combustion, The combustion Institute, 1984, 1619.
11. Kuo J.T. and Hwang L. H., Mass and thermal analysis of burning wood spheres, Combustion Science and Technology, 2003, 175, 665.
12. Wurzenberger J. C., Wallner S., Raupenstrauch H and Khinast J. G., Thermal conversion of biomass: comprehensive reactor and particle modeling, 2002, AIChE Journal, vol 48, No. 10, 2398.
13. Sotirchos S. V. and Burganos V. N., Intraparticle diffusion and char combustion, Chemical Engineering Science, 1986, 1599.
14. Yang Y. B., Sharifi V. N., Swithenbank J., Ma L., Darvell L. I., Jones J. M., Pourkashanian M. and Williams A., Combustion of a single particle of biomass, Energy & Fuels, 2008, 22, 306.
15. Smith I. W.,The combustion rates of coal chars: a review, Nineteenth Symposium (International) on Combustion, The combustion Institute, 1982, 1045.
16. Jiménez S. and Ballester J., Study of the evolution of particle size distributions and its effects on the oxidation of pulverized coal, Combustion and Flame, 2007, 151, 482.
17. Coda B. and Tognotti L., The prediction of char combustion kinetics at high temperature, Experimental Thermal and fluid science, 2000, 21, 79.
18. Ballester J. and Jiménez S., Kinetic parameters for the oxidation of pulverized coal as measured from drop tube tests, Combustion and Flame, 2005, 142, 210.
19. Mitchell R. E., Ma L. and Kim B., On the burning behaviour of pulverized coal chars, Combustion and Flame, 2007, 151, 426.
20. Ranz W.E. and Marshall W.R. Jr, Evaporation from drops, Chemical Engineering Progress, 1952, 48, 141,173.
21. Danner R.P. and Daubert T.E., Journal of Chemical and Engineering Data, 1982, 27.
22. Kunii D. and Levenspiel O., Fluidization Engineering, 1991, Butterworth-Heinemann.
23. Fogler H.S., Elements of Chemical reaction Engineering, 3rd edition, Prentice Hall International Editions
24. Bird R.B., Stewart W.E. and Lightfoot E.N., Transport Phenomena, 2nd edition, Wiley
25. Mermoud F., Salvador S., Van de Steene L. and Glofier F., Influence of the pyrolysis heating rate on the steam gasification rate of large wood char particles, Fuel, 2006, 85, 1473.
26. Lin W., Personal communication, Department of Chemical and Biochemical Engineering, Technical University of Denmark, 2006
27. Senneca O., Kinetics of pyrolysis,combustion and gasification of three biomass fuels, Fuel Processing Technology, 2007, 88, 67.

CHAPTER 6

CONCLUSION

6.1 CONCLUSION

A measurement campaign was carried out at Avedøreværket's Unit 2, a 800 MWth, once-through suspension-fired boiler where oil, pulverised wood and natural gas are co-fired. Sieving of the collected samples showed that the mills in operation at the plant ground the wood particles to smaller sizes than those of the received wood pellets. Half of the sample mass was made up of particles with sieve sizes below 300-430 μm after milling.

Different boiler operating conditions and fuel combinations were tested. The measured CO level at the top of the combustion chamber was very low and increased only when the excess oxygen concentration was as low as 1.5%. The excess oxygen was varied during the campaign from about 1.5 to about 4.5% O_2 after the boiler; in all cases the measured emission of CO (CO concentration after the boiler) was extremely low, generally below 5 ppm. Under all of the applied conditions the wood fuel was found to have reached a very high degree of burnout of at least 99.7%.

The pyrolysis of pulverised wood particles in the conditions typical of a pulverised wood boiler was studied. Pyrolysis experiments at different temperatures were carried out in an Entrained Flow Reactor (EFR) and in a thermogravimetric analyzer (STA) with sieved pine wood and beech sawdust with a nominal size of 90-125 μm and 250-355 μm. Rapid heating (10^4 – 10^5 K/s) to high temperatures in the EFR yielded very little char (1-6 % daf) and caused major transformation in the particles' morphology. Pine char particles from high heating rate pyrolysis were spherical with large internal cavities; this is considered the result of particle melting during this type of fast pyrolysis. Beech char particles were less spherical than pine char particles but still porous with a smooth surface, indicating that some plasticity was attained during high heating rate pyrolysis. It is believed that the higher ash content of beech sawdust (in particular higher Ca and K content) may be responsible for the difference in char particles morphology.

Chars produced at high heating rates in the EFR were more reactive than chars from the STA pyrolised at the same temperature, indicating that the structure attained at high heating rates maintained a certain degree of disorder in spite of the high temperatures applied. Char thermal

deactivation was also observed during high heating rate pyrolysis; the reactivity of EFR pine chars decreased by a factor of 3 when the pyrolysis temperature was risen from 1073 K to 1273 K and by 2 orders of magnitude with a further increase from 1273 K to 1573 K. In the same temperature interval (1273 – 1573 K), on the other hand, EFR beech chars deactivated only by a factor of 10. The mineral matter content of the fuels was also related to the differences in char reactivity, in that the catalytic action of Ca and K may explain the higher reactivity of beech chars with respect to pine chars. Moreover, this study has shown that pyrolysis time has little influence on char reactivity compared with pyrolysis temperature and pyrolysis heating rate.

A simple single particle combustion model was developed that combines the description of the char combustion with the characteristics of the Avedøre Unit 2 furnace. Char reactivity and char sizes obtained during the experimental work were used as input to the model, while char density and porosity were varied over a range based on literature data. At a furnace temperature of 1200 K the model predicts that the time for a 70 μm radius particle to achieve 99.80% burnout is 94% shorter for highly reactive char compared with low reactivity char. The influence of the particle's reactivity is lower at higher temperatures, when the combustion of the chars is mainly controlled by transport processes. Due to radiation to the cold furnace wall low reactive char particles with radius 70 μm burn at temperatures lower than the surrounding gas, whereas highly reactive chars of the same size reach peak temperatures that are about 100 K above that of the bulk gas.

It was found that increasing the oxygen concentration in the bulk gas leads to higher combustion temperatures and shifts the controlling step of the combustion towards diffusion. A low reactive char particle with 70 μm radius reaches 99.80% conversion after 165 s and 3.4 s when the oxygen concentration in the bulk gas is 0.1% and 4.0%, respectively; the burning temperature of the particle was found to be about 50 K higher in the case of 4.0% oxygen with respect to 0.1% oxygen.

The results show that higher particle densities lead to a longer time of conversion: for a low reactivity char with radius 250 μm burning in gas at 1200 K and 2% oxygen the time to achieve 99.80% conversion is 13.6 s and 18.4 s for particles with densities of 170 kg/m^3 and 493 kg/m^3, respectively. Moreover, it was found that the residence time of larger particles in the furnace is longer than for the gas (up to 6.4 s for a 250 μm radius particle, 4.6 s for the gas), which helps to achieve higher particle conversion in the boiler.

The model predicts that low reactivity char particles burning in gas at 1200 K do not reach high conversion (99.80%) in the boiler (35 m above the burners' level). In these conditions the

temperature of the walls influences very much the conversion: a particle with a 100 μm radius would reach 99.80% conversion 74 m above the burner's level when the wall temperature is 800 K, compared with 52 m when the wall is at 1100 K. In fact, due to lower thermal deactivation, char reactivity is generally expected to be higher at lower temperatures and therefore the likelihood of low reactive chars burning in gas at 1200 K is low.

The level of burnout of highly reactive chars at the top of the furnace is not influenced by the wall temperature. The model predicts that high reactive chars with radius up to 285 μm attain a conversion of at least 99.80% in the furnace when burning in gas at 1200 K with 2% oxygen; in 1500 K and 1700 K gas with 2% oxygen 99.80% burnout or higher is reached by low reactive particles with radius up to 260 μm and 300 μm and highly reactive chars with radius up to 315 μm and 335 μm, respectively (char particles with radius 260 - 335 μm correspond to wood fuel particles with sieve size 1450-1850 μm). On the other hand, the char burnout measured at the top of the furnace of the main boiler of Avedøre Unit 2 was above 99.20% in all the tested conditions and the largest char radius in the boiler after pyrolysis, estimated based on the full scale char size distribution and on the experimental work on pyrolysis, was 350 μm, corresponding to a wood fuel particle's sieve size of 2000 μm. Thus, the model is found to give a reasonable prediction of the conversion of wood char at the top of the pulverised fuel boiler considered in this work.

6.2 SUGGESTIONS FOR FURTHER WORK

In order to be able to predict the combustion of wood in pulverised fuel power plants with better accuracy, a wider range of experimental data on char characteristics is needed. Carrying out pyrolysis experiments in the EFR with other wood fuels would allow a better understanding of the relation between parent wood and char characteristics. The produced chars should be analysed with respect to their morphology, density, porosity and reactivity. Investigating how these characteristics depend not only on the conditions of pyrolysis, but also on the ash content and ash composition of the wood, may lead to the development of tools for the prediction of char characteristics. Moreover, it was shown that on the one hand there is a relation between heating rate and char morphology (extent of melting / morphological changes between parent fuel and char) and on the other hand the heating rate during pyrolysis has a very strong influence on char reactivity: it would be useful to

investigate how the appearance of morphological changes at a given temperature depends on the wood particle size, and thereby establish a correlation between the size of the parent wood particle and the reactivity of the char particle. This would be of great advantage for a good description of combustion in full-scale boilers since characteristics such as char density and char reactivity have a great impact on the achieved conversion in a furnace.

It has been shown how important the size of the char is in determining the wood burnout. In this respect, two areas need to be investigated further. On the one hand, a rigorous study on the shrinkage of wood particles during pyrolysis in boiler-like conditions is critical to have a precise size distribution of the burning char particles. On the other hand, the occurrence and extent of particle fragmentation needs to be assessed, as fragmentation may change the size distribution during combustion.

Finally, the model used in this work would benefit from a better knowledge of the conditions in the full scale boiler. A detailed temperature profile in the boiler would help describe the burning particle's temperature history in the furnace more realistically. Moreover, it may help to include a better description of the particle's flow in the furnace in the model. Yet, it would be worth evaluating whether extensive efforts to obtain a detailed CFD simulation of the boiler would bring about substantial improvement. A first, much simpler, step would be to evaluate the gas flow due to combustion air, volatiles released during pyrolysis and combustion product gas with more accuracy for different loads of the boiler and, in the specific case of the Avedøre Unit 2 boiler, different fuels combinations too. This would enable more accurate residence times for the gas and the char particles during different operations of the boiler to be calculated and would thereby improve burnout predictions.